USGS
science for a changing world

# Synthesis of Petrographic, Geochemical, and Isotopic Data for the Boulder Batholith, Southwest Montana

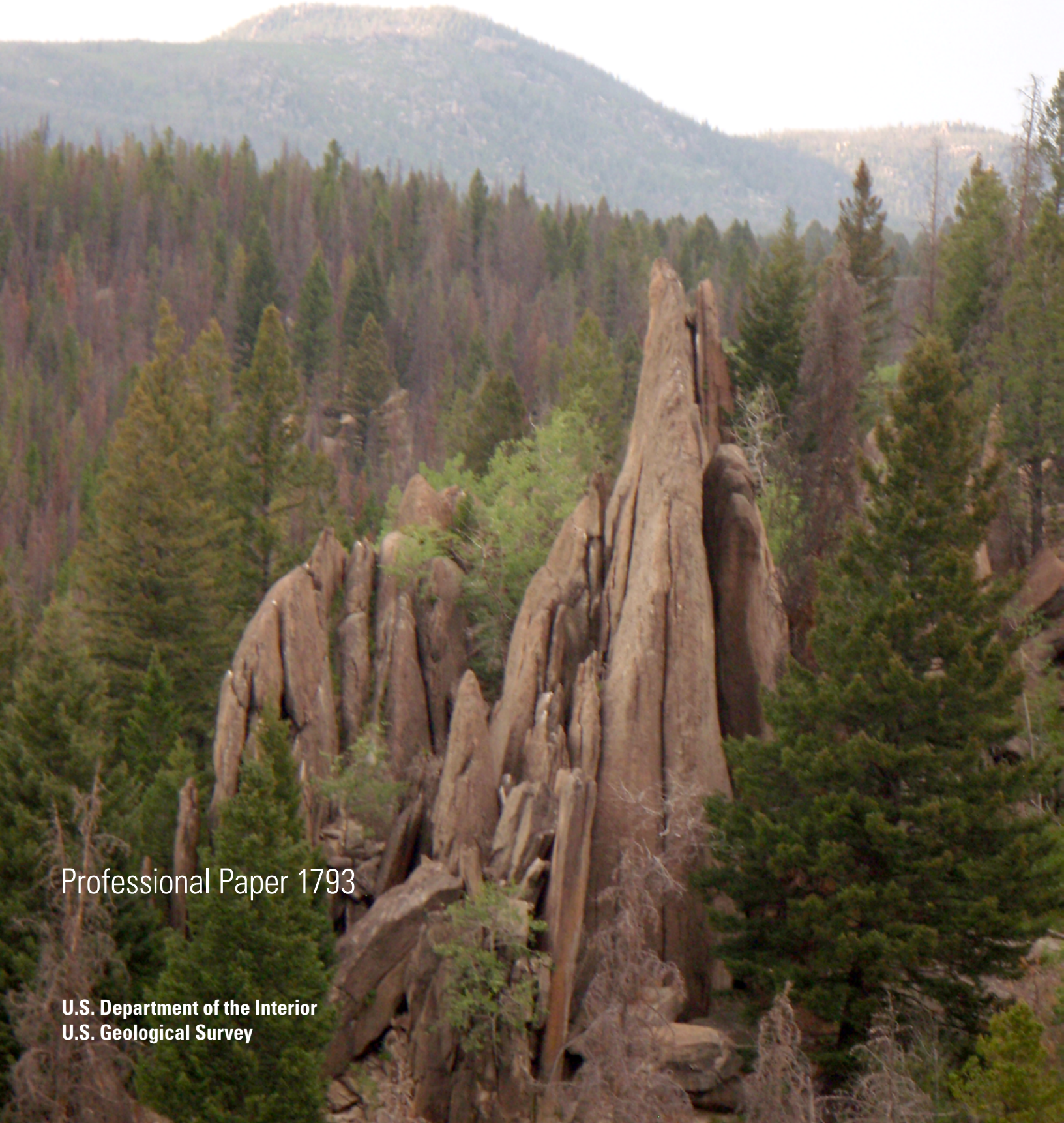

Professional Paper 1793

U.S. Department of the Interior
U.S. Geological Survey

**Cover photograph:** Planar jointed, spheroidal weathered Butte Granite at Homestake Pass, Montana.

# Synthesis of Petrographic, Geochemical, and Isotopic Data for the Boulder Batholith, Southwest Montana

By Edward A. du Bray, John N. Aleinikoff, and Karen Lund

Professional Paper 1793

**U.S. Department of the Interior**
**U.S. Geological Survey**

**U.S. Department of the Interior**
KEN SALAZAR, Secretary

**U.S. Geological Survey**
Marcia K. McNutt, Director

U.S. Geological Survey, Reston, Virginia: 2012



Suggested citation:
du Bray, E.A., Aleinikoff, J.N., and Lund, Karen, 2012, Synthesis of petrographic, geochemical, and isotopic data for the Boulder batholith, southwest Montana: U.S. Geological Survey Professional Paper 1793, 39 p.

# Contents



# Figures

## Tables



## Appendix

# Synthesis of Petrographic, Geochemical, and Isotopic Data for the Boulder Batholith, Southwest Montana

By Edward A. du Bray, John N. Aleinikoff, and Karen Lund

## Abstract

The Late Cretaceous Boulder batholith in southwest Montana consists of the Butte Granite and a group of associated smaller intrusions emplaced into Mesoproterozoic to Mesozoic sedimentary rocks and into the Late Cretaceous Elkhorn Mountains Volcanics. The Boulder batholith is dominated by the voluminous Butte Granite, which is surrounded by as many as a dozen individually named, peripheral intrusions. These granodiorite, monzogranite, and minor syenogranite intrusions contain varying abundances of plagioclase, alkali feldspar, quartz, biotite, hornblende, rare clinopyroxene, and opaque oxide minerals. Mafic, intermediate, and felsic subsets of the Boulder batholith intrusions are defined principally on the basis of color index. Most Boulder batholith plutons have inequigranular to seriate textures although several are porphyritic and some are granophyric (and locally miarolitic). Most of these plutons are medium grained but several of the more felsic and granophyric intrusions are fine grained. Petrographic characteristics, especially relative abundances of constituent minerals, are distinctive and foster reasonably unambiguous identification of individual intrusions.

Seventeen samples from plutons of the Boulder batholith were dated by SHRIMP (Sensitive High Resolution Ion Microprobe) zircon U-Pb geochronology. Three samples of the Butte Granite show that this large pluton may be composite, having formed during two episodes of magmatism at about 76.7 ± 0.5 Ma (2 samples) and 74.7 ± 0.6 million years ago (Ma) (1 sample). However, petrographic and chemical data are inconsistent with the Butte Granite consisting of separate, compositionally distinct intrusions. Accordingly, solidification of magma represented by the Butte Granite appears to have spanned about 2 million years (m.y.). The remaining Boulder batholith plutons were emplaced during a 6–10 m.y. span (81.7 ± 1.4 Ma to 73.7 ± 0.6 Ma).

The compositional characteristics of these plutons are similar to those of moderately differentiated subduction-related magmas. The plutons form relatively coherent, distinct but broadly overlapping major oxide composition clusters or linear arrays on geochemical variation diagrams. Rock compositions are subalkaline, magnesian, calc-alkalic to calcic, and metaluminous to weakly peraluminous. The Butte Granite intrusion is homogeneous with respect to major oxide abundances. Each of the plutons is also characterized by distinct trace element abundances although absolute trace element abundance variations are relatively minor. Limited Sr and Nd isotope data for whole-rock samples of the Boulder batholith are more radiogenic than those for plutonic rocks of western Idaho, eastern Oregon, the Salmon River suture, and most of the Big Belt Mountains. Initial strontium ($Sr_i$) values are low and epsilon neodymium ($\varepsilon_{Nd}$) values are comparable relative to those of other southwest Montana basement and Mesozoic intrusive rocks. Importantly, although the Boulder batholith hosts significant mineral deposits, including the world-class Butte Cu-Ag deposit, ore metal abundances in the Butte Granite, as well as in its peripheral plutons, are not elevated but are comparable to global average abundances in igneous rocks.

## Introduction

The Boulder batholith encompasses about 4,000 square kilometers ($km^2$) in southwest Montana (bounded by latitudes 45.6° and 46.7°N. and longitudes 112.75° and 111.5°W.) and lies in the Helena embayment of the Mesoproterozoic Belt Supergroup and in the foreland of the Late Cretaceous fold and thrust belt (figs. 1 and 2). In this setting, the Boulder batholith is far to the east (inboard) of other Late Cretaceous batholiths, such as the Idaho batholith, of the North American Cordillera.

The batholith is the subject of many detailed studies, including the duration of magmatism, petrology of constituent plutons, and their relations to nearby volcanic rocks and associated mineral deposits, that led to modern models of batholith-scale intrusive systems. Extensive mapping and petrologic studies by U.S. Geological Survey scientists helped characterize the igneous rocks of the Boulder batholith region (Becraft and Pinkney, 1961; Becraft and others, 1963; Emmons and Weed, 1897; Klepper and others, 1957, 1971b, 1974; Knopf, 1913, 1950, 1957, 1963; Robinson and others, 1968; Ruppel, 1963; Smedes, 1966; Tilling, 1964; Tilling and others, 1968; and Tilling and Gottfried, 1969). These studies established the field relations, modal composition, and geochemistry of individual intrusions that constitute the batholith. Important related and follow-on studies pertain to (1) ages of plutonic rocks (Knopf, 1956, 1964; Tilling and others, 1969; Tilling, 1974), (2) relations between the mineral deposits and their

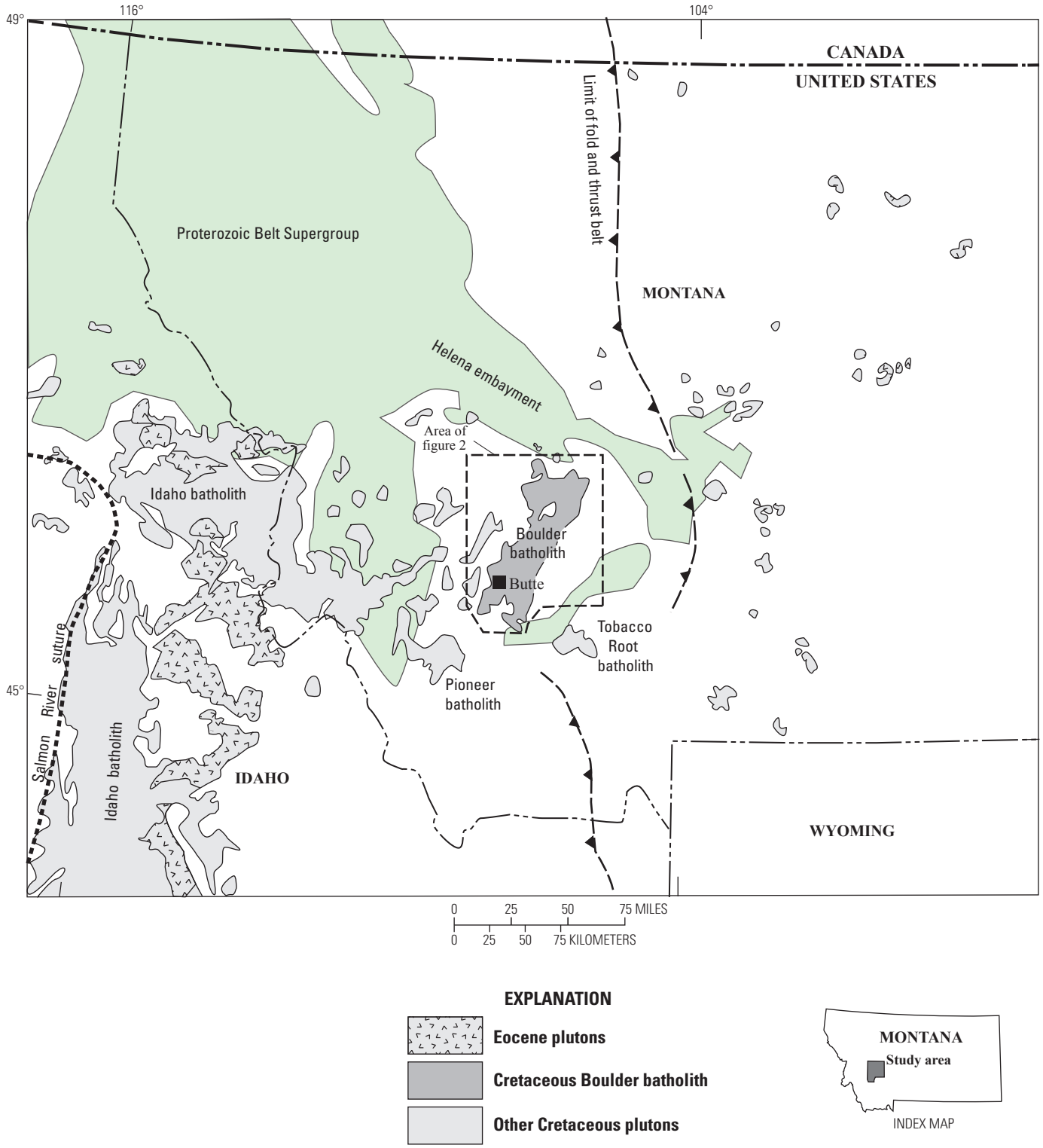


**Figure 1.** Location of Boulder batholith relative to major geologic features in the region.

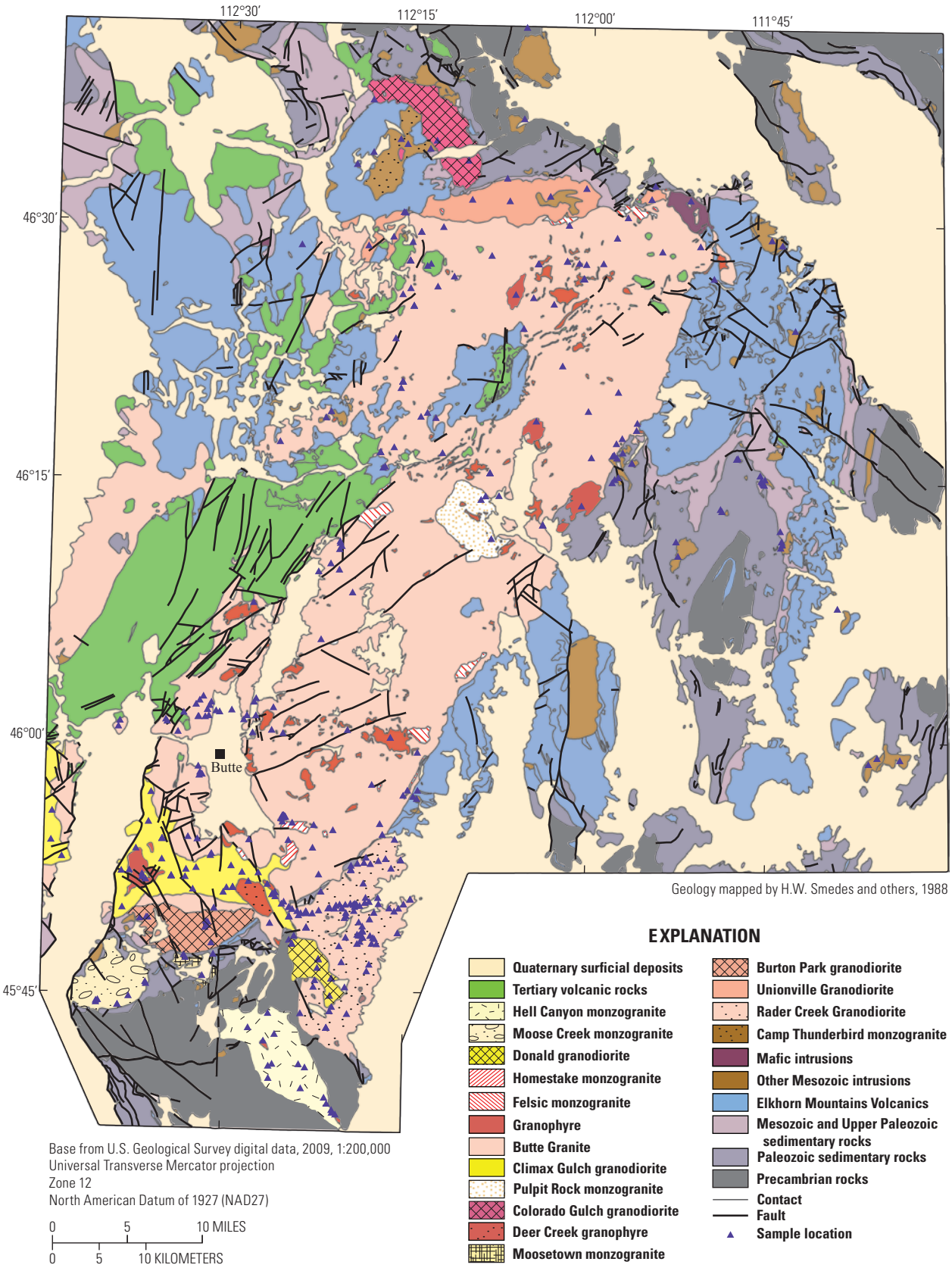


**Figure 2.** Boulder batholith, southwest Montana (modified from Smedes and others, 1988).

Boulder batholith host rocks (Doe and others, 1968; Knopf, 1913; Tilling, 1977; and Weed, 1912; ), (3) the geometric and genetic relations between the batholith and the nearby Elkhorn Mountains Volcanics (Davis and others, 1963, 1965; Hamilton and Myers, 1967; Klepper and others, 1971a, 1974; Robinson and others, 1968; Rutland and others, 1989; and Tilling, 1974), (4) the thickness and crustal geometry of the batholith (Berger and others, 2011; Biehler and Bonini, 1969; and Schmidt and others, 1990) and (5) the isotopic and petrologic characteristics of these rocks, which have been used to define the petrogenetic evolution of associated magmas (Lambe, 1981; Tilling, 1968, 1973, and 1974).

Early studies demonstrated that the Boulder batholith consists of a series of related plutons (fig. 2) that were emplaced into Mesoproterozoic to Mesozoic sedimentary rocks and into reportedly cogenetic rocks of the Late Cretaceous Elkhorn Mountains Volcanics (Hamilton and Myers, 1967; Klepper and others, 1971a, b; Lambe, 1981; Robinson and others, 1968; Rutland and others, 1989; and Tilling, 1974). About 70 percent of the batholith is composed of the voluminous Butte Granite, but it includes as many as a dozen individually named, peripheral plutons (and many more named and unnamed exposures of plutonic rocks) that surround the Butte Granite.

A Cretaceous age for the Boulder batholith was established during early K-Ar dating investigations (Knopf, 1956). Subsequent K-Ar studies approximately defined the emplacement sequence of Boulder batholith intrusions (Tilling and others, 1968) and generally confirmed relative ages determined from field relations (Becraft and Pinkney, 1961; Becraft and others, 1963; and Ruppel, 1963). U-Pb zircon geochronologic investigations confirm that all Boulder batholith intrusions were emplaced between about 82 and 74 Ma and, with one exception, confirm the previously established intrusion sequence (Lund and others, 2002). Geochronologic data for the Elkhorn Mountains Volcanics are limited but a combination of fossils associated with distal and presumably cogenetic volcanic rocks and K-Ar ages on hornblende show that volcanism began about 80 Ma (as summarized by Tysdal, 2000) and may have continued until about 73 Ma (Robinson and others, 1968). As part of the United States northern Cordillera, abundant Cretaceous igneous rocks of the Boulder batholith and nearby region have been interpreted as byproducts of subduction-related processes, including back-arc magmatism, which prevailed along the west edge of the North American plate during this time interval (Christiansen and Yeats, 1992, fig. 1; Coney and Reynolds, 1977; and Lipman, 1992).

Mineral deposits associated with rocks of the Boulder batholith are the subjects of many investigations (Brimhall, 1973, 1977, 1979, 1980; Brown, 1894; Emmons and Tower, 1897; Weed, 1912; Knopf, 1913, 1950; Lange and Cheney, 1971; Meyer, 1965; Meyer and others, 1968; Miller, 1973; Proffett, 1973; Roberts, 1975; Rusk and others, 2008; Sales, 1913; Sales and Meyer, 1948, 1949; and Smedes, 1966 ). However, interpretations of relations between mineral deposits and host batholithic rocks have been controversial. Recently, Lund and others (2002) documented the temporal relations between magmatism and diverse types of ore deposits spatially associated with the Boulder batholith. That study also determined that some of the deposits are genetically related to the batholith but many others are related to volumetrically minor, younger Cretaceous intrusions or to Tertiary-age volcanic rocks (Lund and others, 2002; O'Neill and others, 2004; and Taylor and others, 2007). The mineral deposits in the Boulder batholith region are highly significant (see Elliot and others, 1992; and Tysdal and others, 1996) but many questions remain concerning relations to various intrusive episodes, metal sources, and deposit ages.

Geochemical and isotopic studies have been conducted on selected rocks and(or) minerals of the Boulder batholith (Doe and Tilling, 1967; Doe and others, 1968; Greenland and others, 1968, 1971, 1974; Gottfried and others, 1972; Tilling, 1964, 1968, 1973, 1974, 1977; and Tilling and Gottfried, 1969). However, with the exception of these focused studies, the petrology and petrogenesis of the individual plutons or of the batholith as a whole have not been systematically investigated. The primary goal of this report is to use geochemical and petrographic data compiled by du Bray and others (2009), in conjunction with the new SHRIMP U-Pb ages and Sr and Nd isotopic data, to produce a petrogenetic evaluation of geochemical and modal compositional variation of the Late Cretaceous Boulder batholith through time. Because dating studies indicate that significant polymetallic quartz-vein mineral deposits are temporally related to the Butte Granite (Lund and others, 2002), the geochemical data can also be used to investigate the metallogeny of the various Boulder batholith plutons.

## Study Description

The data compilation of du Bray and others (2009) contains geochemical data for almost 400 Boulder batholith samples; in addition, relative abundances of major rock-forming minerals in about 250 of these samples are recorded. Subsequent to publication of the compilation, a small number of new chemical and modal analyses were added to the working version (Appendix 1) of the previously published Boulder batholith database (du Bray and others, 2009). Using criteria described by du Bray and others (2009), all altered samples have been identified and removed from the geochemical dataset; similarly, all censored values (less than, greater than, and so forth) were replaced by blank cells. To mitigate the effects of variable postmagmatic oxidation processes, all iron abundances were converted to equivalent ferrous iron (FeO*). To eliminate disparities caused by variable volatile component contents and to facilitate meaningful comparison of oxide abundances, major oxide analyses were recalculated to 100 percent on a volatile-free basis. Although the compilation of du Bray and others (2009) includes analyses for numerous small stocks and plugs that intruded the Elkhorn Mountains Volcanics north and east of the Boulder

batholith, petrogenetic relations between these rocks and those of the Boulder batholith are not well documented. Accordingly, the compositional features of the satellitic plutons are not further addressed.

In the present study, plutons are referred to by compositional names derived from available modal data; some of these names differ from previous usage. In this regard, the name "Butte Granite" is used as explained by Lund and others (2002). Location names are given for some previously unnamed plutons, including (1) monzogranite of Camp Thunderbird (for granodiorite, undivided, from Knopf, 1950), (2) granophyre of Deer Creek (for previously mapped but unnamed body previously called aplite), and (3) granodiorite of Colorado Gulch (for porphyritic granodiorite from Knopf, 1950). These and other informal names for plutons are retained but simplified in the text, as in Homestake monzogranite (for monzogranite of Homestake). The Butte Granite includes many tabular or sheet-like masses previously referred to as alaskite or aplite. In recognition of their distinctive chill-zone characteristics, including granophyric textures, leucocratic composition, and miarolitic cavities, we refer to the alaskite and aplite masses as granophyre.

## Petrographic Data

As summarized by Bateman (1992, page 25) a pluton consists of "…a body of intrusive rock that is expressed at the surface by a single exposure that is continuous…" and has "…similar composition, texture, and age…" throughout. According to this definition, the Boulder batholith consists of a series of plutons, each with distinctive petrographic characteristics (table 1). Variable color indices (sum of modal biotite, hornblende, pyroxene, and opaque oxide mineral abundances) indicate that plutons of the Boulder batholith form three groups: (1) mafic (Burton Park, Unionville, and Rader Creek), (2) intermediate (Butte, Climax Gulch, Donald, Camp Thunderbird, Hell Canyon, Homestake, Moose Creek, Moosetown, Colorado Gulch, and Pulpit Rock), and (3) felsic (Deer Creek and other granophyric masses). The mafic plutons have color indices (table 1) that range from 17 to 24 and their average compositions are granodiorite [per the International Union of Geological Sciences classification scheme of Streckeisen (1976), fig. 3]. Color indices of the intermediate group plutons range from 6 to 13 and most plutons are composed of monzogranite (although the Donald and Climax Gulch plutons are composed of felsic granodiorite, fig. 3). The felsic plutons have color indices that range from 1 to 2 and their average compositions are monzogranite and syenogranite (fig. 3). Modal data for the Boulder batholith plutons define coherent, mutually overlapping QAP (quartz-alkali feldspar-plagioclase) composition fields. Compositions of single plutons vary sufficiently that some sample compositions plot in modal fields other than that of the average (fig. 3). Alkali-feldspar-plagioclase abundance ratios for average Boulder batholith modal compositions generally correlate with variations in color index among these rocks; plutons with the highest color indices generally have the lowest alkali feldspar/plagioclase.

Most Boulder batholith plutons have inequigranular to seriate, hypidiomorphic textures. Exceptions are the Colorado Gulch, Climax Gulch, Moosetown and Moose Creek plutons that contain phenocrysts, the Butte Granite (which almost attains a porphyritic texture in places), and sheet-like granophyre intrusions and the Deer Creek granophyre (which have xenomorphic, granophyric textures). The Deer Creek and other granophyric intrusions are fine grained but all other Boulder batholith rocks are medium grained. In Boulder batholith rocks, plagioclase is generally moderately oscillatory zoned and forms 2–3 millimeter (mm) euhedral to subhedral laths. Weakly perthitic alkali feldspar is anhedral, interstitial, and forms 2–mm grains. Anhedral quartz, pale green to olive green hornblende, and tan to dark reddish-brown biotite form anhedral grains approximately1 mm in greatest dimension. Although hornblende and biotite are the principal mafic silicate minerals in Boulder batholith plutons, trace amounts of clinopyroxene have been identified in the three plutons of the mafic group, and rarely in the Butte Granite. Plutons of the mafic group contain approximately equal amounts of hornblende and biotite, although hornblende is slightly more abundant. Intermediate-group plutons contain approximately equal amounts of hornblende and biotite, although biotite is most abundant in plutons with lower color indices. The Moosetown and Pulpit Rock monzogranites of the intermediate group are somewhat unusual in having color indices between 7 and 8 but contain no hornblende. Plutons with color indices less than 7 contain essentially no hornblende. Boulder batholith intrusions also contain 1–2 percent opaque oxide minerals; grains are anhedral to subhedral and 0.1–0.2 mm. The accessory mineral suite in these rocks includes combinations of zircon, apatite, titanite, and rare allanite. Glomerocrysts of hornblende, biotite, and opaque oxide minerals are common constituents of the Butte Granite and the granodiorites of Burton Park and Donald. The granophyric masses contain miarolitic cavities; in many places within the Deer Creek granophyre, these cavities contain chalcopyrite and molybdenite (Smedes and others, 1973).

Berger and others (2011) show that the Butte Granite is a composite intrusion underlain by distinct feeder conduits north and south of about latitude 46.2°N. A 2 m.y. age difference (see U-Pb zircon geochronology section) determined for Butte Granite samples from its northern and southern parts is also consistent with a composite intrusion. However, average modal compositions computed for groups of Butte Granite samples from north and south of latitude 46.2°N., respectively, indicate that the relative abundances of the major rock-forming minerals in these two groups of samples are statistically indistinguishable (table 2).

**Table 1.** Summary of petrographic characteristics for plutons of the Boulder batholith, southwest Montana, arranged in order of decreasing color index.

[Plag, plagioclase; Alk fldsp, alkali feldspar, Qtz, quartz; Hb, hornblende; Pyx, pyroxene; Bi, biotite; Opq, opaque oxide minerals. TR, trace. Accessory minerals: ti, titanite; ap, apatite; zr, zircon; al, allanite; mn, monazite; tr, tourmaline; xe, xenotime; gar, garnet. Blank fields constitute not present]

| Unit designation | Pluton short name | Average modal composition | Plag | Alk fldsp | Qtz | Hb | Pyx | Bi | Opq | Color index | Grain size | Texture | Accessory minerals |
|---|---|---|---|---|---|---|---|---|---|---|---|---|---|
| Granodiorite of Burton Park | Burton Park | Granodiorite | 43 | 17 | 15 | 11 | TR | 11 | 2 | 24 | medium | Seriate, hypidiomorphic | ti, ap, zr, al |
| Unionville Granodiorite | Unionville | Granodiorite | 40 | 21 | 19 | 10 | TR | 8 | TR | 18 | medium | Seriate, hypidiomorphic | ap, zr |
| Rader Creek Granodiorite | Rader Creek | Granodiorite | 46 | 18 | 19 | 9 | TR | 6 | 2 | 17 | medium | Seriate, hypidiomorphic | ap, ti, zr |
| Butte Granite | Butte | Monzogranite | 38 | 26 | 22 | 5 | TR | 7 | 1 | 13 | medium | Inequigranular to porphyritic, hypidiomorphic | al, ap, ti, zr, mn, xe, tr |
| Granodiorite of Climax Gulch | Climax Gulch | Granodiorite | 40 | 20 | 28 | 4 | | 6 | 2 | 12 | medium | Inequigranular, hypidiomorphic | ap, ti, al, zr |
| Monzogranite of Camp Thunderbird | Camp Thunderbird | Monzogranite | 34 | 36 | 19 | 4 | | 6 | 1 | 11 | medium | Aplitic/granophyric | zr, ti, ap |
| Granodiorite of Colorado Gulch | Colorado Gulch | Granodiorite | 44 | 22 | 25 | 5 | | 5 | 1 | 11 | medium | Porphyritic | ti, ap, zr, al |
| Monzogranite of Moosetown | Moosetown | Monzogranite | 36 | 27 | 28 | TR | | 8 | 1 | 9 | medium | Inequigranular to porphyritic, hypidiomorphic | al, ap, ti, zr |
| Monzogranite of Hell Canyon | Hell Canyon | Monzogranite | 44 | 25 | 24 | 4 | | 3 | 1 | 8 | medium | Inequigranular, hypidiomorphic | ti, ap, al, zr |
| Monzogranite of Pulpit Rock | Pulpit Rock | Monzogranite | 31 | 33 | 28 | | | 7 | 1 | 8 | medium | Inequigranular, hypidiomorphic | ti, ap, zr |
| Monzogranite of Homestake | Homestake | Monzogranite | 33 | 31 | 28 | 1 | | 6 | TR | 7 | medium | Inequigranular, hypidiomorphic | ap, ti, al, zr |
| Granodiorite of Donald | Donald | Granodiorite | 42 | 22 | 29 | TR | | 5 | 1 | 6 | medium | Seriate, hypidiomorphic | ap, zr, ti |
| Monzogranite of Moose Creek | Moose Creek | Monzogranite | 40 | 25 | 28 | | | 5 | 1 | 6 | medium | Porphyritic, hypidiomorphic | zr, ap, ti, al, gar |
| Granophyre | Granophyre | Syenogranite | 31 | 31 | 35 | TR | | 2 | TR | 2 | fine | Aplitic, granophyric | zr, al, ap, ti, tr |
| Granophyre of Deer Creek | Deer Creek | Monzogranite | ~33 | ~33 | ~33 | | | 1 | TR | 1 | fine | Equigranular, aplitic, granophyric | zr |

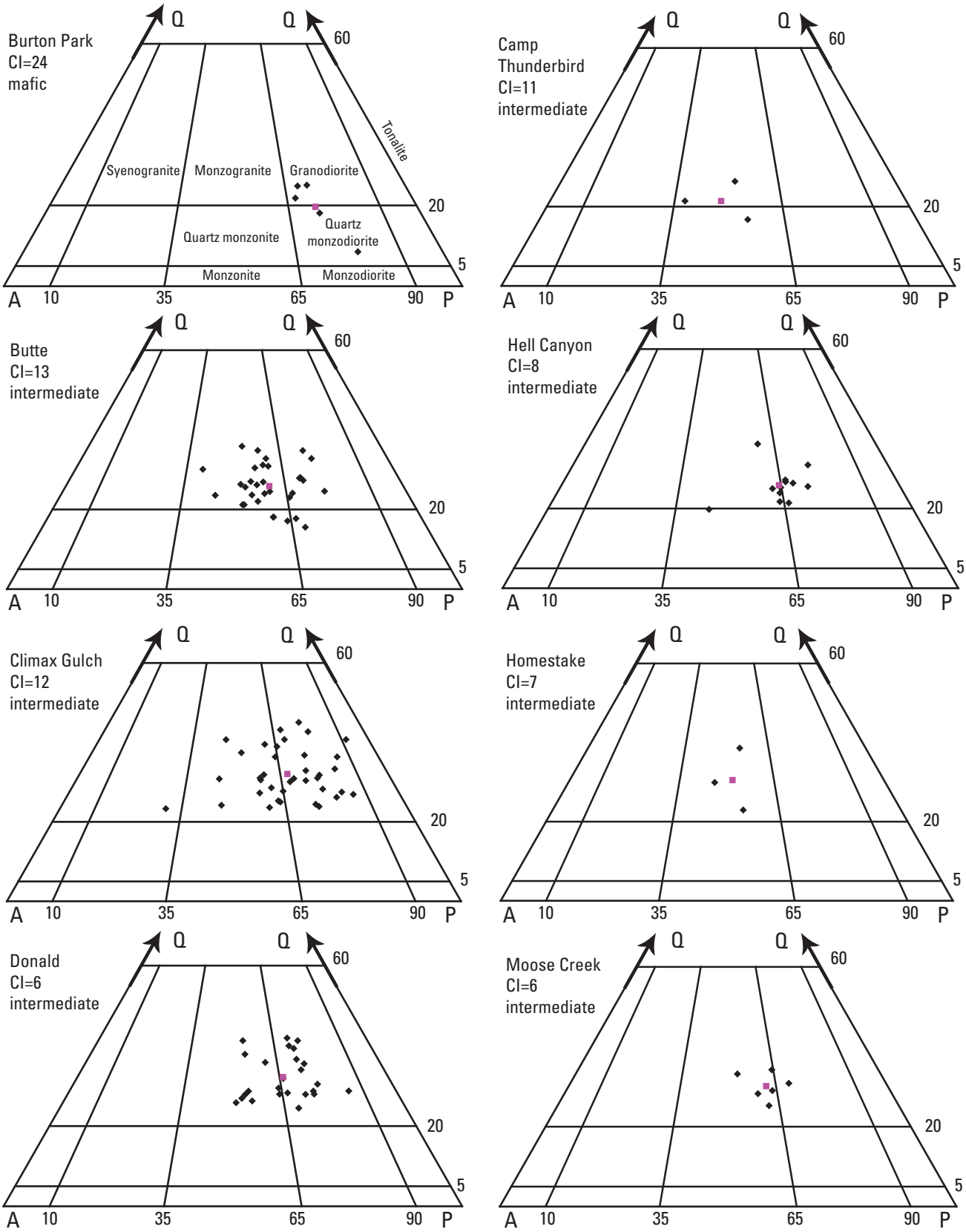


**Figure 3.** Quartz (Q), alkali feldspar (A), plagioclase (P) ternary diagram showing modal compositions of Boulder batholith plutons. Diamond-shaped symbols represent modal compositions of individual samples and square-shaped symbols depict the computed average composition for each intrusion. Classification grid and rock names are those of Streckeisen (1976). Average color index (CI) and mafic, intermediate, or felsic designations are shown for each intrusion.

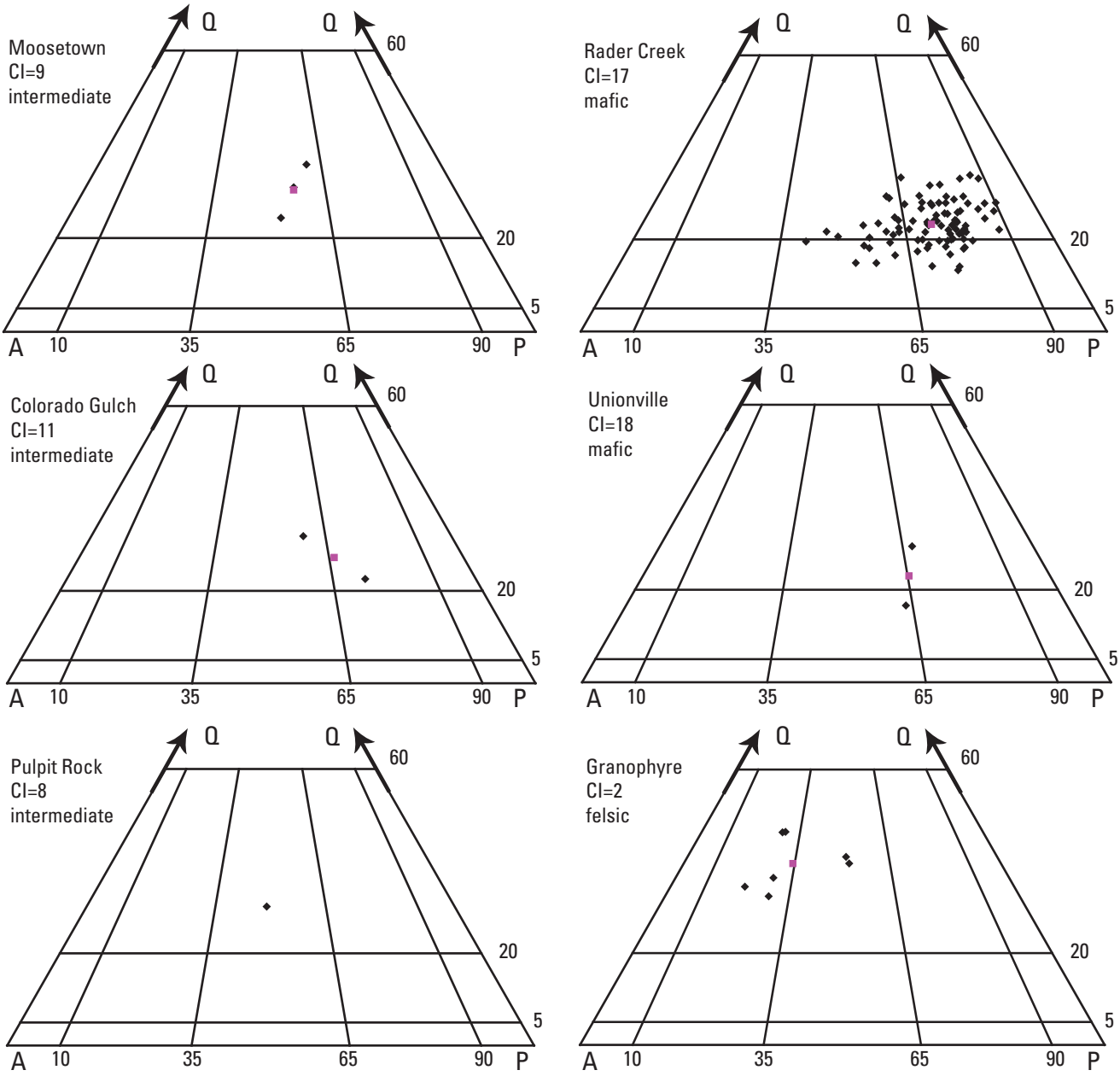


**Figure 3.** Quartz (Q), alkali feldspar (A), plagioclase (P) ternary diagram showing modal compositions of Boulder batholith plutons. Diamond-shaped symbols represent modal compositions of individual samples and square-shaped symbols depict the computed average composition for each intrusion. Classification grid and rock names are those of Streckeisen (1976). Average color index (CI) and mafic, intermediate, or felsic designations are shown for each intrusion.—Continued

**Table 2.** Average mineralogic and chemical compositions of Butte Granite north and south of latitude 46.2°N; Boulder batholith, southwest Montana.

[n=number of analyzed samples; std dev, standard deviation; Plag, plagioclase; Alk fldsp, alkali feldspar, Qtz, quartz; Hb, hornblende; Bi, biotite; Opq, opaque oxide minerals; Acc, accessory minerals]

| | North (n=20) | | South (n=8) | |
|---|---|---|---|---|
| | Mean | std dev | Mean | std dev |
| Plag | 38.0 | 6.0 | 37.7 | 5.5 |
| Alk fldsp | 26.7 | 6.2 | 24.1 | 5.1 |
| Qtz | 21.2 | 5.2 | 23.9 | 4.0 |
| Hb | 5.2 | 3.2 | 5.7 | 2.5 |
| Bi | 6.6 | 2.6 | 7.5 | 2.0 |
| Opq | 1.6 | 0.7 | 1.3 | 0.8 |
| Acc | 0.6 | 0.2 | 0.5 | 0.7 |
| | **North (n=49)** | | **South (n=37)** | |
| | **Mean** | **std dev** | **Mean** | **std dev** |
| $SiO_2$ | 65.97 | 2.74 | 66.11 | 2.29 |
| $TiO_2$ | 0.57 | 0.13 | 0.56 | 0.12 |
| $Al_2O_3$ | 15.63 | 0.79 | 15.57 | 0.55 |
| FeO* | 4.35 | 1.21 | 4.46 | 0.89 |
| MnO | 0.10 | 0.08 | 0.09 | 0.02 |
| MgO | 2.05 | 0.83 | 2.08 | 0.49 |
| CaO | 3.74 | 1.06 | 3.99 | 0.61 |
| $Na_2O$ | 3.14 | 0.46 | 2.92 | 0.16 |
| $K_2O$ | 4.26 | 0.50 | 4.03 | 0.33 |
| $P_2O_5$ | 0.20 | 0.09 | 0.18 | 0.06 |
| LOI | 0.74 | 0.51 | 0.58 | 0.15 |

# Major Oxide Data

Average chemical compositions of the Boulder batholith plutons are summarized in table 3. Major oxide compositions of the northern and southern parts of the Butte Granite, like relative mineral abundances, are statistically indistinguishable (table 2). The $SiO_2$ content of most Boulder batholith rocks ranges continuously from about 60 to 78 weight percent, although a few samples contain less than 60 weight percent $SiO_2$. Samples of the Butte Granite, as well as those of the Climax Gulch granodiorite and Rader Creek Granodiorite, form broad compositional arrays that span as much as 13 weight percent $SiO_2$. In contrast, smaller sample suites for peripheral plutons define more uniform compositional clusters. On geochemical variation diagrams (fig. 4), plutons of the Boulder batholith form relatively coherent composition clusters or linear arrays that are distinct but broadly overlapping. Specific plutons display both absolute and relative major oxide enrichments, or depletions relative to other plutons of the batholith. Absolute enrichments or depletions are by comparison to all Boulder batholith sample data, whereas relative enrichments or depletions indicate high or low concentrations at any given $SiO_2$ concentration. Distinctive major oxide features of the Boulder batholith plutons are as follows (fig. 4):

## Mafic Group

Burton Park Granodiorite: elevated (absolute) $TiO_2$, FeO*, MnO, MgO, CaO, $P_2O_5$ and low (absolute) $Na_2O$
Unionville Granodiorite: elevated (absolute) $TiO_2$, FeO*, MnO, MgO, CaO, $P_2O_5$ and low (absolute) $Na_2O$
Rader Creek Granodiorite: elevated (relative) CaO, $Na_2O$, and Na/K and low (relative) $TiO_2$ and $K_2O$

## Intermediate Group

Butte Granite: elevated (relative) $TiO_2$, $K_2O$, and MgO (slightly) and low (relative) $Al_2O_3$, $Na_2O$, and Na/K
Climax Gulch granodiorite: no distinctive characteristics
Donald granodiorite: slightly elevated (absolute) $SiO_2$ and $Na_2O$ and slightly elevated (relative) $Al_2O_3$, and FeO*
Camp Thunderbird monzogranite: slightly low (relative) FeO*, MgO, and CaO
Hell Canyon monzogranite: slightly elevated (relative) $Al_2O_3$, CaO, and $Na_2O$
Homestake monzogranite: slightly elevated (relative) MgO and $K_2O$ and slightly low (relative) $Al_2O_3$ and $Na_2O$
Moose Creek monzogranite: high (absolute) $Na_2O$, high (relative) MnO and low (relative/absolute) FeO*, $TiO_2$, MgO, and CaO
Moosetown monzogranite: no distinctive characteristics
Colorado Gulch granodiorite: low (relative) MnO and CaO
Pulpit Rock monzogranite: slightly elevated (relative) $P_2O_5$

## Felsic Group

Deer Creek granophyre: no distinctive characteristics
Granophyric intrusions: high (absolute) $SiO_2$, and $K_2O$ and low (absolute) $TiO_2$, $Al_2O_3$, FeO*, MnO, MgO, and CaO

Tilling (1973) and Lambe (1981) showed that the chemistry of Boulder batholith rocks define two distinct magma composition groups, which were identified as the main and sodic magma series, respectively. Relative to major oxide data, plutons of the sodic series (Rader Creek Granodiorite, and the Hell Canyon monzogranite, Donald granodiorite, Climax Gulch granodiorite, Moose Creek monzogranite, and Moosetown monzogranite) were defined as those having higher $Na_2O$ and lower $K_2O$ contents than plutons of main series (Butte Granite, Unionville Granodiorite, and granophyric intrusions); assignment of the Burton Park granodiorite, the Camp Thunderbird monzogranite, and the Colorado Gulch granodiorite to the appropriate magma series was uncertain (Tilling, 1973). Data compiled by du Bray and others (2009) affirm that, at any given silica content, the Rader Creek Granodiorite is more sodic than other Boulder batholith

**Table 3.** Average chemical compositions for plutons of the Boulder batholith, southwest Montana, arranged in order of increasing silica content.

[n=, number of samples upon which major oxide averages are based. Major oxides, in weight percent, recalculated to 100 percent, volatile free. F and Cl abundances in weight percent. All trace element abundances in parts per million. Blank fields constitute no data]

| | Burton Park | Union-ville | Rader Creek | Camp Thunder-bird | Butte | Colorado Gulch | Climax Gulch | Home-stake | Pulpit Rock | Hell Canyon | Donald | Moose-town | Moose Creek | Deer Creek | Grano-phyre |
|---|---|---|---|---|---|---|---|---|---|---|---|---|---|---|---|
| n= | 9 | 9 | 100 | 6 | 86 | 4 | 43 | 4 | 2 | 13 | 29 | 3 | 8 | 2 | 24 |
| $SiO_2$ | 61.35 | 61.60 | 65.13 | 65.32 | 66.02 | 68.72 | 68.44 | 69.49 | 69.56 | 69.74 | 71.46 | 72.24 | 73.16 | 74.67 | 75.29 |
| $TiO_2$ | 0.74 | 0.71 | 0.47 | 0.55 | 0.57 | 0.41 | 0.43 | 0.42 | 0.36 | 0.33 | 0.29 | 0.23 | 0.20 | 0.19 | 0.19 |
| $Al_2O_3$ | 15.84 | 15.30 | 16.13 | 16.66 | 15.59 | 15.55 | 15.53 | 14.75 | 14.98 | 15.80 | 14.84 | 15.16 | 14.99 | 14.05 | 13.64 |
| FeO* | 6.79 | 6.08 | 4.68 | 4.18 | 4.40 | 3.12 | 3.41 | 2.91 | 3.09 | 2.76 | 2.76 | 1.92 | 1.81 | 1.08 | 1.09 |
| MnO | 0.14 | 0.12 | 0.11 | 0.11 | 0.10 | 0.07 | 0.08 | 0.08 | 0.08 | 0.09 | 0.07 | 0.07 | 0.09 | 0.04 | 0.03 |
| MgO | 3.23 | 3.35 | 1.99 | 1.74 | 2.06 | 1.06 | 1.55 | 1.68 | 1.18 | 0.95 | 0.84 | 0.71 | 0.51 | 0.62 | 0.44 |
| CaO | 5.57 | 5.86 | 4.60 | 3.90 | 3.85 | 2.84 | 3.39 | 3.22 | 3.13 | 3.17 | 2.54 | 2.10 | 1.62 | 1.19 | 1.23 |
| $Na_2O$ | 2.88 | 2.86 | 3.65 | 3.51 | 3.05 | 3.46 | 3.19 | 2.87 | 3.13 | 3.62 | 3.65 | 3.70 | 4.01 | 3.54 | 3.20 |
| $K_2O$ | 3.21 | 3.81 | 3.01 | 3.76 | 4.16 | 4.58 | 3.81 | 4.42 | 4.25 | 3.39 | 3.39 | 3.77 | 3.51 | 4.47 | 4.82 |
| $P_2O_5$ | 0.25 | 0.31 | 0.23 | 0.27 | 0.20 | 0.19 | 0.17 | 0.16 | 0.24 | 0.15 | 0.16 | 0.10 | 0.10 | 0.15 | 0.07 |
| vol sum | 0.76 | 0.77 | 0.64 | 0.77 | 0.90 | 0.79 | 0.44 | 0.80 | 0.76 | 0.63 | 0.48 | 0.39 | 0.51 | 0.46 | 0.54 |
| F | | | 0.06 | | | | 0.10 | | | 0.05 | 0.05 | | 0.04 | | 0.06 |
| Cl | | | 0.02 | | | | 0.02 | | | 0.01 | 0.01 | | 0.03 | | 0.01 |
| Ba | | | 1,101 | 1,002 | 746 | 792 | 845 | 609 | | 1,212 | 1,197 | 750 | 1,167 | 739 | |
| Rb | | | 184 | 126 | 148 | | 297 | 171 | | 173 | 245 | 118 | 152 | 144 | |
| Sr | | | 745 | 601 | 426 | | 538 | 371 | | 543 | 527 | 387 | 286 | 240 | |
| Th | 11.6 | 20.6 | 21.7 | 13.0 | 18.3 | | 54.3 | 23.1 | | 44.3 | 34.5 | 21.3 | 24.0 | 14.4 | 29.1 |
| U | 3.50 | 5.04 | 2.24 | 2.70 | 4.57 | | 5.80 | 5.29 | | 3.41 | 3.28 | | 2.28 | 2.34 | 5.19 |
| Co | | | 29 | 8 | | | 22 | 30 | | 100 | 25 | | 12 | | |
| Ni | 45 | | 33 | | | | 30 | 27 | | 16 | 18 | 15 | 11 | | |
| V | | | 63 | 74 | | | 85 | | | 69 | 39 | | 51 | | |

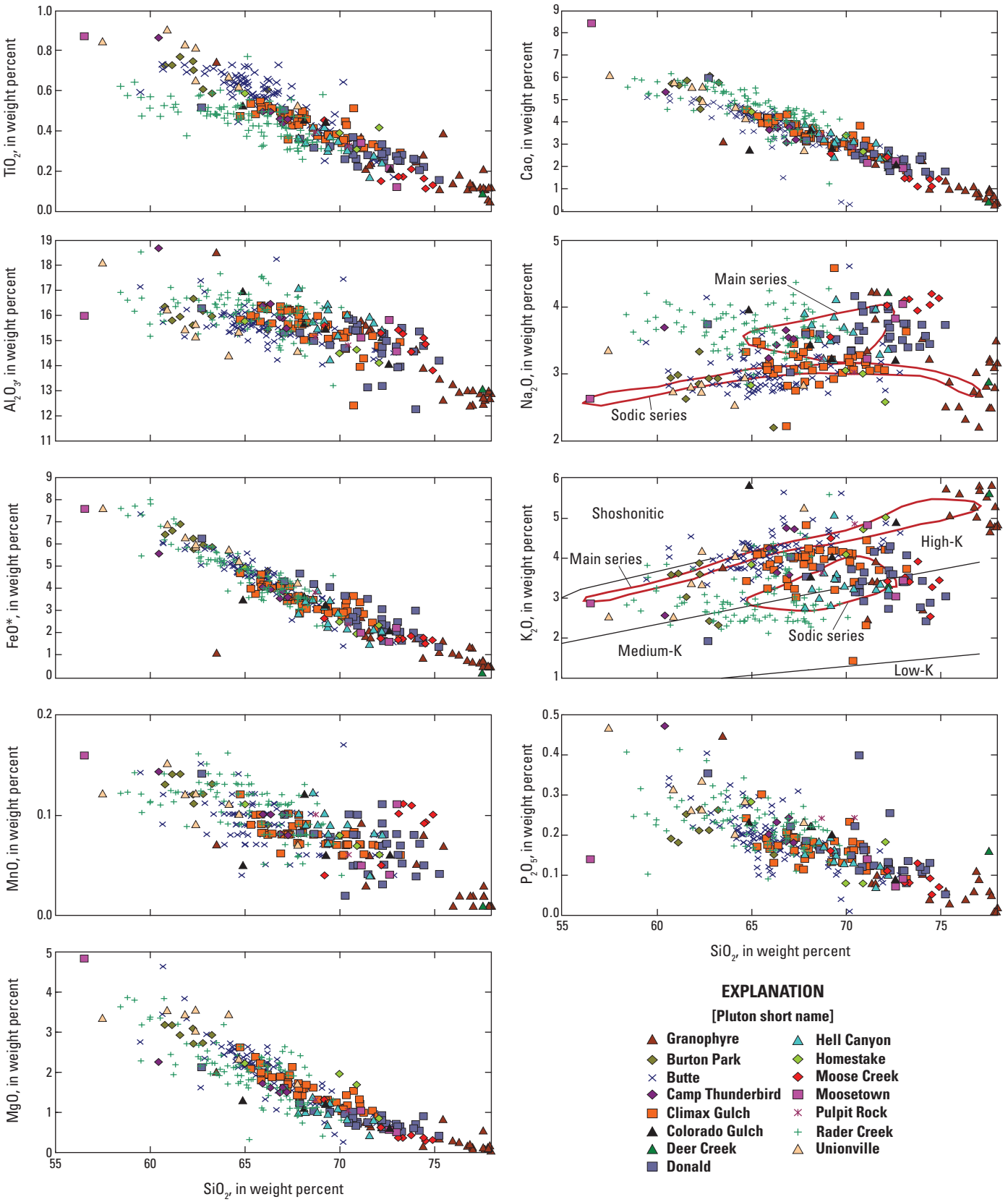


**Figure 4.** Variation diagrams showing major oxide abundances, in weight percent, in samples of the Boulder batholith, southwest Montana. Black field boundaries on $K_2O$ versus $SiO_2$ diagram from Le Maitre and others (1989); high K-shoshonite dividing line from Ewart (1982). Red field boundaries on $K_2O$ versus $SiO_2$ and $Na_2O$ versus $SiO_2$ diagrams from Tilling (1973).

intrusions, and indicate, in particular, that Na/K ratios for Rader Creek Granodiorite samples are distinctly elevated relative to all other batholith samples. Other plutons included in Tilling's sodic series contain more $Na_2O$ and less $K_2O$ than main series intrusions but simply define compositional continua from main series intrusion compositions toward those characteristic of the compositionally distinct Rader Creek Granodiorite. $Na_2O$ and $K_2O$ contents of the Rader Creek Granodiorite are distinct relative to those of other Boulder batholith rocks but the existence of separate sodic and main magma series within the batholith is not convincingly demonstrated by available major oxide data.

Among the Boulder batholith rocks, concentrations of $TiO_2$, $Al_2O_3$, FeO*, MnO, MgO, CaO, and $P_2O_5$ decrease systematically with increasing $SiO_2$, whereas $K_2O$ contents increase with increasing $SiO_2$; $Na_2O$ contents display no consistent relation with $SiO_2$ content. Average Na/K is 1.0 but ranges from 0.4 to 1.7; as a group, samples of the Rader Creek Granodiorite are distinctly sodic whereas samples of the Butte Granite are distinctly potassic. Relative amounts of $K_2O$ and $SiO_2$ in most Boulder batholith rocks (fig. 4) are coincident with high- to medium-K compositions defined by Gill (1981) and Le Maitre (1989).

Volatile contents of the Boulder batholith rocks are generally similar to those characteristic of granitoid rocks. The majority of the Boulder batholith rocks contain less than 700 parts per million (ppm) F, which is consistent with average (500–900 ppm) F contents of granitoid rocks (Turekian and Wedepohl, 1961). However, a group of about 20 samples of the Climax Gulch granodiorite contain distinctly elevated F abundances that range from about 900 ppm to almost 1,700 ppm. Average Cl contents of granitoid rocks range from about 100 to 200 ppm (Turekian and Wedepohl, 1961), and most Boulder batholith rocks have Cl abundances in this range. A few samples of the Rader Creek Granodiorite, Climax Gulch and Donald granodiorites, and Moose Creek and Hell Canyon monzogranites have Cl abundances in the 200–550 ppm range.

Major oxide compositions of the Boulder batholith are similar to those of subduction-related igneous rocks. Relative to standard metrics, they are subalkaline (Irvine and Baragar, 1971), magnesian (Frost and others, 2001), calc-alkalic to calcic (Frost and others, 2001; Miyashiro, 1974), and metaluminous to weakly peraluminous (Shand, 1951). On variation diagrams (figs. 5–8) associated with these metrics, each of the Boulder batholith plutons forms a relatively coherent compositional cluster or array; however, compositions of the various plutons are broadly overlapping.

# Trace Element Data

Trace element abundances (du Bray and others, 2009) for the plutons of the Boulder batholith form clusters that are broadly diagnostic of their constituent plutons. The Climax Gulch and Donald granodiorites and the Hell Canyon monzogranite are distinctly enriched in incompatible trace elements (table 3). Distinctive trace element features (absolute, unless otherwise indicated) of the Boulder batholith plutons are as follows:

## Mafic Group

Burton Park granodiorite: elevated Cu, Ni, Pb (relative), Sc, Y, Zn, Zr, and low Th
Unionville Granodiorite: elevated Ni, Sc, U, Zn, and low Sr
Rader Creek Granodiorite: elevated Ba, Ni, Sr, low U, and low V and Th (relative)

## Intermediate Group

Butte Granite: elevated Cu, Sc, U, Y (relative), Zr, Zn, low Ba, Pb, and Sr
Climax Gulch granodiorite: elevated F, Rb, Th, V, Zn, and low Cu
Donald granodiorite: elevated Ba, Pb, Rb, Th, and low Ni and V
Camp Thunderbird monzogranite: elevated Zn
Hell Canyon monzogranite: elevated Co, Mo, and Th
Homestake monzogranite: low Ba
Moose Creek monzogranite: low Ni and Sr
Moosetown monzogranite: elevated Zn
Colorado Gulch granodiorite: no distinctive characteristics
Pulpit Rock monzogranite: low Co and Pb

## Felsic Group

Deer Creek granophyre: low Co, Cr, Sc, and Zn
Granophyric intrusions: low Sr and Zn

Large-ion lithophile element (LILE) and high-field-strength element (HFSE) abundances for Boulder batholith samples are similar to those of convergent-margin, broadly calc-alkaline, subduction-related igneous rocks such as in the Andean, Kamchatka, and Central American arcs (GEOROC, 2007). Tectonic classification schemes based on relative trace element abundances, including Rb versus Y + Nb of Pearce and others (1984), are consistent with plutons of the Boulder batholith having an origin in a subduction-related magmatic arc environment (fig. 9). Magma genesis in this type of tectonic setting is further indicated by incompatible trace element ratios. Wood and others (1979) and Gill (1981) established that Ba/Ta, Ba/Nb, and La/Nb ratios for modern arc rocks are greater than 450, greater than 26, and 2–7, respectively. Average Ba/Ta, Ba/Nb, and La/Nb for all Boulder batholith samples are 793, 50, and 2.4, respectively (du Bray and others, 2009). Insufficient trace element data are available to determine whether individual Boulder batholith plutons have distinctive ranges of values for each of these trace element parameters.

Relative abundances of K, Rb, and Sr in samples of most Boulder batholith plutons form broadly diagnostic

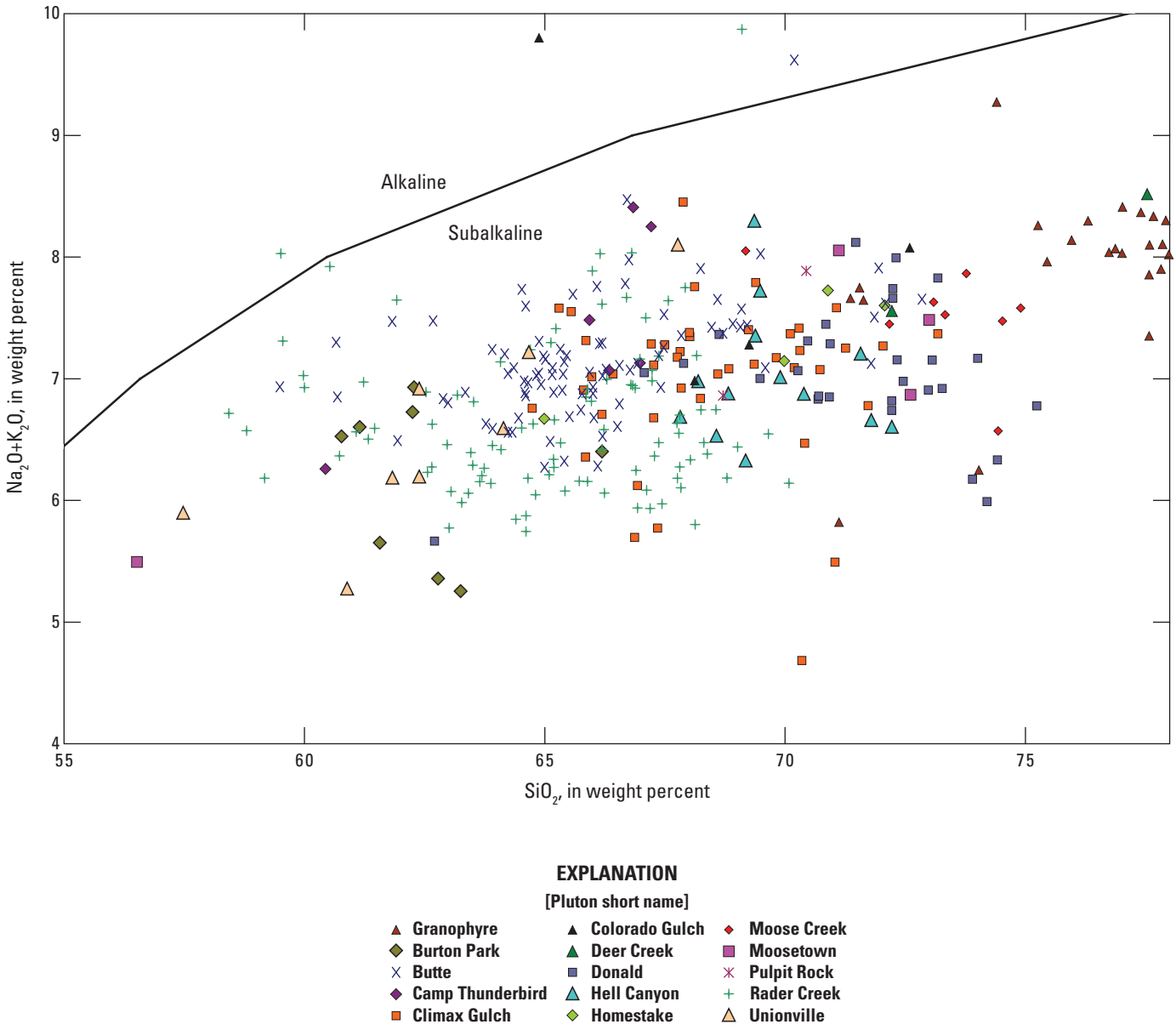


**Figure 5.** Total alkali-silica variation diagram showing compositions of the Boulder batholith, southwest Montana. Alkaline and subalkaline fields defined by Irvine and Baragar (1971).

compositional clusters (fig. 10) and have relatively Sr-enriched compositions; Rader Creek Granodiorite samples, in particular, are strongly Sr-enriched (fig. 10). Samples of the Moose Creek and Homestake monzogranites and of granophyre have progressively K- and Rb-enriched compositions; a sample of the Deer Creek granophyre has the most evolved composition of any Boulder batholith sample.

As summarized by John and others (2010), genesis of porphyry copper deposits has been linked with adakites, magmatic arc rocks with unique geochemical compositions whose genesis may have involved components derived from subducted slab partial melting. Richards and Kerrich (2007) summarize the geochemistry of these rocks and suggest that among other characteristics, Sr/Y greater than or equal to 20, Y less than or equal to 18 ppm, $SiO_2$ greater than or equal to 56 percent, Yb less than or equal to 1.9 ppm, Ni greater than or equal to 20 ppm, Cr greater than or equal to 30 ppm, and La/Yb greater than or equal to 20 are diagnostic of adakites. Most of the analyzed Boulder batholith rocks do have Sr/Y greater than or equal to 20 and $SiO_2$ greater than or equal to 56 percent, but data for the few Boulder batholith samples for which La/Yb and abundances of Y, Yb, Ni, and Cr have been determined are only marginally similar to those diagnostic of adakites.

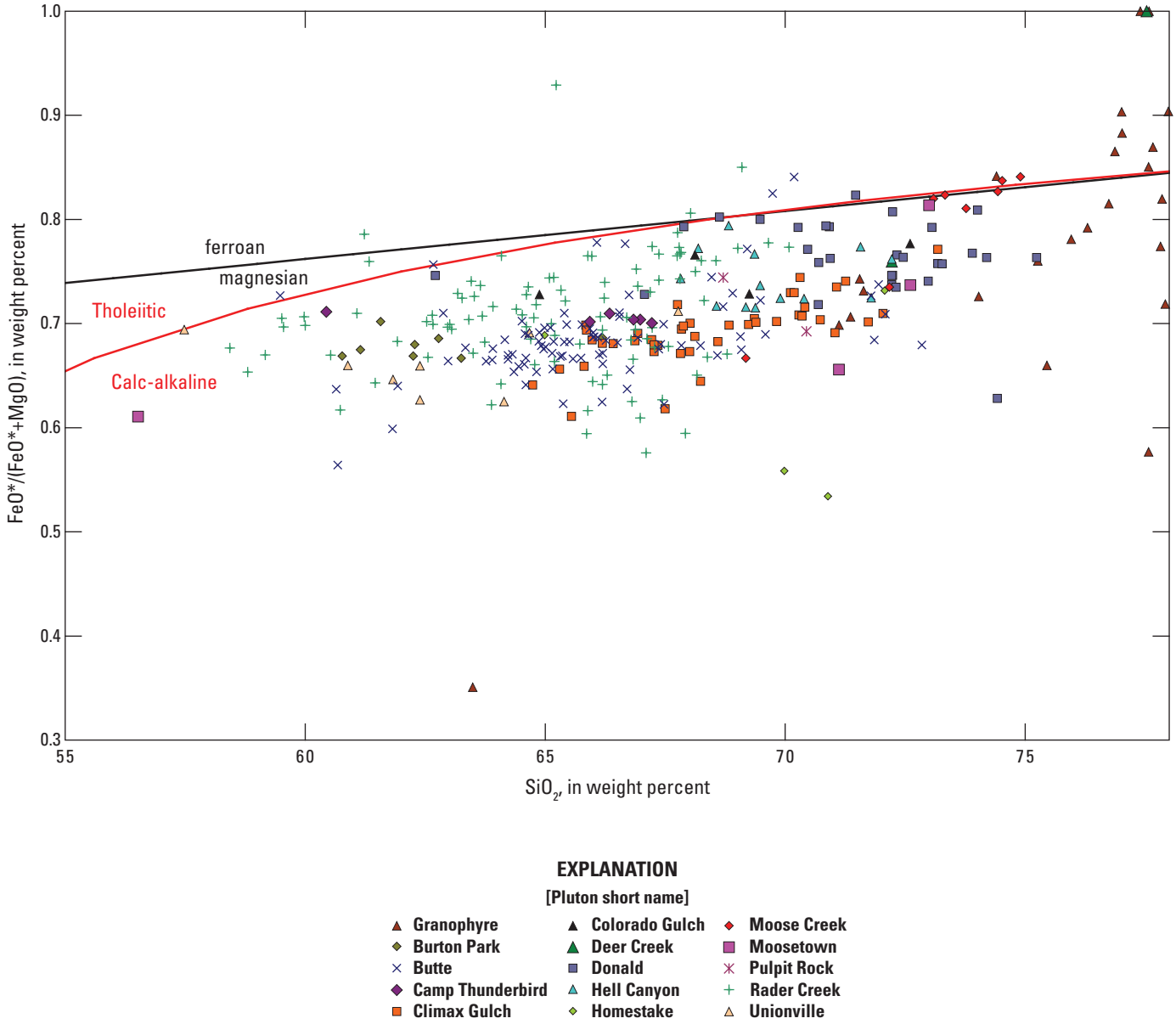


**Figure 6.** FeO*/(FeO*+MgO) versus $SiO_2$ variation diagram showing the compositions of the Boulder batholith, southwest Montana. FeO*, total iron expressed as ferrous iron. Ferroan versus magnesian boundary (black line) from Frost and others (2001); tholeiitic versus calc-alkaline boundary (red line) from Miyashiro (1974).

Abundances of most trace elements in Boulder batholith rocks are only weakly correlated with $SiO_2$ abundance variations. Among all Boulder batholith samples for which trace element data are available, Cr, Cu, Ni, Sc, Zn, and Zr contents decrease (somewhat inconsistently for some of these elements) with increasing $SiO_2$, whereas Pb concentrations increase somewhat inconsistently with increasing $SiO_2$ content (du Bray and others, 2009). The lack of additional and better correlated relations between trace element concentrations and variable silica content is uncharacteristic of igneous rock geochemical variation patterns and shows a lack of accuracy and(or) precision of trace element data for samples (analyzed by a variety of techniques) included in the Boulder batholith geochemical compilation. However, the compilation of du Bray and others (2009) includes high quality data for a group of 23 samples analyzed by modern techniques (with good associated accuracy and precision). These samples include five samples with "02HW" as first four characters of their sample designation, 17 samples with "KL" as the third and fourth characters of their sample designation,

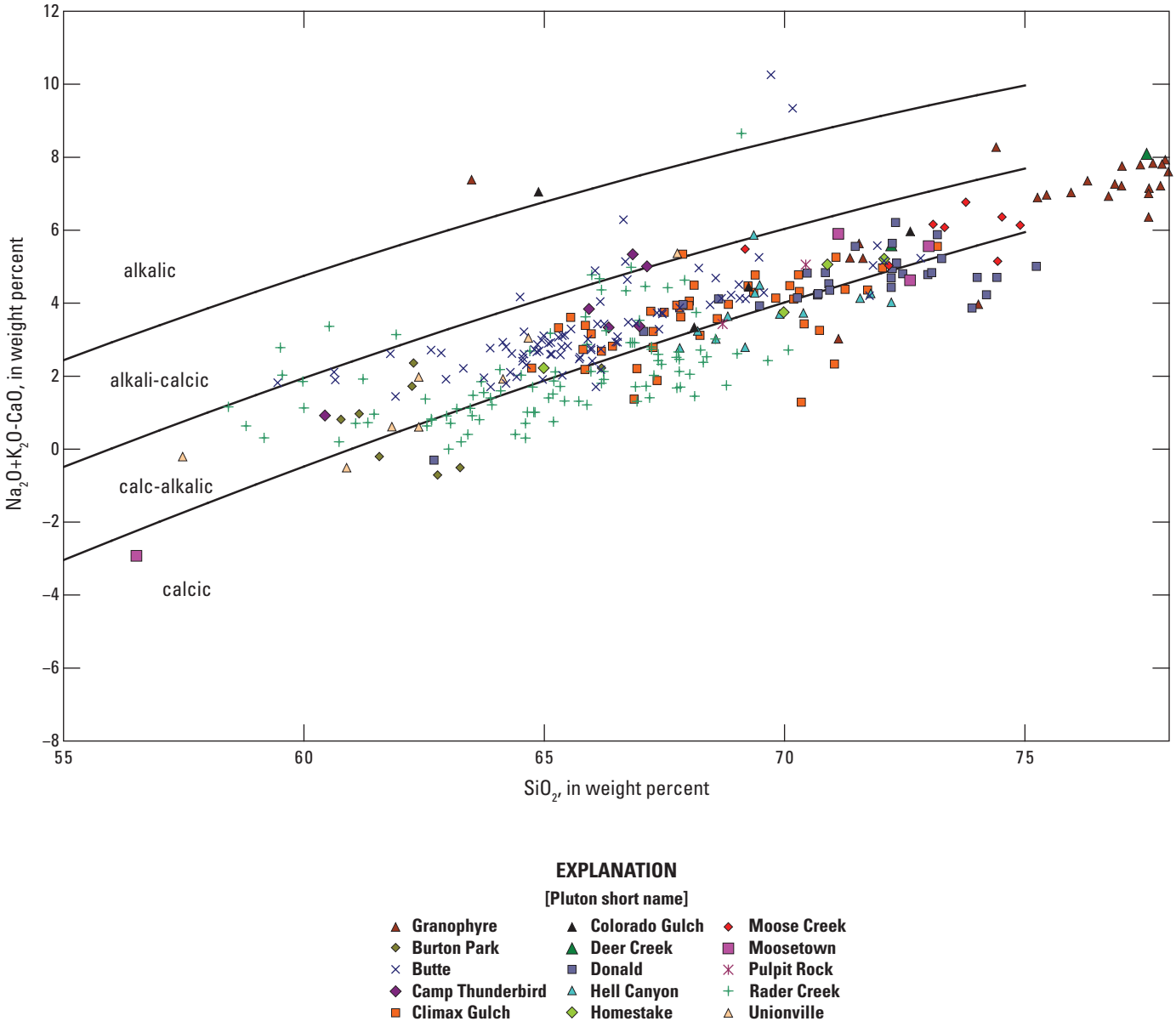


**Figure 7.** $Na_2O+K_2O$-CaO versus $SiO_2$ variation diagram showing the compositions of the Boulder batholith, southwest Montana. Boundaries between various rock series from Frost and others (2001).

and the sample with the identifier "Macdonald." Samples in this subset of the compilation have Ba, Pb, Nb, and Rb contents that increase with $SiO_2$ and contents of Cs, Co, Cu, Cr, Ga, Sc, V, Y, Zn, and Zr that decrease with increasing $SiO_2$. With the exception of Co, Ga, Nb, Sc, Th, V, and Zn, these covariation arrays are somewhat inconsistent. Even among more well-correlated abundance variations, many of the concentration increases or decreases are of moderate relative magnitude ([highest concentration-lowest concentration]/highest concentration ): Ba (+56 percent), Pb (+67 percent), Nb (+63 percent), and Rb (+64 percent); Cs (–60 percent), Co (–95 percent), Cu (–81 percent), Cr (–96 percent), Ga (–28 percent), Sc (–82 percent), V (–89 percent), Y (–62 percent), Zn (–76 percent), and Zr (–86 percent).

The limited amount of ore metal abundance data (specifically for Cu, Mo, Pb, and Zn) available for unmineralized Boulder batholith samples (du Bray and others, 2009) are comparable to ore metal global average abundances (Turekian and Wedepohl, 1961) in basalt (100, 1, 5, and 100 parts per million, respectively) and granite (10, 2, 20, and 40 parts per million,

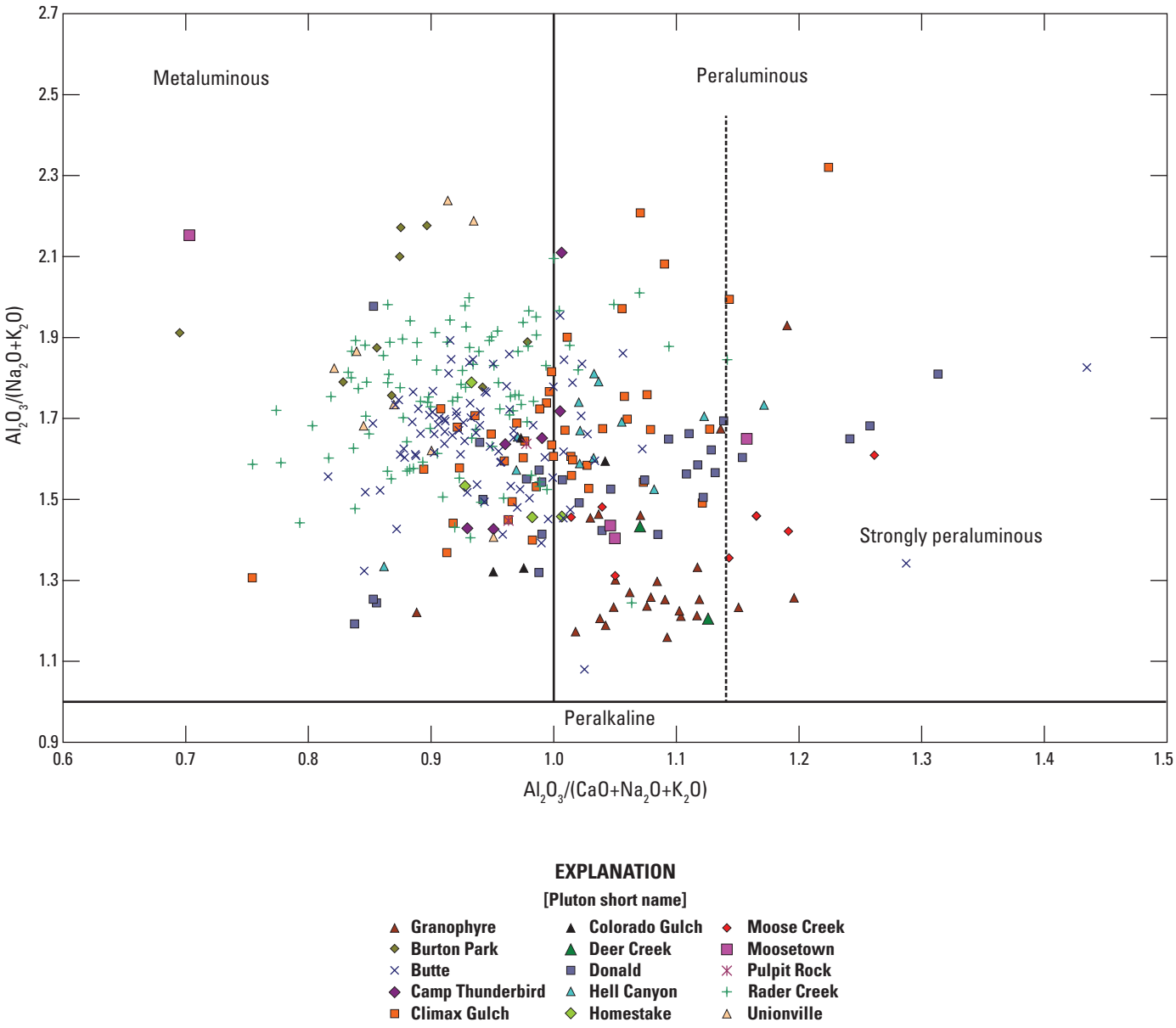


**Figure 8.** Variation diagram showing molar major oxide compositions the Boulder batholith, southwest Montana as a function of alumina and alkali saturation.

respectively). Copper concentrations in Boulder batholith rocks range from several parts per million (ppm) to about 45 ppm (average approximately 17 ppm). Molybdenum concentrations range from less than 1 to 20 ppm (average approximately 8 ppm). Lead concentrations range from about 4 to 36 ppm (average approximately 21 ppm). Zinc concentrations range from about 7 to 69 ppm (average approximately 61 ppm). Consequently, with the exception of Mo, abundances of the Cu, Mo, Pb, and Zn in Boulder batholith rocks are not significantly elevated relative to ordinary igneous rocks. The majority of the Mo concentrations available for Boulder batholith rocks reflect analyses conducted more than 30 years ago by undocumented methods (du Bray and others, 2009) and are of uncertain accuracy and precision. With two exceptions, the group of about 23 recent, high quality analyses (described in the preceding paragraph) contain less than 2 ppm Mo; one additional sample contains 3 ppm Mo and a sample bearing visible molybdenite in miarolitic cavities (Deer Creek granophyre) contains 156 ppm Mo. Consequently, although polymetallic quartz vein deposits are approximately coeval with the younger plutons

and are hosted by the batholith (Lund, 2007; Lund and others, 2002), unmineralized Boulder batholith magmas do not contain elevated abundances of the metals (Cu, Mo, Pb, and Zn) that are significant constituents of those deposits.

Accurate and precise rare earth element (REE) data available for Boulder batholith samples are restricted to the representative set of 23 samples (described two paragraphs previously). Chondrite-normalized REE patterns for Boulder batholith rocks (fig. 11) are typical of intermediate composition, calc-alkaline subduction-related igneous rocks (for example, Cameron and Cameron, 1985; Feeley and Davidson, 1994; Gill, 1981; Wark, 1991). Boulder batholith REE patterns have negative slopes and most have insignificant to small negative europium anomalies although the Rader Creek Granodiorite (Eu/Eu* = 1.09), Donald granodiorite (Eu/Eu* = 1.18), and Hell Canyon monzogranite (Eu/Eu* = 1.28) have small, unusual positive Eu anomalies consistent with plagioclase accumulation. Eu/Eu* ranges from 0.69 to 1.28 (average, 0.87) and the magnitude of Eu anomalies is unrelated to $SiO_2$ content. Among Boulder batholith samples, those with the highest $SiO_2$ content have slightly low total REE contents and slightly clockwise-rotated REE patterns (relatively higher light [LREE] and lower heavy REE [HREE] concentrations). Overall, LREE pattern segments are somewhat more steeply sloping than HREE segments, which are flat to slightly U-shaped.

With several exceptions, REE abundances (fig. 11) in Boulder batholith pluton samples vary within a relatively restricted range, yield calculated negative europium anomalies of similar magnitude, and define REE patterns that are essentially parallel ($La_N/Yb_N$ values vary minimally). In particular, REE abundance patterns for seven Butte Granite samples (representative of the full Butte Granite age array) are indistinguishable within the limits of analytical uncertainty. Presuming that these samples are representative of the entire Butte Granite pluton, they show that the composition of this large intrusive is remarkably homogeneous. In contrast, the LREE content of the Homestake monzogranite is low relative to other Boulder batholith rocks. REE patterns for the Donald granodiorite, Hell Canyon monzogranite, and Deer Creek granophyre are somewhat distinctive. All three plutons are distinguished by atypically low HREE abundances; HREE abundances for the Homestake monzogranite are similarly low. These samples also have the three lowest Eu contents among the Boulder batholith samples; Eu for the Deer Creek sample, in particular, is dramatically lower than that of any other Boulder batholith rock. Finally, the Deer Creek granophyre and Hell Canyon monzogranite, and to a lesser extent, the Donald granodiorite have unusually low LREE contents that are distinct relative to all other Boulder batholith rocks.

Primitive mantle-normalized trace element patterns for Boulder batholith plutons are gently negatively sloping, having high large-ion lithophile element (LILE) abundances and low high-field-strength element (HFSE) abundances common among moderately differentiated subduction-related magmas (fig. 12). These patterns depict systematic but relatively limited geochemical variation among Boulder batholith plutons; patterns for seven Butte Granite samples are essentially parallel, clustered, and represent consistent reservoir-wide petrogenetic processes. Large negative Nb-Ta anomalies, similar to those characteristic of subduction-related magmatism (Wood and others, 1979; Gill, 1981; Pearce and others, 1984), are also characteristic of Boulder batholith samples.

The three most mafic Boulder batholith plutons and all but the Deer Creek granophyre and Hell Canyon monzogranite have primitive mantle-normalized patterns that are essentially indistinguishable. The Deer Creek granophyre and Hell Canyon monzogranite define distinctive primitive mantle-normalized patterns that have almost uniformly low trace element (and as described above, particularly REE) abundances; the Homestake monzogranite exhibits some of these same characteristics.

Tilling (1973) and Lambe (1981) showed that Sr abundances are high and Rb abundances low in sodic series rocks relative to main series rocks; Tilling (1973) and Lambe (1981) also show that concentrations of Ba, Nb, Cu, Th, and U are distinct for samples of the two magma series. The compilation of du Bray and others (2009) indicates that among the well-analyzed Boulder batholith samples, Sr and Ba concentrations are distinctly elevated in Rader Creek Granodiorite samples whereas Rb, Th, and U contents are low relative to other Boulder batholith rocks. In addition, Y, Cs, Zr, Hf, and REE (especially HREE) contents are slightly lower in the Tilling (1973) sodic series rocks than in main series rocks. However, the geochemistry of plutons previously interpreted as part of the sodic series is otherwise not statistically distinct relative to that of other Boulder batholith rocks. As earlier inferred from major oxide data, the Rader Creek Granodiorite has some distinctive compositional attributes but trace element data do not indicate a definitive geochemical distinction between plutons previously designated as constituents of the sodic and main magma series.

# U-Pb Zircon Geochronology

Previously, Lund and others (2002) published ages of four plutons (Rader Creek, Unionville, Butte Granite, and Pulpit Rock) of the Boulder batholith. This study presents new data and ages for an additional 12 plutons and a sample of granophyre, all associated with the batholith (fig. 13, table 4). In addition, zircons from each of the previously dated plutons (Lund and others, 2002) were reanalyzed to produce an internally consistent dataset.

## Methods

Rock samples were collected from outcrops throughout the Boulder batholith and zircons were extracted from these samples using standard mineral separation techniques of crushing, pulverizing, Wilfley table, Frantz magnetic

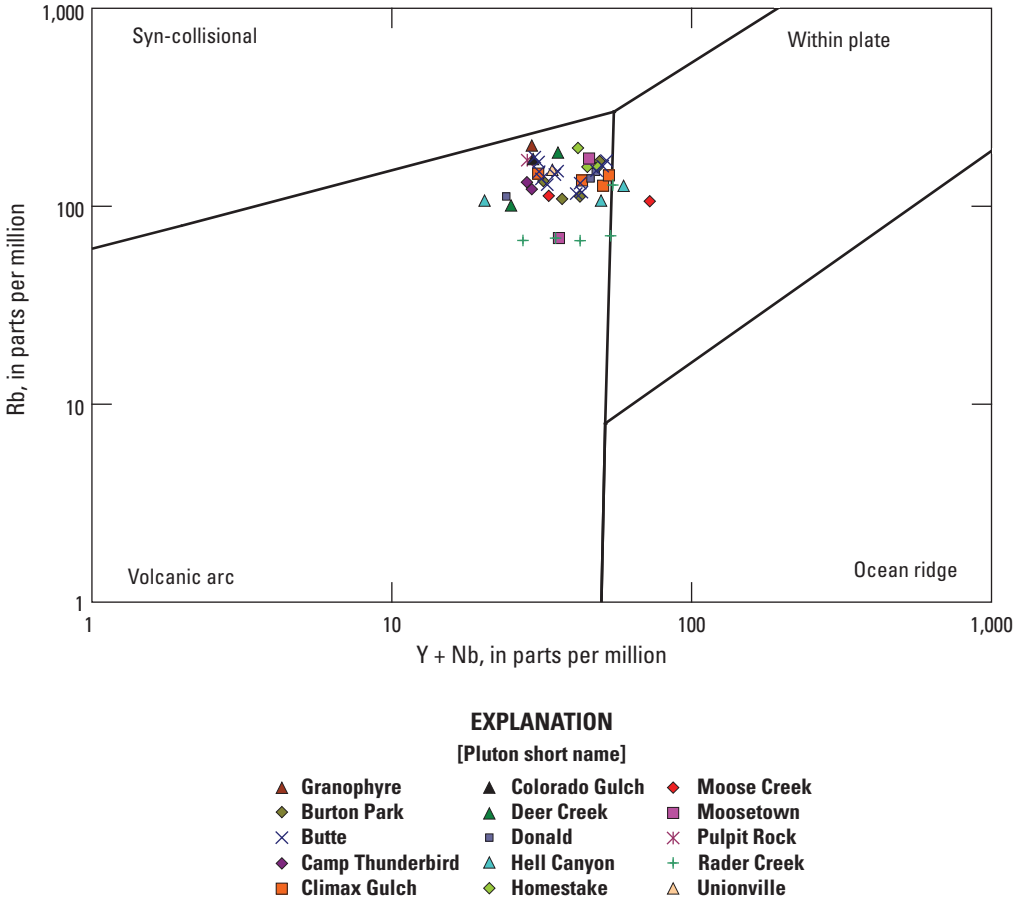


**Figure 9.** Trace-element, tectonic-setting-discrimination variation diagram showing the composition of samples of the Boulder batholith and its peripheral plutons, southwest Montana. Tectonic setting-composition boundaries from Pearce and others (1984).

separator, and Methylene Iodide. Grains were handpicked onto double-stick tape, cast in epoxy, ground to about half thickness, and polished with 6 micrometers (µm) and 1µm diamond suspension.

All grains were imaged in reflected and transmitted light on a petrographic microscope and in cathodoluminescence (CL) on the USGS-Denver JEOL 5800LV scanning electron microscope (fig. 13). These images were used as guides for the location of ion microprobe analysis spots. U-Pb geochronologic analyses (table 4) were made using the USGS/Stanford University sensitive high resolution ion microprobe-reverse geometry (SHRIMP-RG) instrument. The primary ion beam was focused to extract material from a pit about 25–30 µm in diameter. Mass stations were cycled through five iterations per analysis. $^{206}Pb/^{238}U$ ratios were calibrated against zircon standard R33 (419 Ma; Black and others, 2004). Raw data were reduced using SQUID (Ludwig, 2001); results are shown on Tera-Wasserburg concordia plots and weighted averages plots created using Isoplot 3 (Ludwig, 2003). Concordia plots were used to assess which analyses should be included in the age calculations; the weighted average of selected $^{206}Pb/^{238}U$ ages was used to determine the age of each sample (fig. 13).

The primary focus of the geochronologic analyses was to determine Boulder batholith pluton crystallization ages; zircon grains and spots selected for analysis were chosen accordingly. Only pristine (and in most cases, homogeneous) grains were selected for SHRIMP analysis. Results for all dated plutons are summarized in table 5.

## Results

All sampled plutons yielded elongate, colorless, euhedral zircons with various degrees of oscillatory zoning indicative of crystallization in a magma. Most of these zircons have modest U concentrations (about 100–500 ppm) and low common Pb content. All of the dated grains from the plutons yielded concordant U-Pb data. In contrast, zircons from sample 03KL071 (granophyre of Deer Creek) are dark to opaque, equant to

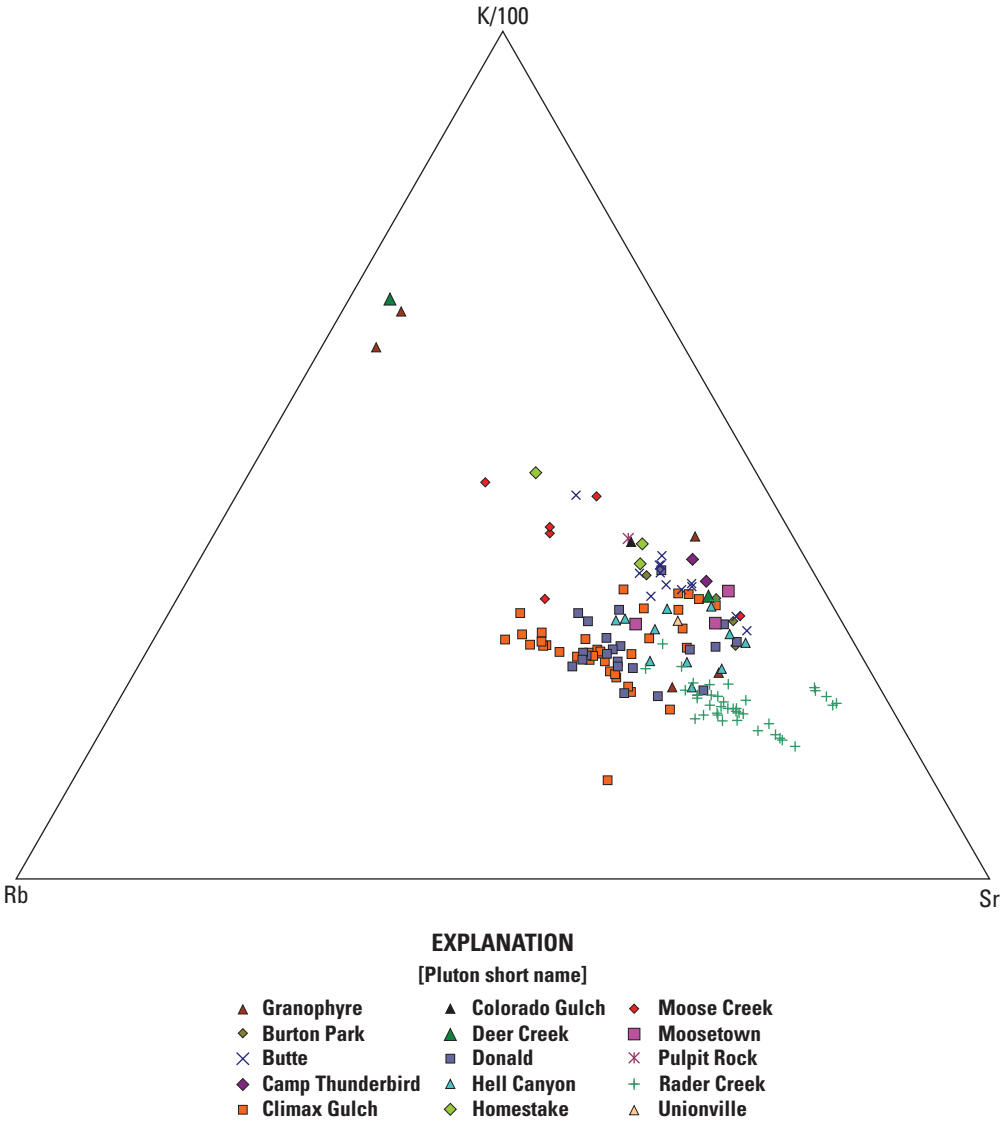


**Figure 10.** Variation diagram showing relative proportions of rubidium, potassium, and strontium in samples of the Boulder batholith and its peripheral plutons, southwest Montana.

stubby, show little or no oscillatory zoning (fig. 13), and are speckled with numerous small, irregularly distributed domains that are bright in CL images. All grains from this sample have high U (2,000–6,000) and common Pb contents (table 4). Although the six oldest grains indicate an age of about 78 Ma, four other grains are discordant (table 4). Thus, this study cannot determine a reliable age for the granophyre of Deer Creek.

SHRIMP U-Pb geochronology of zircon shows that plutons of the Boulder batholith were emplaced and solidified over a period of 6–10 m.y. (81.7 ± 1.4 to 73.7 ± 0.6 Ma; table 5). Zircons in the Rader Creek Granodiorite contain abundant Archean and Paleoproterozoic inheritance in rounded cores (Lund and others, 2002). In all other plutons, inheritance seems to be minimal, although the apparent lack of older material may reflect sampling bias. Alternatively, Boulder batholith plutons that lack inherited zircon may have followed different emplacement and temperature paths that either limited assimilation of inherited zircon or, having incorporated exotic zircon grains, caused them to be completely dissolved.

U-Pb zircon ages of most Boulder batholith plutons are correlated with intrusion composition. The three most mafic plutons (Rader Creek, Unionville, and Burton Park), whose ages range from 80.7 to 77.3 Ma, are among the oldest components of the batholith. The voluminous, intermediate composition Butte Granite was the next phase of the batholith to be emplaced (about 76.7 Ma); a second apparent pulse of Butte Granite magmatism may have occurred at about 74.7 Ma. The progressively more felsic peripheral plutons were emplaced at about 76.7 to 73.7 Ma (table 5).

## Radiogenic Isotope Data

Neodymium and strontium isotopic data were obtained for 12 representative Boulder batholith samples (table 6). Initial $^{87}Sr/^{86}Sr$ ($Sr_i$) values for most of these samples cluster between about 0.707 and 0.709 and are similar to those reported for Boulder batholith rocks by Doe and others (1968) and Foster and others (2006) and unpublished data described by Taylor and others (2007). $\varepsilon_{Nd}$ values for these samples are variable, ranging from –11.9 to –22.9. Neither $\varepsilon_{Nd}$ nor $Sr_i$ variations are well correlated with age, although the two youngest Boulder batholith samples (Moose Creek and Hell Canyon monzogranites) have distinctly more radiogenic $Sr_i$ values. Three samples of Butte Granite and one sample of Pulpit Rock monzogranite, have the highest $\varepsilon_{Nd}$ values (–11.9 to –12.1) of the analyzed Boulder batholith samples; these samples define a small range of $Sr_i$ values (0.70685 to 0.70726) that is comparable to most other Boulder batholith samples. Data for the Rader Creek Granodiorite, Donald granodiorite, and Homestake monzogranite define a second cluster having the lowest $\varepsilon_{Nd}$ values (–18.5 to –22.9); $Sr_i$ data for these samples define a narrow range from 0.70695 to 0.70702. Five plutons (Unionville Granodiorite, Burton Park and Climax Gulch granodiorites, and Moose Creek and Hell Canyon monzogranites) yielded intermediate $\varepsilon_{Nd}$ values (–14.1 to –16.4) and more radiogenic $Sr_i$ values (0.70716 to 0.70892).

As shown by Taylor and others (2007), strongly negative $\varepsilon_{Nd}$ values and relatively high $Sr_i$ values for all analyzed (table 6) samples of the Boulder batholith indicate that these rocks were derived from Precambrian crust, an interpretation supported by ubiquitous 2.4–3.4 Ga cores in zircons from the Rader Creek Granodiorite (Lund and others, 2002). Samples from other plutons include little or no inheritance; however, because the focus of geochronologic results reported here was determination of emplacement ages, not source ages, the apparent lack of inheritance may represent a sampling issue. Sr and Nd isotopic data for Boulder batholith rocks are more radiogenic than those for plutons from accreted terranes in western Idaho and eastern Oregon, from the Salmon River suture, and from most of the Big Belt Mountains plutonic rocks (figs. 1 and 14; Fleck and Criss, 1985; 2004; Fleck, 1990; Gunn, 1991; Lund, 2007; Unruh and others, 2008). $Sr_i$ values for the Boulder batholith are significantly less radiogenic than those for the Late Cretaceous Idaho batholith (to the west) but $\varepsilon_{Nd}$ values are more radiogenic; whereas, the converse is true relative to Late Cretaceous Pioneer batholith rocks (to the southwest). $Sr_i$ values for the Boulder batholith are most similar to Eocene plutons on the eastern side of the Idaho batholith (Fleck and Criss, 1985; 2004).

## Petrogenetic Implications of Geochemical and Isotopic Data

As documented above in the U-Pb zircon geochronology section, the age of the Butte Granite spans about 2 m.y. Consequently, either (1) the Butte Granite consists of 2 or more intrusive phases that solidified at different times or (2) U-Pb zircon ages of the Butte Granite depict a solidification process that spanned 2 m.y. Petrographic and geochemical characteristics of the northern and southern parts of the Butte Granite are indistinguishable. Given the diversity of petrographic and geochemical features characteristic of adjacent plutons in batholithic terranes (Bateman, 1992), it is unlikely that the Butte Granite is a composite mass composed of two fortuitously identical intrusions with regard to petrographic and geochemical characteristics. Consequently, the second hypothesis, that the Butte Granite solidified during 2 m.y., seems most consistent with geochronologic, petrographic, and geochemical attributes of these rocks.

Geochemical and isotopic data for the Boulder batholith rocks are consistent with their genesis in a subduction-related tectonic setting. Although not particularly diagnostic, major oxide abundances are similar to those of other continental magmatic arc rocks (du Bray and others, 1995; 2006; 2009). Trace element abundances are significantly more definitive in identifying the Boulder batholith magma as subduction related. In particular, relative abundances of Rb versus Y + Nb, Ba/Nb, Ba/Ta, La/Nb, and well-developed negative Nb-Ta anomalies show that all of the Boulder batholith rocks are the products of magmatic arc, subduction-related magmatism. In addition, primitive mantle-normalized trace element diagrams for Boulder batholith plutons include variably developed small negative Ba anomalies, prominent positive Pb anomalies and small to moderate negative P and Ti anomalies: each of these are similar to anomalies characteristic of intermediate composition, subduction-related, MASH-zone (Hildreth and Moorbath (1988) magmas that evolved by separation from restite during partial melting and(or) moderate fractionation of early crystallized minerals.

Down-going slab dehydration and attendant volatile-induced flux melting of lithospheric mantle beneath the western edge of the North American continent likely fostered the ascent of relatively mafic magmas into the lower crust. On the basis of radiogenic isotopic data, Foster and others (2006) suggest that the Paleoproterozoic basement, which underlies most of the Boulder batholith, was a fertile crustal source for partial melt generation. Mantle-derived, subduction-related partial melts may themselves have initiated additional partial melting of material included in the basement terrane, and mixed with those magmas to produce more voluminous, felsic

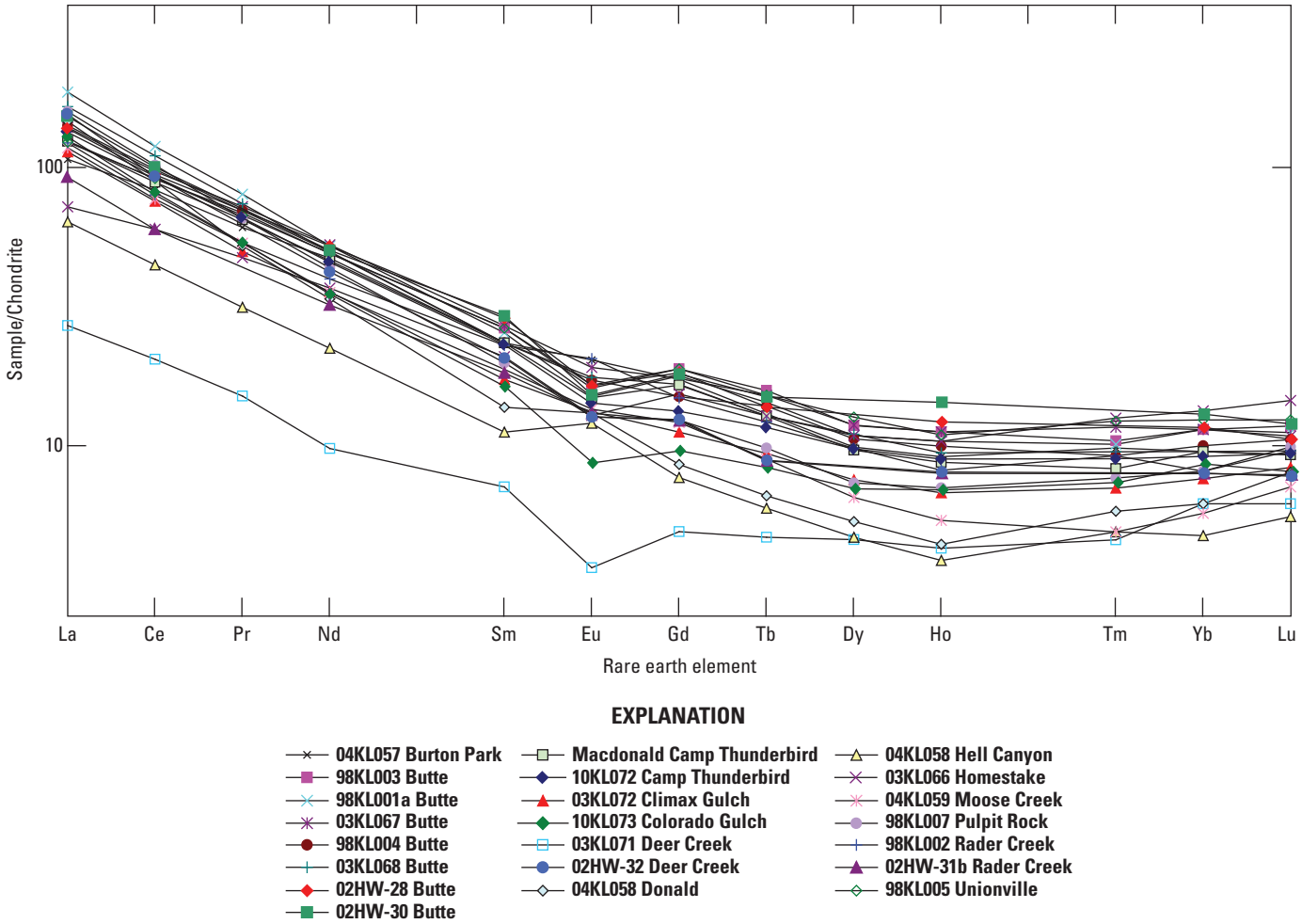


**Figure 11.** Chondrite-normalized rare-earth element diagrams for Boulder batholith samples; chondrite abundances from Anders and Ebiharra (1982).

magmas such as those represented by the Boulder batholith. The presence of magmatic arc rocks well inboard from the western, subduction-zone delimited margin of western North America in the Late Cretaceous is consistent with low angle subduction (Coney and Reynolds, 1977; Lipman, 1992) and inboard deflection of the critical depth required for genesis of subduction-related magmas. Subsequently, as the convergence rate decreased, the subduction zone steepened and the hinge-line of the down-going oceanic slab (and subduction-related magmatism) retreated westward (Coney and Reynolds, 1977; Lipman, 1992).

Distinct isotopic compositions within constituent plutons of the Boulder batholith probably represent different proportions of mafic, mantle-derived magma and crustally-derived partial melts. $Sr_i$ and $\varepsilon_{Nd}$ isotopic variation preserved in the Boulder batholith rocks may also indicate isotopic inhomogeneities in the underlying continental basement that mixed with upwardly buoyant, mantle-derived mafic magma. Magmatism responsible for the Climax Gulch granodiorite and the Moose Creek and Hell Canyon monzogranites involved a component that was elevated with respect to radiogenic Sr, whereas that responsible for Butte granite and Pulpit Rock monzogranite was more primitive with regard to $\varepsilon_{Nd}$ than other Boulder batholith rocks and that responsible for the Donald granodiorite involved a source with elevated $\varepsilon_{Nd}$.

Trace element abundances of Boulder batholith rocks show that the associated magmas experienced limited differentiation. In evolving magmatic systems affected by plagioclase separation, melt compositions become relatively Sr depleted and K enriched, and in the case of advanced fractionation, Rb enriched, with differentiation (Hanson, 1980). Relative abundances of K, Rb, and Sr in these rocks are dominated by Sr, which is consistent with minimal differentiation involving plagioclase fractionation (fig. 10). REE data for the Boulder batholith rocks are also consistent with limited magma differentiation. These rocks have minimal

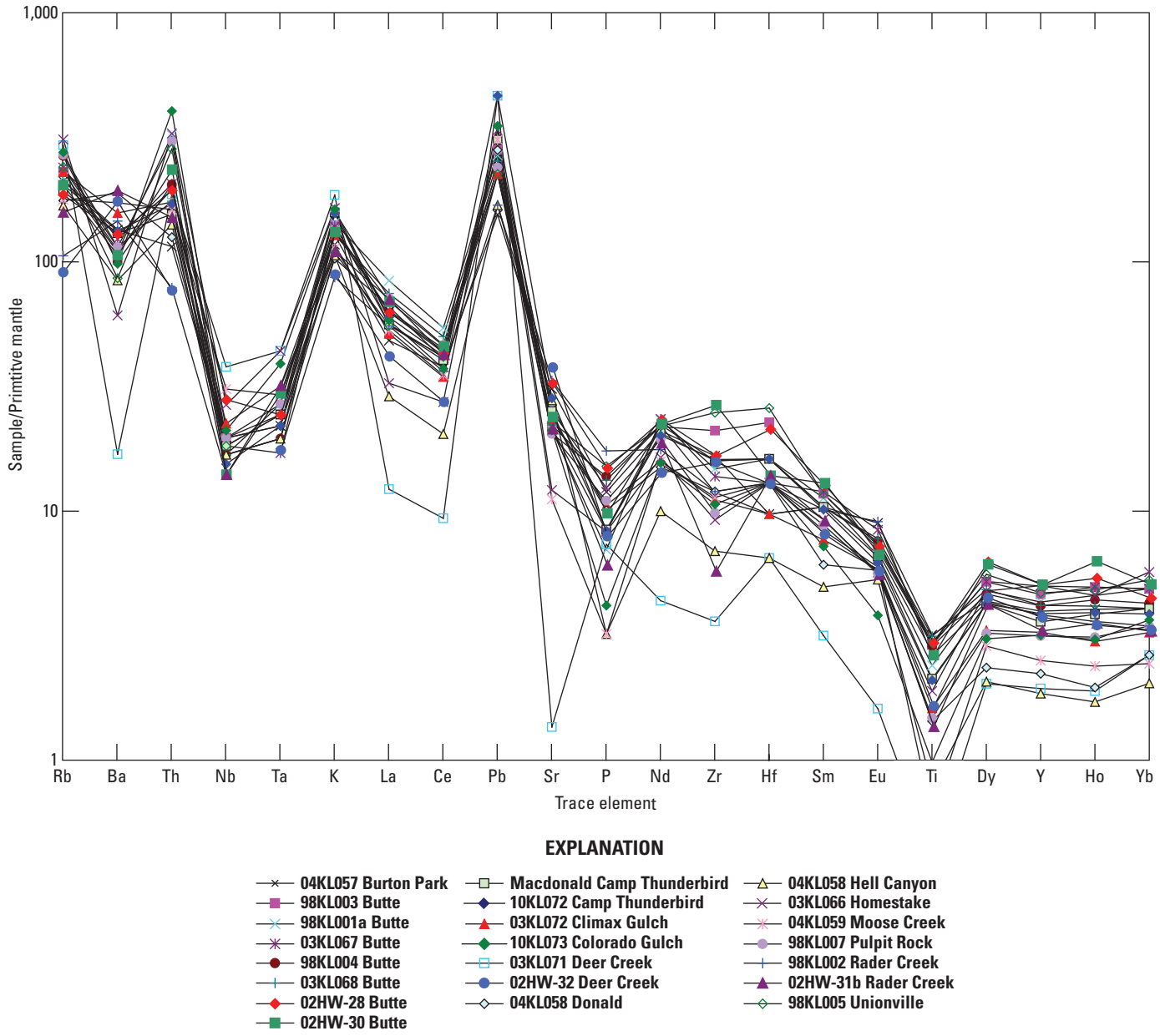


**Figure 12.** Primitive mantle-normalized (Sun and McDonough, 1989) trace-element diagrams for Boulder batholith samples. Trace elements arranged in order of increasing compatibility to the right.

to nonexistent negative Eu anomalies (fig. 11), which also reflect insignificant plagioclase fractionation. REE patterns for various Boulder batholith rocks are essentially parallel, which indicates minimal relative REE fractionation. Consequently, REE-enriched accessory phases, such as titanite, apatite, and zircon, cannot have been removed in significant quantities from the representative magmas. Noteworthy middle (MREE) to HREE depletions among the plutonic constituents of the Boulder batholith rocks probably reflect variable amphibole fractionation because amphibole fractionation causes Dy/Yb to decrease (Davidson and others, 2007). The Deer Creek granophyre has distinctly depleted LREE abundances that may reflect fractionation of LREE-enriched titanite or allanite (Sawka and others, 1984) from the associated magma. Alternatively, the aplitic character of the Deer Creek granophyre indicates that it could have interacted with late-stage (exsolved) magmatic fluids that destroyed LREE-enriched accessory minerals and flushed LREE from the magmatic system, thereby selectively reducing LREE abundances. Less pronounced LREE depletion, characteristic of the Hell Canyon monzogranite, may reflect similar processes.

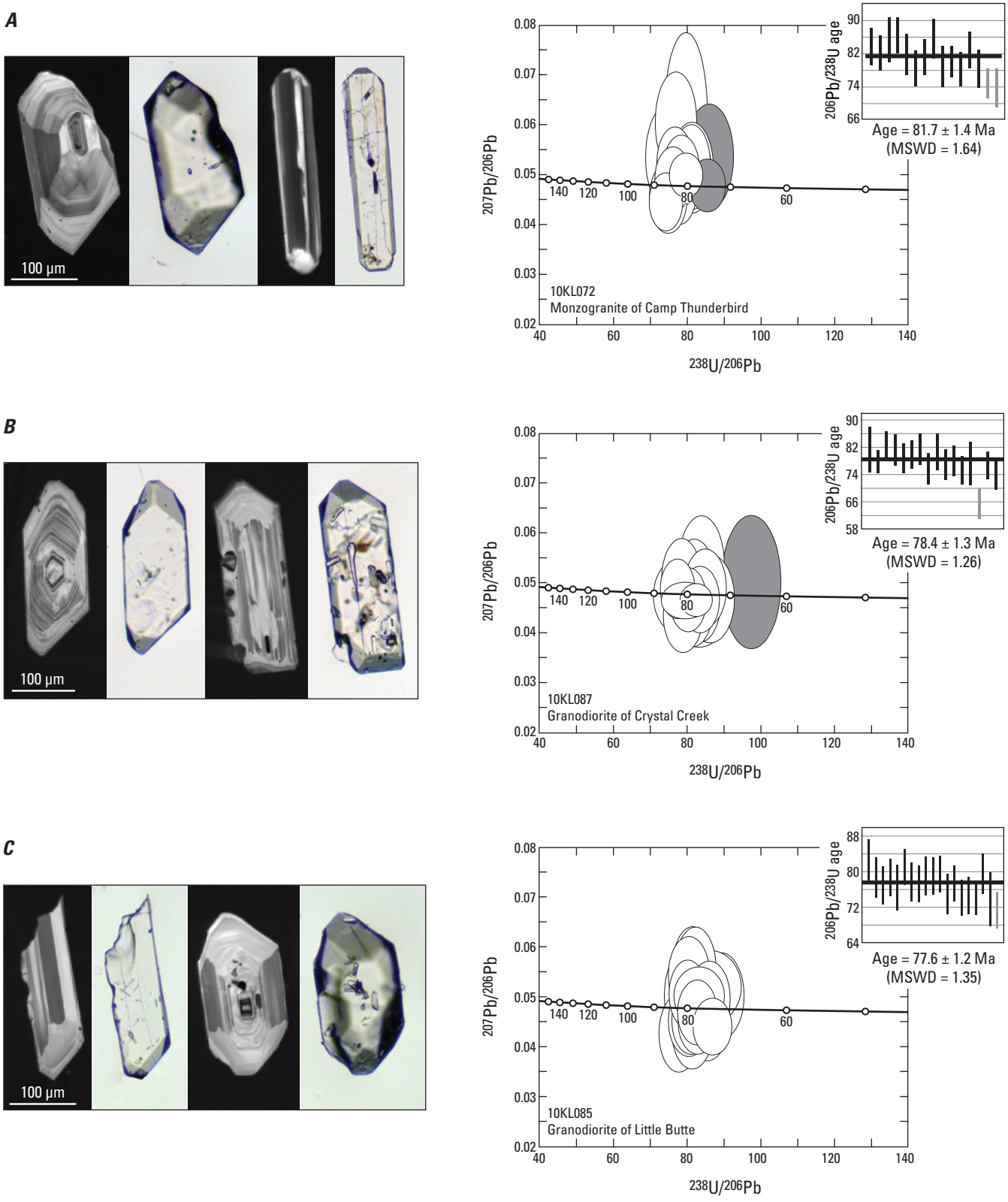


**Figure 13.** Photographs of representative zircons and Tera-Wasserburg plots of sensitive high resolution ion microprobe (SHRIMP) U-Pb dates from each sample dated in this study. In image pairs, cathodoluminescence images are on the left and transmitted-light images are on the right. SHRIMP data for each sample are shown as Tera-Wasserburg plots to the right of images. Data shown by gray error ellipses and error bars are excluded from weighted average age calculations. MSWD, mean square of weighted deviates.

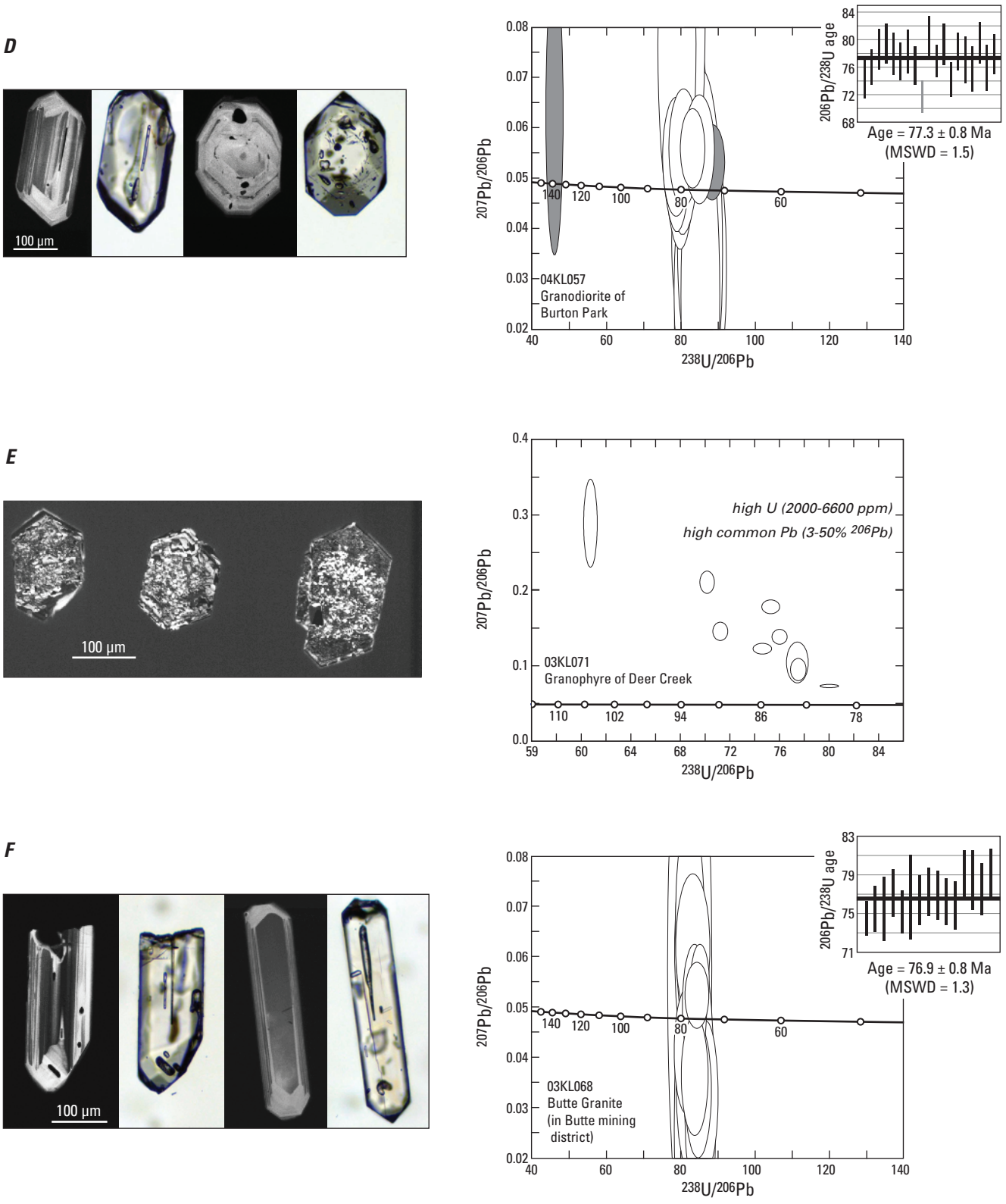


**Figure 13.** Photographs of representative zircons and Tera-Wasserburg plots of sensitive high resolution ion microprobe (SHRIMP) U-Pb dates from each sample dated in this study. In image pairs, cathodoluminescence images are on the left and transmitted-light images are on the right. SHRIMP data for each sample are shown as Tera-Wasserburg plots to the right of images. Data shown by gray error ellipses and error bars are excluded from weighted average age calculations. MSWD, mean square of weighted deviates.—Continued

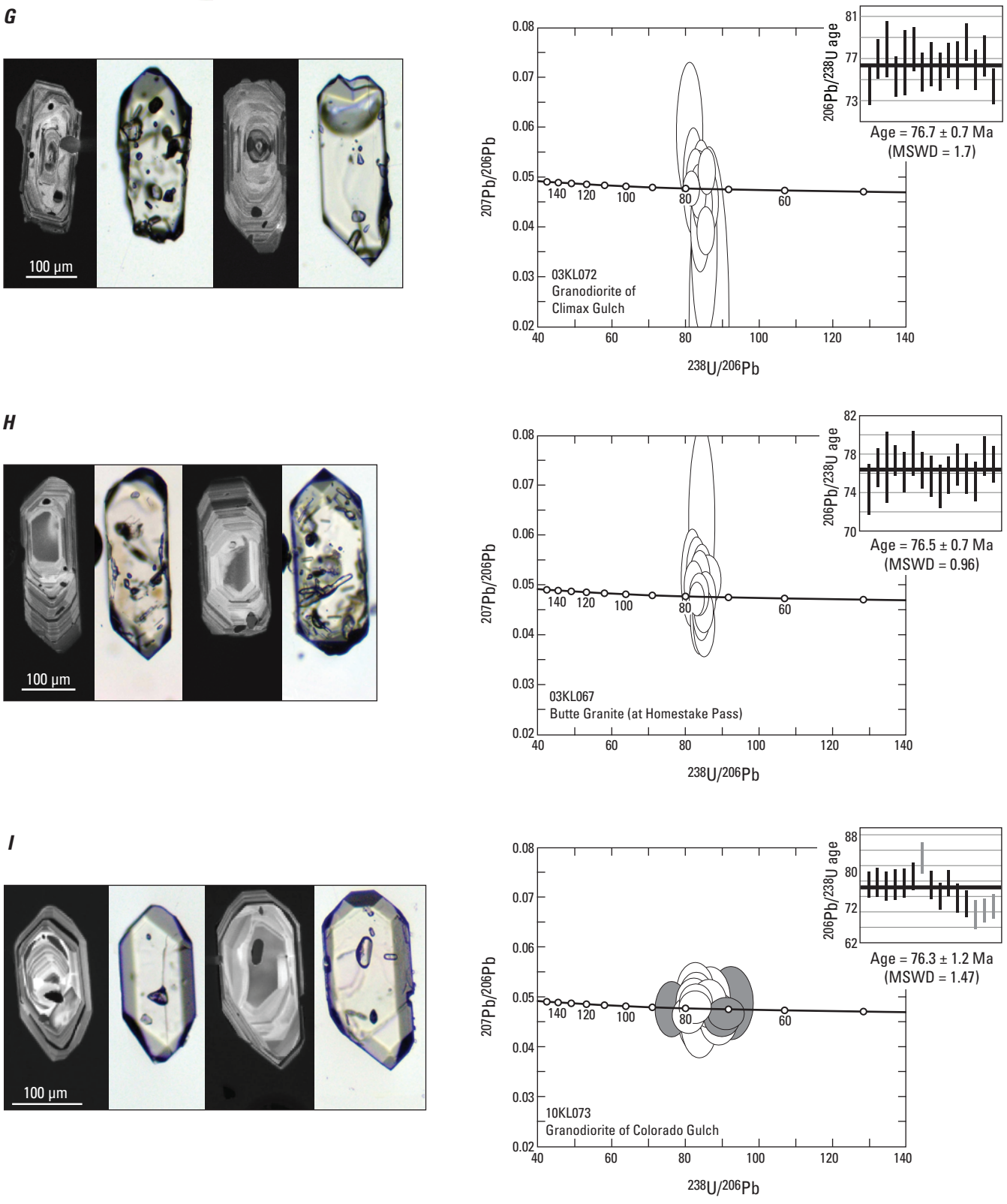


**Figure 13.** Photographs of representative zircons and Tera-Wasserburg plots of sensitive high resolution ion microprobe (SHRIMP) U-Pb dates from each sample dated in this study. In image pairs, cathodoluminescence images are on the left and transmitted-light images are on the right. SHRIMP data for each sample are shown as Tera-Wasserburg plots to the right of images. Data shown by gray error ellipses and error bars are excluded from weighted average age calculations. MSWD, mean square of weighted deviates.—Continued

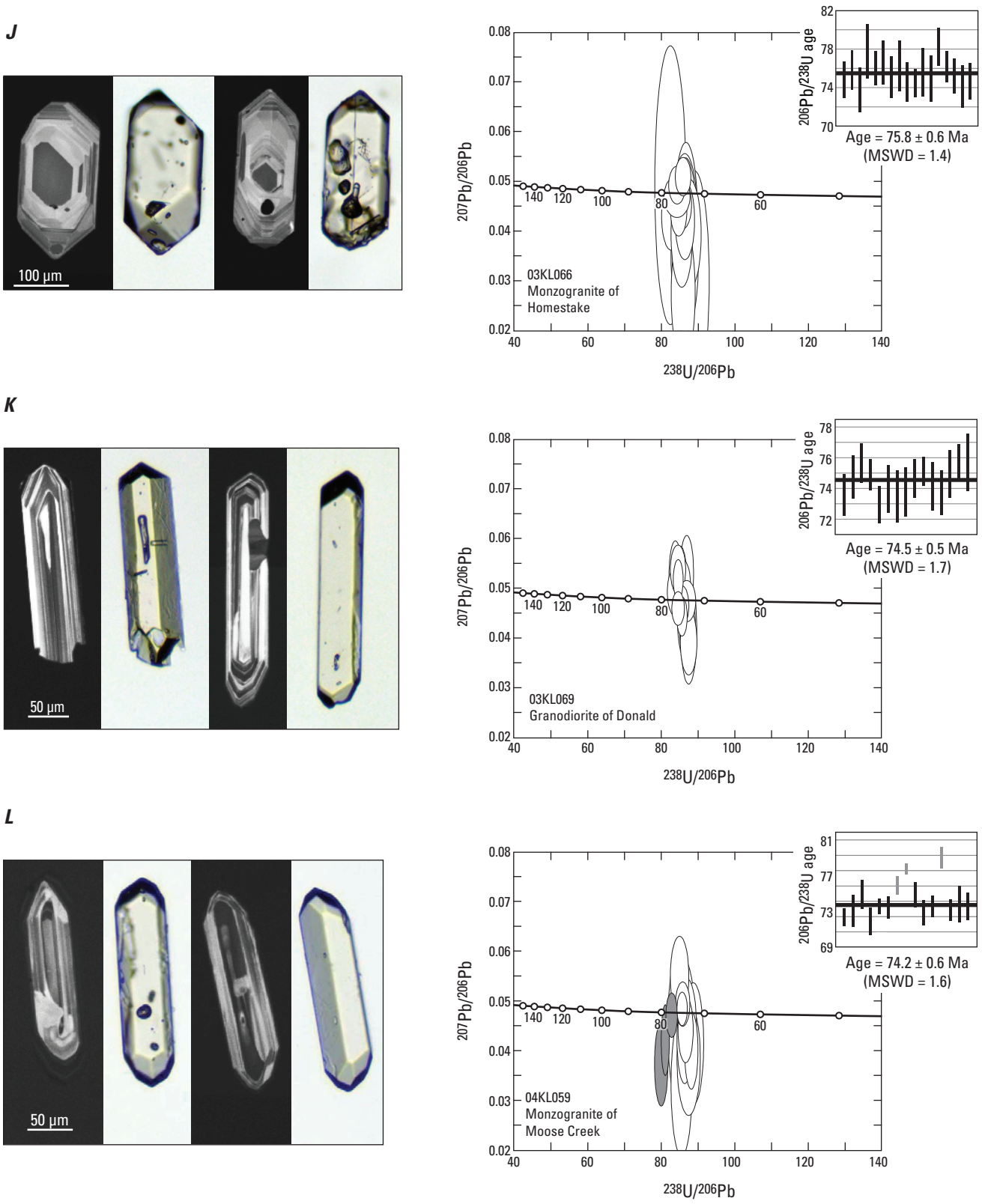


**Figure 13.** Photographs of representative zircons and Tera-Wasserburg plots of sensitive high resolution ion microprobe (SHRIMP) U-Pb dates from each sample dated in this study. In image pairs, cathodoluminescence images are on the left and transmitted-light images are on the right. SHRIMP data for each sample are shown as Tera-Wasserburg plots to the right of images. Data shown by gray error ellipses and error bars are excluded from weighted average age calculations. MSWD, mean square of weighted deviates.—Continued

**Table 4.** SHRIMP U-Th-Pb data for zircon from plutons of Boulder batholith, southwest Montana.

[%, percent; ---, no data]

| Sample | Measured $^{204}Pb/^{206}Pb$ | Measured $^{207}Pb/^{206}Pb$ | % common $^{206}Pb$ | U (ppm) | Th/U | $^{206}Pb^{1}/^{238}U$ (Ma) | err [2] (Ma) | $^{238}U^{3}/^{206}Pb$ | err[2] (%) | $^{207}Pb^{3}/^{206}Pb$ | err[2] (%) |
|---|---|---|---|---|---|---|---|---|---|---|---|
| Sample 10KL072 (Monzogranite of Camp Thunderbird) [latitude 46.5819° N, longitude –112.27227° W] | | | | | | | | | | | |
| 10KL072–1.1 | 0.002432 | 0.0494 | 0.21 | 172 | 1.33 | 83.8 | 2.2 | 76.23 | 2.6 | .0494 | 5.4 |
| 10KL072–2.1 | --- | 0.0477 | 0.01 | 171 | 0.89 | 82.2 | 2.1 | 77.95 | 2.5 | .0477 | 6.2 |
| 10KL072–3.1 | --- | 0.0538 | 0.76 | 67 | 1.03 | 85.4 | 2.7 | 74.45 | 3.1 | .0538 | 7.7 |
| 10KL072–4.1 | 0.000482 | 0.0449 | –0.35 | 176 | 1.03 | 86.4 | 2.2 | 74.34 | 2.5 | .0449 | 5.2 |
| 10KL072–5.1 | 0.001710 | 0.0607 | 1.64 | 79 | 1.06 | 81.8 | 2.5 | 77.00 | 3.0 | .0607 | 6.8 |
| 10KL072–6.1 | 0.000884 | 0.0511 | 0.45 | 124 | 0.57 | 78.6 | 2.1 | 81.19 | 2.7 | .0511 | 6.2 |
| 10KL072–7.1 | 0.001596 | 0.0511 | 0.44 | 147 | 0.64 | 81.3 | 2.1 | 78.49 | 2.6 | .0511 | 5.7 |
| 10KL072–8.1 | –0.001121 | 0.0457 | –0.25 | 135 | 0.87 | 85.7 | 2.4 | 74.94 | 2.8 | .0457 | 6.3 |
| 10KL072–9.1 | 0.002733 | 0.0621 | 1.83 | 82 | 0.84 | 78.9 | 2.4 | 79.70 | 3.0 | .0621 | 10.8 |
| 10KL072–10.1 | 0.000618 | 0.0502 | 0.33 | 390 | 1.69 | 80.1 | 1.9 | 79.68 | 2.3 | .0502 | 3.6 |
| 10KL072–11.1 | 0.001134 | 0.0524 | 0.61 | 170 | 0.85 | 78.4 | 2.0 | 81.20 | 2.6 | .0524 | 6.1 |
| 10KL072–12.1 | 0.001211 | 0.0525 | 0.61 | 129 | 0.59 | 82.9 | 2.2 | 76.81 | 2.6 | .0525 | 5.7 |
| 10KL072–13.1 | 0.000690 | 0.0517 | 0.52 | 96 | 0.60 | 78.4 | 2.3 | 81.33 | 2.9 | .0517 | 7.1 |
| 10KL072–14.1 | –0.000107 | 0.0482 | 0.08 | 280 | 1.02 | 74.9 | 1.8 | 85.52 | 2.4 | .0482 | 4.4 |
| 10KL072–15.1 | --- | 0.0539 | 0.81 | 83 | 0.69 | 73.9 | 2.3 | 86.05 | 3.1 | .0539 | 7.9 |
| Sample 98BL002 (Rader Creek Granodiorite) [latitude 45.8389° N, longitude –112.3139° W] | | | | | | | | | | | |
| 98BL002–1.1 | 0.002872 | 0.0589 | 1.43 | 70 | 0.96 | 80.2 | 2.0 | 78.79 | 2.3 | .0589 | 9.6 |
| 98BL002–2.1 | –0.000331 | 0.0599 | 1.55 | 87 | 0.95 | 81.8 | 1.8 | 77.06 | 2.2 | .0599 | 7.2 |
| 98BL002–3.1 | 0.002523 | 0.1276 | 10.07 | 124 | 1.38 | 83.4 | 1.7 | 69.06 | 1.9 | .1276 | 4.1 |
| 98BL002–4.1 | 0.004681 | 0.0660 | 2.30 | 67 | 0.96 | 84.8 | 2.4 | 73.82 | 2.8 | .0660 | 7.8 |
| 98BL002–5.1 | --- | 0.0605 | 1.63 | 68 | 0.95 | 79.4 | 2.0 | 79.41 | 2.4 | .0605 | 7.7 |
| 98BL002–6.1 | --- | 0.0828 | 4.43 | 61 | 0.94 | 80.9 | 2.2 | 75.66 | 2.6 | .0828 | 7.2 |
| 98BL002–7.1 | 0.001243 | 0.0646 | 2.14 | 85 | 1.02 | 80.9 | 1.9 | 77.45 | 2.2 | .0646 | 7.5 |
| 98BL002–8.1 | 0.005765 | 0.0937 | 5.81 | 54 | 1.04 | 77.3 | 2.2 | 78.04 | 2.7 | .0937 | 7.1 |
| 98BL002–9.1 | 0.003437 | 0.0920 | 5.61 | 174 | 0.91 | 74.1 | 1.3 | 81.63 | 1.7 | .0920 | 4.3 |
| 98BL002–10.1 | 0.020579 | 0.2888 | 30.50 | 116 | 5.36 | 57.8 | 1.7 | 77.23 | 1.9 | .2888 | 4.0 |
| 98BL002–11.1 | –0.000517 | 0.0539 | 0.78 | 48 | 0.98 | 84.2 | 2.4 | 75.47 | 2.8 | .0539 | 10.2 |
| 98BL002–12.1 | 0.019342 | 0.3615 | 39.56 | 91 | 1.19 | 80.9 | 2.5 | 47.86 | 2.1 | .3615 | 2.7 |
| 98BL002–13.1 | 0.003082 | 0.0736 | 3.31 | 187 | 0.89 | 71.1 | 1.2 | 87.20 | 1.6 | .0736 | 4.4 |
| 98BL002–14.1 | 0.003866 | 0.0862 | 4.87 | 50 | 1.06 | 77.1 | 2.3 | 79.11 | 2.8 | .0862 | 7.8 |
| 98BL002–15.1 | 0.002364 | 0.0589 | 1.42 | 79 | 1.02 | 80.4 | 1.8 | 78.59 | 2.2 | .0589 | 7.2 |
| 98BL002–16.1 | 0.001755 | 0.2002 | 17.87 | 76 | 1.97 | 436.0 | 11.9 | 11.74 | 2.6 | .2002 | 2.8 |
| 98BL002–17.1 | 0.003273 | 0.0542 | 0.82 | 96 | 0.86 | 81.9 | 1.7 | 77.54 | 2.1 | .0542 | 6.9 |
| 98BL002–18.1 | 0.000832 | 0.0743 | 3.37 | 42 | 1.18 | 78.3 | 2.5 | 79.07 | 3.1 | .0743 | 9.6 |
| Sample 10KL087 (Granodiorite of Crystal Creek) [latitude 46.4824° N, longitude –111.8448° W] | | | | | | | | | | | |
| 10KL087–1.1 | 0.000534 | 0.0477 | 0.01 | 111 | 1.10 | 81.3 | 3.3 | 78.76 | 4.1 | .0477 | 6.7 |
| 10KL087–1.2 | 0.000104 | 0.0469 | –0.08 | 670 | 0.94 | 77.8 | 1.7 | 82.47 | 2.2 | .0469 | 2.8 |
| 10KL087–2.1 | 0.000658 | 0.0491 | 0.18 | 184 | 0.84 | 82.6 | 2.0 | 77.44 | 2.5 | .0491 | 4.9 |
| 10KL087–3.1 | --- | 0.0509 | 0.41 | 95 | 0.76 | 81.3 | 2.3 | 78.50 | 2.8 | .0509 | 6.6 |
| 10KL087–4.1 | –0.002177 | 0.0453 | –0.29 | 109 | 1.18 | 78.8 | 2.2 | 81.50 | 2.7 | .0453 | 6.9 |
| 10KL087–5.1 | --- | 0.0470 | –0.08 | 147 | 0.56 | 79.9 | 2.0 | 80.29 | 2.6 | .0470 | 5.5 |
| 10KL087–6.1 | --- | 0.0439 | –0.47 | 105 | 0.87 | 81.5 | 2.3 | 78.92 | 2.8 | .0439 | 6.9 |
| 10KL087–7.1 | --- | 0.0537 | 0.78 | 80 | 0.82 | 75.8 | 2.3 | 83.92 | 3.0 | .0537 | 7.5 |
| 10KL087–8.1 | 0.000262 | 0.0468 | –0.11 | 459 | 1.47 | 80.6 | 2.7 | 79.54 | 3.3 | .0468 | 3.2 |
| 10KL087–9.1 | 0.000662 | 0.0468 | –0.10 | 96 | 0.88 | 77.0 | 2.2 | 83.34 | 2.9 | .0468 | 7.2 |
| 10KL087–10.1 | 0.001317 | 0.0503 | 0.34 | 96 | 1.08 | 78.0 | 2.2 | 81.92 | 2.9 | .0503 | 7.1 |
| 10KL087–11.1 | 0.002110 | 0.0493 | 0.23 | 117 | 0.83 | 75.3 | 2.1 | 84.95 | 2.7 | .0493 | 6.4 |
| 10KL087–12.1 | 0.001321 | 0.0456 | –0.24 | 94 | 0.75 | 77.2 | 3.2 | 83.19 | 4.1 | .0456 | 7.2 |

**Table 4.** SHRIMP U-Th-Pb data for zircon from plutons of Boulder batholith, southwest Montana.—Continued

[%, percent; ---, no data]

| Sample | Measured $^{204}Pb/^{206}Pb$ | Measured $^{207}Pb/^{206}Pb$ | % common $^{206}Pb$ | U (ppm) | Th/U | $^{206}Pb^{1}/^{238}U$ (Ma) | err [2] (Ma) | $^{238}U^{3}/^{206}Pb$ | err [2] (%) | $^{207}Pb^{3}/^{206}Pb$ | err [2] (%) |
|---|---|---|---|---|---|---|---|---|---|---|---|
| 10KL087–13.1 | 0.000967 | 0.0505 | 0.40 | 81 | 0.80 | 65.7 | 2.2 | 97.28 | 3.4 | .0505 | 10.7 |
| 10KL087–14.1 | 0.000404 | 0.0470 | –0.07 | 154 | 1.15 | 76.8 | 2.0 | 83.48 | 2.6 | .0470 | 5.7 |
| 10KL087–15.1 | --- | 0.0471 | –0.05 | 91 | 0.73 | 74.4 | 2.3 | 86.20 | 3.1 | .0471 | 7.6 |
| Sample 98BL005 (Unionville Granodiorite) [latitude 46.5125° N, longitude –112.2597° W] | | | | | | | | | | | |
| 98KL005–1.1 | 0.001001 | 0.0568 | 1.16 | 221 | 1.18 | 77.0 | 1.2 | 82.26 | 1.5 | .0568 | 4.6 |
| 98KL005–2.1 | 0.000249 | 0.0493 | 0.21 | 390 | 1.47 | 78.9 | 1.0 | 80.98 | 1.2 | .0493 | 3.7 |
| 98KL005–3.1 | 0.000669 | 0.0538 | 0.79 | 242 | 0.94 | 79.3 | 1.2 | 80.20 | 1.4 | .0538 | 4.4 |
| 98KL005–4.1 | 0.001281 | 0.0481 | 0.07 | 313 | 1.10 | 78.1 | 1.1 | 82.01 | 1.3 | .0481 | 5.2 |
| 98KL005–5.1 | --- | 0.0491 | 0.20 | 243 | 1.18 | 77.1 | 1.2 | 82.95 | 1.4 | .0491 | 6.6 |
| 98KL005–6.1 | 0.000701 | 0.0494 | 0.23 | 275 | 1.09 | 79.3 | 1.1 | 80.62 | 1.4 | .0494 | 4.2 |
| 98KL005–7.1 | 0.001531 | 0.0570 | 1.19 | 198 | 1.09 | 78.3 | 1.3 | 80.81 | 1.6 | .0570 | 4.8 |
| 98KL005–8.1 | 0.001224 | 0.0526 | 0.64 | 225 | 1.15 | 78.2 | 1.2 | 81.42 | 1.5 | .0526 | 4.7 |
| 98KL005–9.1 | 0.000380 | 0.0478 | 0.02 | 237 | 1.13 | 79.4 | 1.2 | 80.64 | 1.4 | .0478 | 4.7 |
| 98KL005–10.1 | 0.000501 | 0.0518 | 0.53 | 323 | 1.27 | 78.1 | 1.0 | 81.63 | 1.3 | .0518 | 3.9 |
| 98KL005–11.1 | 0.000340 | 0.0533 | 0.72 | 345 | 1.42 | 78.2 | 1.0 | 81.36 | 1.3 | .0533 | 3.8 |
| 98KL005–12.1 | 0.000008 | 0.0486 | 0.13 | 365 | 0.99 | 77.9 | 1.0 | 82.10 | 1.3 | .0486 | 3.8 |
| 98KL005–13.1 | –0.000204 | 0.0501 | 0.31 | 361 | 1.39 | 78.8 | 1.0 | 81.02 | 1.2 | .0501 | 3.8 |
| 98KL005–14.1 | –0.001175 | 0.0456 | –0.24 | 224 | 1.23 | 78.3 | 1.2 | 81.99 | 1.5 | .0456 | 5.1 |
| 98KL005–15.1 | –0.000831 | 0.0523 | 0.60 | 208 | 1.19 | 76.8 | 1.2 | 82.94 | 1.5 | .0523 | 4.9 |
| 98KL005–16.1 | –0.000366 | 0.0470 | –0.07 | 232 | 1.22 | 77.2 | 1.2 | 83.02 | 1.5 | .0470 | 5.0 |
| Sample 10KL085 (Granodiorite of Little Butte) [latitude –111.8558° N, longitude 46.5195° W] | | | | | | | | | | | |
| 10KL085–1.1 | 0.001016 | 0.0431 | –0.58 | 95 | 0.77 | 82.7 | 2.3 | 77.93 | 2.8 | .0431 | 7.3 |
| 10KL085–2.1 | --- | 0.0547 | 0.89 | 122 | 0.83 | 78.7 | 2.2 | 80.68 | 2.8 | .0547 | 5.7 |
| 10KL085–3.1 | --- | 0.0559 | 1.06 | 109 | 0.95 | 76.9 | 2.1 | 82.43 | 2.7 | .0559 | 6.1 |
| 10KL085–4.1 | 0.000647 | 0.0495 | 0.24 | 132 | 1.04 | 78.8 | 2.1 | 81.14 | 2.6 | .0495 | 5.7 |
| 10KL085–5.1 | --- | 0.0505 | 0.38 | 220 | 1.30 | 76.5 | 2.6 | 83.40 | 3.3 | .0505 | 4.7 |
| 10KL085–6.1 | 0.000523 | 0.0506 | 0.37 | 192 | 0.78 | 81.1 | 2.0 | 78.66 | 2.4 | .0506 | 6.7 |
| 10KL085–7.1 | 0.001198 | 0.0558 | 1.04 | 104 | 0.63 | 77.7 | 2.2 | 81.63 | 2.8 | .0558 | 6.2 |
| 10KL085–8.1 | –0.001141 | 0.0473 | –0.04 | 162 | 0.79 | 77.4 | 2.0 | 82.87 | 2.6 | .0473 | 5.6 |
| 10KL085–9.1 | 0.000810 | 0.0433 | –0.55 | 108 | 1.01 | 79.0 | 2.2 | 81.52 | 2.7 | .0433 | 6.8 |
| 10KL085–10.1 | 0.001429 | 0.0457 | –0.24 | 129 | 0.75 | 79.0 | 2.1 | 81.26 | 2.6 | .0457 | 6.1 |
| 10KL085–11.1 | --- | 0.0509 | 0.42 | 144 | 1.01 | 79.4 | 2.0 | 80.31 | 2.6 | .0509 | 5.4 |
| 10KL085–12.1 | 0.001820 | 0.0463 | –0.15 | 86 | 0.82 | 75.0 | 2.2 | 85.57 | 2.9 | .0463 | 7.7 |
| 10KL085–13.1 | 0.000816 | 0.0455 | –0.26 | 144 | 1.07 | 77.4 | 2.0 | 82.96 | 2.6 | .0455 | 5.9 |
| 10KL085–14.1 | --- | 0.0500 | 0.31 | 127 | 0.77 | 74.2 | 2.0 | 86.13 | 2.7 | .0500 | 6.1 |
| 10KL085–15.1 | --- | 0.0477 | 0.03 | 103 | 0.96 | 74.7 | 2.1 | 85.80 | 2.8 | .0477 | 7.3 |
| 10KL085–16.1 | 0.001039 | 0.0445 | –0.38 | 203 | 1.19 | 74.0 | 1.8 | 86.97 | 2.5 | .0445 | 5.2 |
| 10KL085–17.1 | --- | 0.0456 | –0.26 | 124 | 0.66 | 79.6 | 2.3 | 80.66 | 2.8 | .0456 | 6.3 |
| 10KL085–18.1 | 0.000470 | 0.0523 | 0.61 | 142 | 1.02 | 73.9 | 3.0 | 86.24 | 4.0 | .0523 | 5.7 |
| 10KL085–19.1 | --- | 0.0506 | 0.39 | 101 | 0.78 | 71.5 | 2.1 | 89.30 | 2.8 | .0506 | 6.9 |
| Sample 04KL057 (Granodiorite of Burton Park) [latitude 45.8193° N, longitude 112.5203° W] | | | | | | | | | | | |
| 04KL057–1.1 | –0.000293 | 0.0515 | 0.50 | 111 | 0.75 | 74.4 | 1.4 | 85.25 | 1.9 | 0.0558 | 7.8 |
| 04KL057–2.1 | 0.000000 | 0.0559 | 1.06 | 154 | 0.72 | 76.0 | 1.3 | 83.41 | 1.6 | 0.0559 | 5.7 |
| 04KL057–3.1 | 0.003059 | 0.0541 | 0.82 | 119 | 0.69 | 78.6 | 1.5 | 85.74 | 2.8 | | |
| 04KL057–4.1 | 0.001454 | 0.0840 | 4.43 | 86 | 0.46 | 135.2 | 2.7 | 46.34 | 2.0 | 0.0630 | 18.2 |
| 04KL057–5.1 | 0.001368 | 0.0487 | 0.14 | 120 | 0.80 | 79.4 | 1.4 | 82.68 | 2.1 | 0.0280 | 33.4 |
| 04KL057–6.1 | –0.001209 | 0.0503 | 0.34 | 117 | 0.65 | 78.0 | 1.5 | 80.08 | 2.5 | 0.0676 | 19.1 |
| 04KL057–7.1 | 0.001582 | 0.0509 | 0.42 | 136 | 0.75 | 76.9 | 1.4 | 85.52 | 2.5 | 0.0270 | 56.4 |
| 04KL057–8.1 | –0.000366 | 0.0507 | 0.40 | 103 | 0.71 | 78.3 | 1.6 | 81.00 | 2.0 | 0.0561 | 8.4 |

**Table 4.** SHRIMP U-Th-Pb data for zircon from plutons of Boulder batholith, southwest Montana.—Continued

[%, percent; ---, no data]

| Sample | Measured $^{204}Pb/^{206}Pb$ | Measured $^{207}Pb/^{206}Pb$ | % common $^{206}Pb$ | U (ppm) | Th/U | $^{206}Pb^{1}/^{238}U$ (Ma) | err [2] (Ma) | $^{238}U^{3}/^{206}Pb$ | err[2] (%) | $^{207}Pb^{3}/^{206}Pb$ | err[2] (%) |
|---|---|---|---|---|---|---|---|---|---|---|---|
| 04KL057–9.1 | 0.000224 | 0.0585 | 1.38 | 133 | 0.77 | 76.3 | 1.4 | 83.16 | 2.2 | 0.0552 | 20.3 |
| 04KL057–10.1 | 0.000076 | 0.1047 | 3.09 | 231 | 0.19 | 1162.0 | 7.4 | 4.91 | 0.7 | 0.1036 | 0.9 |
| 04KL057–11.1 | 0.000000 | 0.0532 | 0.72 | 171 | 0.62 | 71.8 | 1.2 | 88.68 | 1.6 | 0.0532 | 5.7 |
| 04KL057–12.1 | –0.000370 | 0.0489 | 0.16 | 117 | 0.59 | 80.4 | 1.5 | 79.02 | 1.9 | 0.0543 | 8.8 |
| 04KL057–13.1 | 0.001559 | 0.0525 | 0.63 | 185 | 1.26 | 77.0 | 1.1 | 85.18 | 1.9 | 0.0290 | 35.8 |
| 04KL057–14.1 | 0.000945 | 0.0516 | 0.51 | 117 | 0.91 | 79.3 | 1.5 | 81.77 | 2.0 | 0.0375 | 19.6 |
| 04KL057–15.1 | 0.001686 | 0.0574 | 1.25 | 154 | 0.70 | 74.2 | 1.2 | 88.00 | 2.1 | 0.0321 | 35.2 |
| 04KL057–16.1 | 0.002399 | 0.0504 | 0.36 | 135 | 0.69 | 78.3 | 1.4 | 85.34 | 2.4 | | |
| 04KL057–17.1 | 0.001311 | 0.0560 | 1.06 | 87 | 0.77 | 77.1 | 1.7 | 84.33 | 2.4 | 0.0364 | 27.5 |
| 04KL057–18.1 | 0.000958 | 0.0500 | 0.31 | 89 | 0.80 | 75.8 | 1.6 | 85.84 | 2.7 | 0.0357 | 41.0 |
| 04KL057–19.1 | 0.001902 | 0.0462 | –0.18 | 111 | 0.68 | 79.6 | 1.5 | 83.60 | 2.5 | 0.0171 | 84.1 |
| 04KL057–20.1 | –0.002302 | 0.0494 | 0.24 | 89 | 0.73 | 76.0 | 1.6 | 80.67 | 3.1 | 0.0819 | 21.4 |
| 04KL057–21.1 | –0.002405 | 0.0423 | –0.67 | 118 | 0.69 | 78.0 | 1.4 | 79.20 | 2.6 | 0.0764 | 19.7 |
| Sample 03KL071 (Granophyre of Deer Creek) [latitude 45.8595° N, longitude 112.4647° W] | | | | | | | | | | | |
| 03KL071–1.1 | 0.016349 | 0.2902 | 35.21 | 2365 | 0.25 | 67.1 | 6.4 | 88.94 | 4.8 | | |
| 03KL071–2.1 | 0.009091 | 0.1809 | 19.35 | 2650 | 0.46 | 68.6 | 2.4 | 90.75 | 1.5 | 0.0677 | 34.1 |
| 03KL071–3.1 | 0.005501 | 0.1260 | 12.31 | 2614 | 0.23 | 76.3 | 1.7 | 81.99 | 1.0 | 0.0624 | 20.9 |
| 03KL071–4.1 | 0.011057 | 0.2129 | 23.99 | 4284 | 0.34 | 68.9 | 3.2 | 89.00 | 1.7 | 0.0772 | 37.6 |
| 03KL071–5.1 | 0.001829 | 0.0771 | 4.64 | 3137 | 0.26 | 76.2 | 0.7 | 83.00 | 0.5 | 0.0557 | 7.7 |
| 03KL071–5.2 | 0.004005 | 0.1078 | 9.45 | 2046 | 0.12 | 75.4 | 1.9 | 83.11 | 1.8 | 0.0613 | 29.3 |
| 03KL071–6.1 | 0.006221 | 0.1417 | 11.88 | 3873 | 0.27 | 74.2 | 1.3 | 86.08 | 1.0 | 0.0503 | 31.2 |
| 03KL071–7.1 | 0.007027 | 0.1485 | 15.84 | 4071 | 0.15 | 75.9 | 2.4 | 81.68 | 1.8 | 0.0679 | 28.2 |
| 03KL071–8.1 | 0.027167 | 0.4411 | 49.69 | 6633 | 0.48 | 61.9 | 7.8 | 105.42 | 6.0 | | |
| 03KL071–9.1 | 0.003796 | 0.0986 | 8.02 | 5095 | 0.23 | 77.0 | 1.3 | 82.35 | 1.2 | 0.0541 | 22.9 |
| Sample 03KL068 (Butte Granite, in Butte mining district) [latitude 46.0390° N, longitude 112.5320° W] | | | | | | | | | | | |
| 03KL068–1.1 | –0.000286 | 0.0511 | 0.45 | 390 | 1.16 | 74.5 | 0.9 | 85.20 | 1.2 | 0.0552 | 5.4 |
| 03KL068–2.1 | 0.000000 | 0.0525 | 0.63 | 160 | 0.86 | 75.5 | 1.2 | 84.37 | 1.5 | 0.0525 | 5.0 |
| 03KL068–3.1 | –0.000748 | 0.0512 | 0.46 | 257 | 0.69 | 75.5 | 1.6 | 83.30 | 2.3 | 0.0620 | 9.6 |
| 03KL068–4.1 | 0.001205 | 0.0480 | 0.06 | 178 | 0.74 | 77.2 | 1.2 | 84.90 | 1.8 | 0.0298 | 27.0 |
| 03KL068–5.1 | 0.001139 | 0.0498 | 0.29 | 186 | 1.03 | 75.2 | 1.1 | 86.79 | 1.6 | 0.0327 | 18.5 |
| 03KL068–6.1 | 0.007084 | 0.1611 | 14.32 | 264 | 0.67 | 76.7 | 2.2 | 82.41 | 3.0 | 0.0580 | 43.3 |
| 03KL068–7.1 | –0.000863 | 0.0490 | 0.18 | 132 | 0.69 | 76.4 | 1.3 | 82.38 | 2.0 | 0.0615 | 14.6 |
| 03KL068–8.1 | 0.000862 | 0.0494 | 0.23 | 161 | 0.70 | 77.2 | 1.2 | 84.11 | 1.7 | 0.0365 | 18.0 |
| 03KL068–9.1 | 0.000768 | 0.0453 | –0.28 | 147 | 0.65 | 76.9 | 1.3 | 84.75 | 1.7 | 0.0338 | 16.0 |
| 03KL068–10.1 | 0.000042 | 0.0510 | 0.43 | 175 | 0.82 | 76.3 | 1.2 | 83.72 | 1.6 | 0.0504 | 9.9 |
| 03KL068–11.1 | –0.001060 | 0.0513 | 0.47 | 149 | 0.71 | 75.8 | 1.2 | 82.48 | 2.0 | 0.0665 | 14.2 |
| 03KL068–12.1 | 0.000641 | 0.0448 | –0.35 | 159 | 0.72 | 79.0 | 1.3 | 82.36 | 1.8 | 0.0352 | 20.2 |
| 03KL068–13.1 | 0.001657 | 0.0513 | 0.47 | 95 | 0.86 | 78.5 | 1.5 | 83.84 | 2.7 | 0.0262 | 62.2 |
| 03KL068–14.1 | 0.000746 | 0.0479 | 0.05 | 135 | 0.72 | 77.5 | 1.3 | 83.83 | 1.7 | 0.0368 | 13.1 |
| 03KL068–15.1 | 0.000548 | 0.0497 | 0.26 | 142 | 0.72 | 79.0 | 1.3 | 81.72 | 1.7 | 0.0415 | 12.2 |
| Sample 03KL072 (Granodiorite of Climax Gulch) [latitude 45.8702° N, longitude 112.5519° W] | | | | | | | | | | | |
| 03KL072–1.1 | 0.000297 | 0.0497 | 0.28 | 315 | 0.62 | 74.5 | 0.9 | 86.25 | 1.3 | 0.0453 | 5.9 |
| 03KL072–2.1 | 0.000509 | 0.0482 | 0.08 | 382 | 0.57 | 77.0 | 0.9 | 83.97 | 1.3 | 0.0406 | 9.3 |
| 03KL072–3.1 | –0.000677 | 0.0492 | 0.20 | 292 | 0.75 | 77.9 | 1.3 | 81.11 | 1.8 | 0.0590 | 9.7 |
| 03KL072–4.1 | 0.000295 | 0.0507 | 0.40 | 333 | 0.60 | 75.3 | 1.0 | 85.27 | 1.3 | 0.0463 | 6.6 |
| 03KL072–5.1 | 0.002076 | 0.0532 | 0.71 | 187 | 0.72 | 76.6 | 1.5 | 86.39 | 2.6 | 0.0216 | 65.6 |
| 03KL072–6.1 | 0.000102 | 0.0508 | 0.41 | 301 | 0.64 | 77.9 | 1.0 | 82.07 | 1.4 | 0.0494 | 8.8 |
| 03KL072–7.1 | –0.000257 | 0.0474 | –0.02 | 403 | 0.65 | 75.7 | 0.9 | 84.25 | 1.2 | 0.0512 | 5.1 |
| 03KL072–8.1 | –0.000143 | 0.0472 | –0.05 | 260 | 0.65 | 76.5 | 1.0 | 83.63 | 1.3 | 0.0493 | 5.1 |

**Table 4.** SHRIMP U-Th-Pb data for zircon from plutons of Boulder batholith, southwest Montana.—Continued

[%, percent; ---, no data]

| Sample | Measured $^{204}Pb/^{206}Pb$ | Measured $^{207}Pb/^{206}Pb$ | % common $^{206}Pb$ | U (ppm) | Th/U | $^{206}Pb^{1}/^{238}U$ (Ma) | err [2] (Ma) | $^{238}U^{3}/^{206}Pb$ | err [2] (%) | $^{207}Pb^{3}/^{206}Pb$ | err [2] (%) |
|---|---|---|---|---|---|---|---|---|---|---|---|
| 03KL072–9.1 | 0.000551 | 0.0477 | 0.03 | 453 | 0.52 | 75.7 | 0.9 | 85.46 | 1.2 | 0.0395 | 4.9 |
| 03KL072–10.1 | 0.000031 | 0.0478 | 0.04 | 688 | 0.56 | 76.8 | 0.8 | 83.44 | 1.1 | 0.0474 | 4.6 |
| 03KL072–11.1 | 0.001052 | 0.0518 | 0.54 | 208 | 0.61 | 76.4 | 1.1 | 85.10 | 1.7 | 0.0361 | 20.5 |
| 03KL072–12.1 | 0.000000 | 0.0479 | 0.04 | 605 | 0.54 | 78.6 | 0.9 | 81.53 | 1.1 | 0.0479 | 3.0 |
| 03KL072–13.1 | 0.000344 | 0.0498 | 0.28 | 527 | 0.59 | 75.9 | 0.9 | 84.71 | 1.3 | 0.0447 | 5.2 |
| 03KL072–14.1 | 0.000195 | 0.0527 | 0.65 | 331 | 0.92 | 77.3 | 1.0 | 82.70 | 1.2 | 0.0499 | 4.9 |
| 03KL072–15.1 | –0.000105 | 0.0497 | 0.28 | 518 | 0.62 | 74.4 | 0.8 | 85.75 | 1.1 | 0.0513 | 3.6 |
| Sample 03KL067 (Butte Granite, at Homestake Pass) [latitude 45.9230° N, longitude 112.4170° W] | | | | | | | | | | | |
| 03KL067–1.1 | 0.000000 | 0.0510 | 0.44 | 268 | 0.64 | 74.3 | 1.3 | 85.83 | 1.7 | 0.0510 | 4.0 |
| 03KL067–2.1 | 0.000000 | 0.0483 | 0.09 | 392 | 0.62 | 76.6 | 1.0 | 83.57 | 1.3 | 0.0483 | 3.6 |
| 03KL067–3.1 | 0.002992 | 0.0577 | 1.28 | 66 | 0.55 | 76.6 | 1.8 | 87.45 | 3.1 | | |
| 03KL067–4.1 | 0.000179 | 0.0500 | 0.30 | 778 | 0.69 | 77.3 | 0.8 | 82.91 | 1.0 | 0.0473 | 2.9 |
| 03KL067–5.1 | 0.000000 | 0.0517 | 0.53 | 271 | 0.65 | 76.1 | 1.0 | 83.73 | 1.3 | 0.0517 | 4.1 |
| 03KL067–6.1 | –0.000281 | 0.0474 | –0.03 | 191 | 0.66 | 78.0 | 1.2 | 81.69 | 1.5 | 0.0515 | 7.7 |
| 03KL067–7.1 | 0.000349 | 0.0506 | 0.38 | 350 | 0.54 | 76.3 | 0.9 | 84.20 | 1.2 | 0.0454 | 5.7 |
| 03KL067–8.1 | –0.000230 | 0.0481 | 0.07 | 509 | 0.60 | 75.7 | 1.0 | 84.27 | 1.4 | 0.0515 | 5.3 |
| 03KL067–9.1 | –0.000820 | 0.0510 | 0.45 | 174 | 0.70 | 74.6 | 1.1 | 84.22 | 1.7 | 0.0629 | 12.2 |
| 03KL067–11.1 | –0.000046 | 0.0442 | –0.41 | 298 | 0.62 | 75.8 | 1.0 | 84.78 | 1.2 | 0.0449 | 3.9 |
| 03KL067–12.1 | –0.000202 | 0.0494 | 0.23 | 234 | 0.63 | 76.9 | 1.1 | 82.87 | 1.4 | 0.0523 | 5.7 |
| 03KL067–13.1 | 0.000390 | 0.0480 | 0.07 | 395 | 0.55 | 76.0 | 1.0 | 84.91 | 1.4 | 0.0423 | 6.2 |
| 03KL067–14.1 | 0.000000 | 0.0478 | 0.03 | 249 | 0.65 | 75.1 | 1.0 | 85.26 | 1.3 | 0.0478 | 4.3 |
| 03KL067–15.1 | 0.000000 | 0.0499 | 0.30 | 264 | 0.65 | 77.8 | 1.0 | 82.08 | 1.3 | 0.0499 | 4.0 |
| 03KL067–16.1 | 0.000277 | 0.0475 | –0.01 | 356 | 0.63 | 77.0 | 0.9 | 83.70 | 1.2 | 0.0434 | 6.6 |
| Sample 98BL007 (Monzogranite of Pulpit Rock) [latitude 46.1960° N, longitude –112.1330° W] | | | | | | | | | | | |
| 98BL007–1.1 | 0.000335 | 0.0515 | 0.50 | 466 | 0.60 | 75.8 | 0.9 | 84.10 | 1.2 | .0515 | 3.4 |
| 98BL007–2.1 | –0.001166 | 0.0573 | 1.23 | 215 | 0.60 | 75.3 | 1.2 | 84.05 | 1.6 | .0573 | 4.8 |
| 98BL007–3.1 | 0.000806 | 0.0491 | 0.20 | 329 | 0.58 | 76.9 | 1.0 | 83.13 | 1.3 | .0491 | 4.1 |
| 98BL007–4.1 | –0.000194 | 0.0514 | 0.48 | 325 | 0.57 | 76.4 | 1.0 | 83.50 | 1.3 | .0514 | 4.1 |
| 98BL007–5.1 | 0.001000 | 0.0543 | 0.85 | 507 | 0.59 | 77.9 | 0.9 | 81.55 | 1.1 | .0543 | 3.8 |
| 98BL007–6.1 | 0.000967 | 0.0552 | 0.96 | 399 | 0.61 | 76.3 | 0.9 | 83.20 | 1.2 | .0552 | 3.5 |
| 98BL007–7.1 | 0.000513 | 0.0521 | 0.58 | 504 | 0.53 | 77.0 | 0.9 | 82.74 | 1.2 | .0521 | 3.2 |
| 98BL007–8.1 | 0.000718 | 0.0561 | 1.09 | 406 | 0.55 | 75.4 | 0.9 | 84.05 | 1.2 | .0561 | 3.4 |
| 98BL007–9.1 | 0.001088 | 0.0499 | 0.30 | 247 | 0.54 | 73.7 | 1.1 | 86.70 | 1.5 | .0499 | 4.7 |
| 98BL007–10.1 | 0.000795 | 0.0486 | 0.14 | 362 | 0.59 | 77.2 | 1.0 | 82.91 | 1.3 | .0486 | 3.9 |
| 98BL007–11.1 | 0.000019 | 0.0508 | 0.42 | 271 | 0.65 | 75.8 | 1.1 | 84.16 | 1.4 | .0508 | 4.4 |
| 98BL007–12.1 | 0.001229 | 0.0517 | 0.53 | 378 | 0.65 | 75.4 | 1.0 | 84.50 | 1.3 | .0517 | 3.7 |
| Sample 10KL073 (Granodiorite of Colorado Gulch) [latitude 46.5761° N, longitude –112.2009° W] | | | | | | | | | | | |
| 10KL073–1.1 | 0.000242 | 0.0492 | 0.21 | 610 | 0.26 | 77.2 | 1.7 | 82.82 | 2.2 | .0492 | 3.0 |
| 10KL073–2.1 | 0.000213 | 0.0492 | 0.20 | 305 | 0.62 | 77.7 | 1.9 | 82.26 | 2.4 | .0492 | 4.0 |
| 10KL073–3.1 | --- | 0.0451 | –0.31 | 221 | 0.53 | 76.7 | 1.9 | 83.77 | 2.4 | .0451 | 6.3 |
| 10KL073–4.1 | 0.000659 | 0.0509 | 0.42 | 200 | 0.54 | 77.2 | 2.0 | 82.69 | 2.6 | .0509 | 4.9 |
| 10KL073–5.1 | --- | 0.0466 | –0.13 | 234 | 0.45 | 77.6 | 1.9 | 82.67 | 2.4 | .0466 | 6.3 |
| 10KL073–6.1 | –0.000514 | 0.0466 | –0.13 | 515 | 0.51 | 79.3 | 1.8 | 80.85 | 2.2 | .0466 | 3.2 |
| 10KL073–7.1 | –0.000450 | 0.0478 | 0.01 | 205 | 0.46 | 83.9 | 2.0 | 76.29 | 2.4 | .0478 | 4.7 |
| 10KL073–8.1 | 0.000324 | 0.0499 | 0.30 | 265 | 0.71 | 77.0 | 1.8 | 82.96 | 2.4 | .0499 | 4.3 |
| 10KL073–9.1 | –0.000662 | 0.0489 | 0.18 | 330 | 0.53 | 74.1 | 1.7 | 86.34 | 2.3 | .0489 | 4.0 |
| 10KL073–10.1 | 0.000105 | 0.0482 | 0.08 | 597 | 0.63 | 77.4 | 1.7 | 82.67 | 2.1 | .0482 | 2.7 |
| 10KL073–11.1 | 0.000642 | 0.0497 | 0.28 | 213 | 0.58 | 73.7 | 1.9 | 86.74 | 2.5 | .0497 | 5.4 |
| 10KL073–12.1 | –0.001032 | 0.0458 | –0.21 | 288 | 0.37 | 72.2 | 1.7 | 89.03 | 2.4 | .0458 | 4.6 |

**Table 4.** SHRIMP U-Th-Pb data for zircon from plutons of Boulder batholith, southwest Montana.—Continued

[%, percent; ---, no data]

| Sample | Measured $^{204}Pb/^{206}Pb$ | Measured $^{207}Pb/^{206}Pb$ | % common $^{206}Pb$ | U (ppm) | Th/U | $^{206}Pb^{1}/^{238}U$ (Ma) | err [2] (Ma) | $^{238}U^{3}/^{206}Pb$ | err [2] (%) | $^{207}Pb^{3}/^{206}Pb$ | err [2] (%) |
|---|---|---|---|---|---|---|---|---|---|---|---|
| 10KL073–13.1 | 0.002064 | 0.0490 | 0.20 | 146 | 0.89 | 69.3 | 1.9 | 92.29 | 2.7 | .0490 | 6.0 |
| 10KL073–14.1 | --- | 0.0469 | –0.07 | 734 | 1.30 | 70.5 | 1.5 | 91.03 | 2.2 | .0469 | 2.8 |
| 10KL073–15.1 | 0.000177 | 0.0460 | –0.18 | 507 | 0.56 | 71.5 | 1.6 | 89.86 | 2.2 | .0460 | 3.2 |
| Sample 03KL066 (Monzogranite of Homestake) [latitude 45.9211° N, longitude 112.4209° W] | | | | | | | | | | | |
| 03KL066–1.1 | 0.000790 | 0.0540 | 0.82 | 329 | 0.63 | 74.8 | 0.9 | 86.20 | 1.2 | 0.0423 | 7.6 |
| 03KL066–2.1 | 0.000500 | 0.0471 | –0.06 | 248 | 0.62 | 75.8 | 1.0 | 85.34 | 1.4 | 0.0396 | 10.9 |
| 03KL066–3.1 | 0.001199 | 0.0484 | 0.12 | 189 | 0.60 | 73.8 | 1.2 | 88.74 | 1.8 | 0.0304 | 29.5 |
| 03KL066–4.1 | 0.002238 | 0.0822 | 4.37 | 282 | 0.63 | 77.8 | 1.4 | 82.20 | 2.1 | 0.0493 | 23.0 |
| 03KL066–5.1 | 0.000000 | 0.0494 | 0.23 | 467 | 0.49 | 76.0 | 0.9 | 84.10 | 1.1 | 0.0494 | 3.1 |
| 03KL066–6.1 | 0.001335 | 0.0479 | 0.05 | 196 | 0.68 | 76.6 | 1.1 | 85.71 | 1.5 | 0.0278 | 20.3 |
| 03KL066–7.1 | 0.001071 | 0.0526 | 0.65 | 217 | 0.64 | 75.1 | 1.1 | 86.53 | 1.7 | 0.0366 | 22.9 |
| 03KL066–8.1 | 0.000000 | 0.0470 | –0.06 | 371 | 0.62 | 76.3 | 1.3 | 84.05 | 1.7 | 0.0470 | 3.6 |
| 03KL066–10.1 | 0.000588 | 0.0512 | 0.47 | 270 | 0.55 | 74.6 | 1.0 | 86.43 | 1.5 | 0.0425 | 14.8 |
| 03KL066–11.1 | –0.000109 | 0.0494 | 0.25 | 1106 | 0.50 | 74.5 | 0.7 | 85.69 | 1.0 | 0.0510 | 3.1 |
| 03KL066–12.1 | 0.000679 | 0.0454 | –0.26 | 216 | 0.68 | 75.6 | 1.2 | 86.12 | 1.8 | 0.0353 | 17.9 |
| 03KL066–13.1 | 0.000586 | 0.0508 | 0.42 | 167 | 0.68 | 74.9 | 1.2 | 86.12 | 1.7 | 0.0421 | 13.1 |
| 03KL066–14.1 | 0.000456 | 0.0500 | 0.30 | 393 | 0.65 | 78.3 | 1.0 | 82.33 | 1.2 | 0.0432 | 6.5 |
| 03KL066–15.1 | 0.000364 | 0.0495 | 0.25 | 765 | 0.62 | 76.2 | 0.8 | 84.47 | 1.0 | 0.0441 | 4.5 |
| 03KL066–16.1 | 0.000206 | 0.0484 | 0.11 | 558 | 0.56 | 75.2 | 0.9 | 85.45 | 1.2 | 0.0454 | 4.4 |
| 03KL066–17.1 | 0.000470 | 0.0466 | –0.11 | 215 | 0.62 | 74.1 | 1.1 | 87.35 | 1.5 | 0.0396 | 11.4 |
| 03KL066–18.1 | 0.000547 | 0.0501 | 0.33 | 364 | 0.53 | 74.7 | 0.9 | 86.44 | 1.4 | 0.0420 | 12.5 |
| Sample 98BL004 (Butte Granite, at Bison Creek) [latitude 46.1917° N, longitude –112.3444° W] | | | | | | | | | | | |
| 98BL004–1.1 | 0.002693 | 0.0547 | 0.91 | 111 | 0.72 | 73.3 | 1.5 | 86.63 | 1.9 | .0547 | 6.3 |
| 98BL004–2.1 | 0.001813 | 0.0529 | 0.68 | 149 | 0.64 | 74.9 | 1.3 | 85.00 | 1.7 | .0529 | 5.7 |
| 98BL004–3.1 | 0.002741 | 0.0541 | 0.83 | 150 | 0.80 | 77.0 | 1.3 | 82.55 | 1.7 | .0541 | 5.7 |
| 98BL004–4.1 | 0.001683 | 0.0524 | 0.61 | 188 | 0.71 | 76.6 | 1.2 | 83.11 | 1.6 | .0524 | 5.0 |
| 98BL004–5.1 | 0.006364 | 0.1173 | 8.80 | 293 | 1.24 | 73.9 | 1.4 | 79.09 | 1.5 | .1173 | 6.3 |
| 98BL004–6.1 | 0.000117 | 0.0523 | 0.60 | 191 | 0.99 | 78.3 | 1.4 | 81.37 | 1.7 | .0523 | 5.6 |
| 98BL004–7.1 | 0.000084 | 0.0502 | 0.34 | 688 | 1.48 | 77.5 | 0.9 | 82.39 | 1.1 | .0502 | 5.2 |
| 98BL004–8.1 | –0.000461 | 0.0564 | 1.12 | 200 | 1.04 | 73.3 | 1.3 | 86.50 | 1.7 | .0564 | 5.5 |
| 98BL004–9.1 | 0.000471 | 0.0530 | 0.69 | 413 | 1.15 | 74.5 | 1.0 | 85.47 | 1.3 | .0530 | 3.9 |
| 98BL004–10.1 | –0.000968 | 0.0566 | 1.15 | 149 | 0.89 | 74.9 | 1.5 | 84.55 | 2.0 | .0566 | 6.6 |
| 98BL004–11.1 | 0.000583 | 0.0554 | 1.00 | 319 | 1.26 | 77.1 | 1.1 | 82.32 | 1.4 | .0554 | 4.2 |
| 98BL004–12.1 | 0.000101 | 0.0545 | 0.88 | 266 | 0.60 | 75.8 | 1.2 | 83.83 | 1.5 | .0545 | 4.9 |
| 98BL004–13.1 | 0.001029 | 0.0602 | 1.59 | 119 | 0.78 | 76.2 | 1.7 | 82.71 | 2.2 | .0602 | 7.0 |
| 98BL004–14.1 | 0.002641 | 0.0516 | 0.52 | 157 | 0.78 | 75.8 | 1.5 | 84.07 | 1.9 | .0516 | 6.3 |
| 98BL004–15.1 | 0.001932 | 0.0615 | 1.77 | 156 | 0.72 | 72.2 | 1.4 | 87.17 | 1.9 | .0615 | 7.9 |
| 98BL004–16.1 | --- | 0.0877 | 4.14 | 178 | 0.64 | 383.2 | 4.5 | 15.65 | 1.2 | .0877 | 2.0 |
| 98BL004–17.1 | 0.000744 | 0.0505 | 0.37 | 393 | 0.64 | 76.5 | 1.0 | 83.41 | 1.3 | .0505 | 4.1 |
| 98BL004–18.1 | –0.000327 | 0.0541 | 0.84 | 730 | 0.41 | 74.5 | 0.8 | 85.35 | 1.1 | .0541 | 3.0 |
| 98BL004–19.1 | 0.003658 | 0.0822 | 4.38 | 181 | 0.74 | 73.0 | 1.4 | 83.93 | 1.8 | .0822 | 4.8 |
| 98BL004–20.1 | –0.000312 | 0.0531 | 0.72 | 284 | 0.68 | 72.9 | 1.1 | 87.27 | 1.5 | .0531 | 4.7 |
| Sample 03KL069 (Granodiorite of Donald) [latitude 45.8493° N, longitude 112.4277° W] | | | | | | | | | | | |
| 03KL069–1 | 0.000565 | 0.0503 | 0.35 | 343 | 0.85 | 73.6 | 0.7 | 87.74 | 1.0 | 0.0419 | 10.2 |
| 03KL069–2 | 0.000192 | 0.0497 | 0.27 | 559 | 1.41 | 74.7 | 0.7 | 85.84 | 0.9 | 0.0468 | 3.5 |
| 03KL069–3 | 0.000000 | 0.0463 | –0.15 | 424 | 1.12 | 75.6 | 0.6 | 84.85 | 0.8 | 0.0463 | 2.9 |
| 03KL069–4 | 0.000209 | 0.0478 | 0.04 | 864 | 1.29 | 74.9 | 0.5 | 85.91 | 0.7 | 0.0447 | 3.5 |
| 03KL069–5 | –0.000411 | 0.0471 | –0.05 | 439 | 1.24 | 73.0 | 0.6 | 87.23 | 0.9 | 0.0531 | 5.8 |
| 03KL069–6 | 0.000462 | 0.0514 | 0.49 | 255 | 0.66 | 74.0 | 0.8 | 86.96 | 1.1 | 0.0445 | 7.7 |

**Table 4.** SHRIMP U-Th-Pb data for zircon from plutons of Boulder batholith, southwest Montana.—Continued

[%, percent; ---, no data]

| Sample | Measured $^{204}Pb/^{206}Pb$ | Measured $^{207}Pb/^{206}Pb$ | % common $^{206}Pb$ | U (ppm) | Th/U | $^{206}Pb^{1}/^{238}U$ (Ma) | err [2] (Ma) | $^{238}U^{3}/^{206}Pb$ | err [2] (%) | $^{207}Pb^{3}/^{206}Pb$ | err [2] (%) |
|---|---|---|---|---|---|---|---|---|---|---|---|
| 03KL069–7.1 | –0.000104 | 0.0462 | –0.16 | 412 | 0.74 | 73.5 | 0.8 | 87.21 | 1.1 | 0.0477 | 3.5 |
| 03KL069–8.1 | 0.000813 | 0.0517 | 0.54 | 217 | 0.70 | 73.8 | 0.8 | 87.73 | 1.1 | 0.0396 | 6.6 |
| 03KL069–9.1 | –0.000347 | 0.0464 | –0.14 | 447 | 1.57 | 74.6 | 0.6 | 85.44 | 0.9 | 0.0515 | 5.7 |
| 03KL069–10.1 | –0.000174 | 0.0494 | 0.24 | 1167 | 1.10 | 75.1 | 0.5 | 84.87 | 0.6 | 0.0520 | 3.1 |
| 03KL069–11.1 | –0.000077 | 0.0497 | 0.27 | 223 | 0.70 | 74.1 | 0.8 | 86.11 | 1.0 | 0.0508 | 4.2 |
| 03KL069–12.1 | 0.000221 | 0.0466 | –0.11 | 275 | 0.68 | 73.7 | 0.7 | 87.37 | 1.0 | 0.0434 | 7.3 |
| 03KL069–13.1 | –0.000355 | 0.0488 | 0.16 | 245 | 1.44 | 74.9 | 0.8 | 84.84 | 1.0 | 0.0540 | 3.7 |
| 03KL069–14.1 | –0.000353 | 0.0478 | 0.04 | 530 | 1.19 | 75.7 | 0.6 | 84.13 | 0.8 | 0.0530 | 5.1 |
| 03KL069–15.1 | –0.000124 | 0.0477 | 0.03 | 470 | 1.06 | 75.7 | 0.9 | 84.44 | 1.2 | 0.0496 | 4.1 |
| 03KL069–15.2 | 0.000003 | 0.1873 | 3.11 | 997 | 0.51 | 2452.7 | 15.8 | 2.09 | 0.5 | 0.1873 | 0.2 |
| Sample 04KL059 (Monzogranite of Moose Creek) [latitude 45.7394° N, longitude 112.6740° W] | | | | | | | | | | | |
| 04KL059–1.1 | 0.000420 | 0.0485 | 0.14 | 827 | 1.35 | 73.0 | 0.6 | 88.35 | 0.8 | 0.0423 | 7.5 |
| 04KL059–2.1 | 0.000558 | 0.0488 | 0.16 | 247 | 0.93 | 73.8 | 1.0 | 87.58 | 1.5 | 0.0405 | 11.3 |
| 04KL059–3.1 | 0.000827 | 0.0478 | 0.03 | 345 | 1.95 | 75.9 | 0.9 | 85.67 | 1.4 | 0.0354 | 16.4 |
| 04KL059–4.1 | 0.000702 | 0.0540 | 0.83 | 343 | 0.59 | 72.5 | 0.9 | 88.88 | 1.3 | 0.0436 | 11.3 |
| 04KL059–5.1 | –0.000068 | 0.0495 | 0.25 | 1152 | 1.03 | 74.4 | 0.5 | 85.80 | 0.7 | 0.0505 | 2.7 |
| 04KL059–6.1 | –0.000044 | 0.0508 | 0.42 | 597 | 1.35 | 74.2 | 0.7 | 85.91 | 0.9 | 0.0515 | 3.5 |
| 04KL059–7.1 | –0.000145 | 0.0471 | –0.06 | 739 | 1.01 | 77.1 | 0.6 | 82.95 | 0.8 | 0.0492 | 3.7 |
| 04KL059–8.1 | 0.000989 | 0.0589 | 1.43 | 2662 | 0.15 | 79.2 | 0.3 | 81.23 | 0.5 | 0.0443 | 6.5 |
| 04KL059–9.1 | 0.000396 | 0.0527 | 0.65 | 381 | 1.09 | 75.9 | 0.8 | 84.51 | 1.3 | 0.0468 | 12.4 |
| 04KL059–10.1 | 0.000255 | 0.0506 | 0.40 | 382 | 1.85 | 73.6 | 0.8 | 87.21 | 1.2 | 0.0469 | 8.4 |
| 04KL059–11.1 | 0.000358 | 0.0498 | 0.29 | 545 | 2.20 | 74.4 | 0.7 | 86.46 | 1.0 | 0.0445 | 8.1 |
| 04KL059–12.1 | 0.000590 | 0.0484 | 0.09 | 579 | 0.95 | 80.7 | 0.7 | 80.15 | 0.9 | 0.0396 | 8.6 |
| 04KL059–13.1 | 0.000057 | 0.0472 | –0.04 | 527 | 0.66 | 73.9 | 0.7 | 86.80 | 1.0 | 0.0464 | 5.8 |
| 04KL059–14.1 | 0.000055 | 0.0469 | –0.08 | 182 | 0.62 | 74.6 | 1.2 | 86.01 | 1.7 | 0.0461 | 12.9 |
| 04KL059–15.1 | –0.000370 | 0.0515 | 0.51 | 329 | 1.05 | 74.4 | 0.9 | 85.09 | 1.2 | 0.0569 | 5.8 |
| Sample 04KL058 (Monzogranite of Hell Canyon) [latitude 45.6353° N, longitude 112.3435° W] | | | | | | | | | | | |
| 04KL058–1.1 | 0.000126 | 0.0505 | 0.38 | 440 | 0.55 | 73.3 | 0.8 | 87.35 | 1.0 | 0.0487 | 5.3 |
| 04KL058–2.1 | 0.000918 | 0.0482 | 0.09 | 346 | 0.56 | 73.9 | 0.8 | 88.21 | 1.3 | 0.0344 | 17.8 |
| 04KL058–3.1 | –0.000333 | 0.0501 | 0.33 | 378 | 0.73 | 73.6 | 0.8 | 86.23 | 1.1 | 0.0550 | 6.1 |
| 04KL058–4.1 | 0.000579 | 0.0475 | 0.00 | 418 | 0.73 | 72.3 | 0.8 | 89.58 | 1.2 | 0.0388 | 11.5 |
| 04KL058–5.1 | 0.000294 | 0.0495 | 0.26 | 270 | 0.62 | 72.8 | 1.0 | 88.33 | 1.3 | 0.0451 | 8.2 |
| 04KL058–6.1 | 0.000102 | 0.0476 | 0.02 | 531 | 0.82 | 74.4 | 0.7 | 86.28 | 0.9 | 0.0461 | 4.7 |
| 04KL058–7.1 | –0.000036 | 0.0479 | 0.05 | 505 | 0.67 | 74.3 | 0.7 | 86.17 | 1.0 | 0.0484 | 3.7 |
| 04KL058–8.1 | –0.000274 | 0.0506 | 0.39 | 305 | 0.62 | 74.2 | 0.9 | 85.57 | 1.3 | 0.0546 | 6.5 |
| 04KL058–9.1 | 0.000466 | 0.0494 | 0.24 | 291 | 0.56 | 72.4 | 0.9 | 89.14 | 1.3 | 0.0424 | 10.4 |
| 04KL058–10.1 | 0.000348 | 0.0519 | 0.56 | 505 | 0.83 | 73.9 | 0.7 | 86.76 | 1.0 | 0.0468 | 7.1 |
| 04KL058–11.1 | 0.000747 | 0.0477 | 0.02 | 274 | 0.59 | 74.5 | 0.9 | 87.20 | 1.4 | 0.0365 | 14.2 |
| 04KL058–12.1 | –0.000083 | 0.0517 | 0.54 | 479 | 0.87 | 72.6 | 0.7 | 87.71 | 0.9 | 0.0529 | 4.1 |
| 04KL058–13.1 | 0.000425 | 0.0509 | 0.44 | 470 | 0.87 | 72.9 | 0.7 | 88.23 | 1.1 | 0.0447 | 10.6 |
| 04KL058–14.1 | 0.000012 | 0.0504 | 0.36 | 334 | 0.62 | 74.1 | 0.9 | 86.17 | 1.4 | 0.0502 | 11.3 |
| 04KL058–15.1 | –0.000081 | 0.0490 | 0.19 | 558 | 1.09 | 75.5 | 0.7 | 84.62 | 0.9 | 0.0502 | 3.3 |

[1] $^{206}Pb/^{238}U$ ages corrected for common Pb using the $^{207}Pb$-correction method. Decay constants from Steiger and Jäger (1977).

[2] 1σ errors.

[3] Radiogenic ratios, corrected for common Pb using the $^{204}Pb$-correction method, based on the Stacey and Kramers (1975) model.

**Table 5.** Summary of age data for plutons of Boulder batholith, southwest Montana.

| Sample number | Unit | Age (Ma) |
|---|---|---|
| 10KL072 | Monzogranite of Camp Thunderbird | 81.7 ± 1.4 |
| 98BL002 | Rader Creek Granodiorite | [1]80.7 ± 0.8 |
| 10KL087 | Granodiorite of Crystal Creek | 78.4 ± 1.3 |
| 98BL005 | Unionville Granodiorite | [1]78.2 ± 0.5 |
| 10KL085 | Granodiorite of Little Butte | 77.6 ± 1.2 |
| 04KL057 | Granodiorite of Burton Park | 77.3 ± 0.8 |
| 03KL071 | Granophyre of Deer Creek | 76.9 ± 0.6 |
| 03KL068 | Butte Granite (in Butte mining district) | 76.9 ± 0.8 |
| 03KL072 | Granodiorite of Climax Gulch | 76.7 ± 0.7 |
| 03KL067 | Butte Granite (at Homestake Pass) | 76.5 ± 0.7 |
| 98BL007 | Monzogranite of Pulpit Rock | [1]76.3 ± 0.5 |
| 10KL073 | Granodiorite of Colorado Gulch | 76.3 ± 1.2 |
| 03KL066 | Monzogranite of Homestake | 75.8 ± 0.6 |
| 98BL004 | Butte Granite (at Bison Creek) | [1]74.7 ± 0.6 |
| 03KL069 | Granodiorite of Donald | 74.5 ± 0.5 |
| 04KL059 | Monzogranite of Moose Creek | 74.2 ± 0.6 |
| 04KL058 | Monzogranite of Hell Canyon | 73.7 ± 0.6 |

[1]Average of data from Lund and others (2002) and new data (this study).

The weakly adakitic character of the Boulder batholith rocks implies an affinity with magmas whose petrogenesis included a subducted-slab partial melt component. However, the equivocal nature of this association and the finding by Richards and Kerrich (2007) that adakitic rocks need not involve subducted slab components indicate that the Boulder batholith rocks reflect magma genesis by ordinary processes typically associated with arc magmatism and subsequent, extensive open system petrogenesis. Consequently, petrogenesis of the Boulder batholith probably does not involve a subducted slab component. The Boulder batholith rocks are not ore metal enriched; consequently, processes that fostered formation of mineral deposits associated with these rocks do not require involvement of metal-enriched magma. Although weakly adakitic, Boulder batholith rocks are known to be as much as 10 m.y. older than spatially associated porphyry copper-molybdenum deposits (Lund and others, 2002), which is in accord with observations by Richards and Kerrich (2007) that adakitic compositions do not necessarily identify plutons with enhanced potential for spatially and genetically associated porphyry copper deposits.

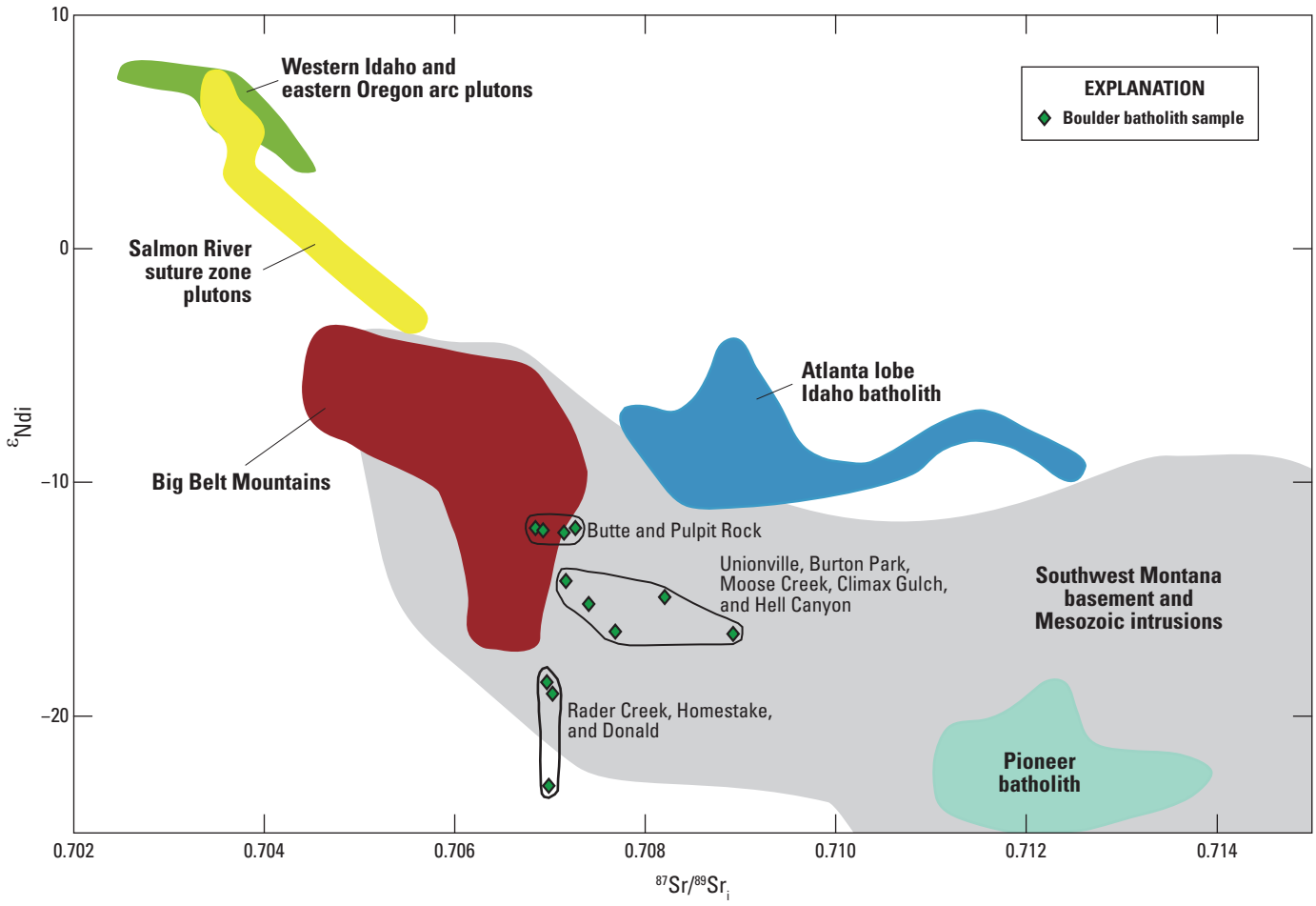


**Figure 14.** Epsilon neodymium versus initial strontium isotopic data for Boulder batholith samples. Fields for specific batholiths and plutons in Idaho and Montana from Taylor and others (2007); Unruh and others (2008).

**Table 6.** Rb-Sr and Sm-Nd isotopic data for samples of the Boulder batholith, southwest Montana.

| Sample | Pluton | Rb | Sr | Sm | Nd | Age | $^{87}Rb/^{86}Sr$ | $^{87}Sr/^{86}Sr$ | Uncertainty 2σ | $^{147}Sm/^{144}Nd$ | $^{143}Nd/^{144}Nd$ | Uncertainty 2σ | Sri | Nd(i) model | eNd(t) model | CHUR (t) |
|---|---|---|---|---|---|---|---|---|---|---|---|---|---|---|---|---|
| 98KL002 | Rader Creek | 67.2 | 703 | 4.5 | 23.9 | 80.7 | 0.267 | 0.70726 | 0.00001 | 0.116 | 0.511647 | 0.000011 | 0.70695 | 0.511586 | –18.5 | 0.512534 |
| 98KL005 | Unionville | 153 | 481 | 5.2 | 29.6 | 78.2 | 0.887 | 0.70815 | 0.00002 | 0.108 | 0.511868 | 0.000007 | 0.70716 | 0.511813 | –14.1 | 0.512537 |
| 04KL057 | Burton Park | 134 | 653 | 4.6 | 28.4 | 77.6 | 0.573 | 0.70803 | 0.00001 | 0.100 | 0.511813 | 0.000009 | 0.70740 | 0.511762 | –15.1 | 0.512538 |
| 98KL004 | Butte | 169 | 431 | 4.6 | 30 | 74.7 | 1.094 | 0.70809 | 0.00001 | 0.095 | 0.511972 | 0.000007 | 0.70693 | 0.511926 | –12.0 | 0.512542 |
| 03KL067 | Butte | 152 | 530 | 5.3 | 31.7 | 76.4 | 0.800 | 0.70813 | 0.00001 | 0.103 | 0.511981 | 0.000012 | 0.70726 | 0.511929 | –11.9 | 0.512540 |
| 03KL068 | Butte | 151 | 467 | 4.6 | 29.8 | 76.5 | 0.902 | 0.70813 | 0.00001 | 0.095 | 0.511969 | 0.000007 | 0.70715 | 0.511921 | –12.1 | 0.512540 |
| 98KL007 | Pulpit Rock | 171 | 430 | 3.9 | 26.2 | 76.3 | 1.110 | 0.70805 | 0.00001 | 0.092 | 0.511975 | 0.000008 | 0.70685 | 0.511929 | –11.9 | 0.512540 |
| 03KL072 | Climax Gulch | 146 | 494 | 3.4 | 21.5 | 76.3 | 0.825 | 0.70857 | 0.00001 | 0.098 | 0.511750 | 0.000006 | 0.70768 | 0.511701 | –16.4 | 0.512540 |
| 03KL066 | Homestake | 197 | 256 | 4.1 | 22.2 | 75.3 | 2.147 | 0.70932 | 0.00001 | 0.114 | 0.511626 | 0.000009 | 0.70702 | 0.511570 | –18.9 | 0.512541 |
| 03KL069 | Donald | 112 | 561 | 2.7 | 20.3 | 74.7 | 0.557 | 0.70758 | 0.00002 | 0.082 | 0.511406 | 0.000009 | 0.70699 | 0.511366 | –22.9 | 0.512542 |
| 04KL059 | Moose Creek | 113 | 235 | 3.7 | 21.4 | 74.2 | 1.342 | 0.70962 | 0.00001 | 0.107 | 0.511835 | 0.000008 | 0.70821 | 0.511783 | –14.8 | 0.512543 |
| 04KL058 | Hell Canyon | 107 | 587 | 2.2 | 13.5 | 73.7 | 0.509 | 0.70945 | 0.00001 | 0.101 | 0.511749 | 0.000011 | 0.70892 | 0.511701 | –16.4 | 0.512543 |

## Conclusions

The volume of the Late Cretaceous Boulder batholith is dominated by the large Butte Granite intrusion but includes at least 14 additional intrusive rock units. The petrographic, geochemical, and geochronologic characteristics of each of these units are distinct and foster identification of each intrusion. Compositions of the Boulder batholith rocks range from moderately mafic granodiorite to monzogranite and felsic granophyre. Standard intrusive rock geochemical metrics for the Boulder batholith rocks are consistent with their genesis being related to subduction and continental magmatic arc processes. A subduction-related origin for these rocks, well inboard from the edge of the Late Cretaceous western margin of North America, requires a high convergence rate and consequent shallow subduction. Accordingly, the critical depth of subduction-related magmatism shifted eastward over time. Subsequently (Late Cretaceous to Paleocene), when the convergence rate decreased along the western margin of North America, the subducted slab steepened and hinge rollback ensued.

Trace element data for the Boulder batholith rocks indicate that the magmas experienced minimal internal differentiation. Sr dominates large ion lithophile abundances and negative Eu anomalies are of limited magnitude. Consequently, magmas represented by these rocks experienced only modest plagioclase fractionation. REE patterns are remarkably similar between plutons. The lack of relative pattern rotation also indicates the limited role of accessory mineral fractionation in the genesis of these rocks. Subtle but systematic MREE to HREE depletions of the Boulder batholith rocks show that amphibole may have significantly affected their petrogenesis. Radiogenic isotope data for these rocks are also consistent with a subduction-related origin, including a significant mantle component. Between-pluton radiogenic isotopic variations probably reflect a combination of processes, including variable assimilation of crustal components by mantle-derived magmas as well as basement isotopic inhomogeneities. Although the Boulder batholith rocks have a weak adakitic geochemical affinity, compelling evidence for involvement of a subducted slab component in the genesis of these rocks is absent.

Magmas represented by the Boulder batholith rocks do not preserve evidence of unusual ore-metal enrichment. Consequently, ore-forming processes responsible for genesis of mineral deposits do not seem to require a particularly unique magma composition. Rather, the genesis of associated mineral deposits seems to reflect a combination of factors, including: a magma (source) containing the ore metals (though not in unusual abundances), hydrothermal fluids with the appropriate ligands and redox conditions (transport medium), conductive structural features (conduits), and reactive/receptive host rocks (sink).

## Acknowledgments

This work was funded by the USGS Mineral Resources Program. We thank Bettina Wiegand for Sr and Nd whole-rock isotopic analyses. We also gratefully acknowledge reviews by C.N. Mercer and C.D. Taylor that helped considerably improve this synthesis.

## References Cited

Anders, E., and Ebihara, Mitsuru, 1982, Solar-system abundances of the elements: Geochimica et Cosmochimica Acta, v. 46, p. 2362–2380.

Bateman, P.C., 1992, Plutonism in the central part of the Sierra Nevada Batholith, California: U.S. Geological Survey Professional Paper 1483, 186 p.

Becraft, G.E., and Pinckney, D.M., 1961, Preliminary geologic map of the northwest quarter of the Boulder quadrangle, Montana: U.S. Geological Survey Miscellaneous Field Studies Map MF–183, scale 1:24,000.

Becraft, G.E., Pinckney, D.M., and Rosenblum, S., 1963, Geology and mineral deposits of the Jefferson City quadrangle, Jefferson and Lewis and Clark counties, Montana, U.S. Geological Survey Professional Paper 428, 101 p.

Berger, B.R., Hildenbrand, T.G., and O'Neill, J.M., 2011, Control of Precambrian basement deformation zones on emplacement of the Laramide Boulder batholith and Butte mining district, Montana, United States: U.S. Geological Survey Scientific Investigations Report 2011–5016, 39 p.

Biehler, S., and Bonini, W.E., 1969, A regional gravity study of the Boulder Batholith, Montana: Geological Society of America Memoir 115, p. 401–422.

Black, L.P., Kamo, S.L., Allen, C.M., Davis, D.W., Aleinikoff, J.N., Valley, J.W., Mundil, R., Campbell, I.H., Korsuch, R.J., Williams, I.S., and Foudoulis, C, 2004, Improved $^{206}Pb/^{238}U$ microprobe geochronology by the monitoring of a trace-element-related matrix effect; SHRIMP, ID–TIMS, ELA–ICP–MS and oxygen isotope documentation for a series of zircon standards: Chemical Geology, v. 205, p. 115–140.

Brimhall, G.H., Jr., 1973, Mineralogy, texture, and chemistry of early wall rock alteration in the deep underground mines and Continental area, Butte district, Montana, *in* Miller, R.N., ed., Guidebook for the Butte field meeting of Society of Economic Geologists: Littleton, Colo., Society of Economic Geologists, p. H1–H5.

Brimhall, G.H., Jr., 1977, Early fracture-controlled disseminated mineralization at Butte, Montana: Economic Geology, v. 72, p. 37–59.

Brimhall, G.H., Jr., 1979, Lithologic determination of mass transfer mechanisms of multiple-stage porphyry copper mineralization at Butte Montana—Vein formation by hypogene leaching and enrichment of potassium-silicate protore: Economic Geology, v. 74, p. 556–589.

Brimhall, G.H., Jr., 1980, Deep hypogene oxidation of porphyry copper potassium-silicate protore at Butte, Montana—A theoretical evaluation of the copper remobilization hypothesis: Economic Geology, v. 75, p. 384–409.

Brown, R.G., 1894, The ore deposits of Butte City: Transactions of the American Institute of Mining and Metallurgical Engineering, v. 24, p. 543–558.

Cameron, K.L., and Cameron, M., 1985, Rare earth element, $^{87}Sr/^{86}Sr$, and $^{143}Nd/^{144}Nd$ compositions of Cenozoic orogenic dacites from Baja California, northwestern Mexico, and adjacent West Texas; evidence for the predominance of a subcrustal component: Contributions to Mineralogy and Petrology, v. 91, p. 1–11.

Christiansen, R.L., and Yeats, R.S., 1992, Post-Laramide geology of the U.S. Cordillera region, *in* Burchfiel, B.C., Lipman, P.W., and Zoback, M.L., eds., The Cordilleran Orogen—Conterminous U.S.: Boulder, Colo., Geological Society of America, The Geology of North America, v. G–3, p. 261–406.

Coney, P.J., and Reynolds, S.J., 1977, Cordilleran Benioff zones: Nature, v. 270, p. 403–406.

Davis, W.E., Kinoshita, W.T., and Smedes, H.W., 1963, Bouguer gravity, aeromagnetic, and generalized geologic map of East Helena and Canyon Ferry quadrangles and part of the Diamond City quadrangle, Lewis and Clark, Broadwater, and Jefferson counties, Montana: U.S. Geological Survey Geophysical Investigations Map GP–444, scale 1:62,500.

Davis, W.E., Kinoshita, W.T., and Robinson, G.D., 1965, Bouguer gravity, aeromagnetic, and generalized geologic map of the western part of the Three Forks Basin, Jefferson, Broadwater, Madison, and Gallatin counties, Montana: U.S. Geological Survey Geophysical Investigations Map GP–497, scale 1:62,500.

Davidson, Jon, Turner, Simon, Handley, Heather, Macpherson, Colin, and Dosseto, Anthony, 2007, Amphibole “sponge” in arc crust?: Geology, v 35, p. 787–790.

Doe, B.R., and Tilling, R.I., 1967, The distribution of lead between coexisting K-feldspar and plagioclase: American Mineralogist, v. 52, p. 805–816.

Doe, B.R., Tilling, R.I., Hedge, C.E., and Klepper, M.R., 1968, Lead and strontium isotope studies of the Boulder batholith, southwestern Montana: Economic Geology, v. 63, no. 8, p. 884–906.

du Bray, E.A., John, D.A., Putirka, Keith, and Cousens, B.L., 2009, Geochemical database for igneous rocks of the ancestral Cascades arc—Southern segment, California and Nevada: U.S. Geological Survey Data Series 439, 1 CD-ROM.

du Bray, E.A., John, D.A., Sherrod, D.R., Evarts, R.C., Conrey, R.M., and Lexa, Jaroslav, 2006, Geochemical database for volcanic rocks of the Western Cascades, Washington, Oregon, and California: U.S. Geological Survey Data Series 155, 49 p.

du Bray, E.A., Ludington, S., Brooks, W.E., Gamble, B.M., Ratte, J.C., Richter, D.R., and Soria-Escalante, E., 1995, Compositional characteristics of middle to upper Tertiary volcanic rocks of the Bolivian Altiplano: U.S. Geological Survey Bulletin 2119, 30 p.

du Bray, E.A., Lund, Karen, Tilling, R.I., Denning, P.D., and DeWitt, Ed, 2009, Geochemical database for the Boulder batholith and its satellitic plutons, southwest Montana: U.S. Geological Survey Data Series 454, 1 CD-ROM.

Elliott, J.E., Wallace, C.A., Lee, G.K., Antweiler, J.C., Lidke, D.J., 1992, Maps showing mineral resource assessment for vein and replacement deposits of gold, silver, copper, lead, zinc, manganese and tungsten in the Butte 1 x 2 degree quadrangle, Montana: U.S. Geological Survey I–2050–D, scale 1:250,000.

Emmons, S.F., and Tower, G.W., Jr., 1897, Economic geology of the Butte special district [Montana]: U.S. Geological Survey Atlas, Butte Folio no. 38, p. 3–8.

Emmons, S.F., and Weed, W.H., 1897, Butte Folio: U.S. Geological Survey Atlas, no. 38, 8 p.

Ewart, Anthony, 1982, The mineralogy and petrology of Tertiary-Recent orogenic volcanic rocks with special reference to the andesitic-basaltic compositional range, *in* Thorpe, R.S., ed., Andesites: Chichester, Wiley, p. 25–87.

Feeley, T.C., and Davidson, J.P., 1994, Petrology of calc-alkaline lavas at Volcan Ollague and the origin of compositional diversity at central Andean stratovolcanoes: Journal of Petrology, v. 35, p. 1295–1340.

Fleck, R.J., 1990, Neodymium, strontium, and trace-element evidence of crustal anatexis and magma mixing in the Idaho batholith, *in* Anderson, J.L. ed., The nature and origin of Cordilleran magmatism: Boulder, Colorado, Geological Society of America Memoir 174, p. 359–373.

Fleck, R.J., and Criss, R.E., 1985, Strontium and oxygen isotopic variations in Mesozoic and Tertiary plutons of central Idaho: Contributions to Mineralogy and Petrology, v. 90, p. 291–308.

Fleck, R.J., and Criss, R.E., 2004, Location, age, and tectonic significance of the western Idaho suture zone (WISZ): U.S. Geological Survey Open-File Report 2004–1039, 48 p.

Foster, D.A., Mueller, P.A., Mogk, D.W., Wooden, J.L., and Vogl, J.J., 2006, Proterozoic evolution of the western margin of the Wyoming Craton—implications for the tectonic and magmatic evolution of the Northern Rocky Mountains: Canadian Journal of Earth Sciences, v. 43, p. 1601–1619.

Frost, B.R., Barnes, C.G., Collins, W.J., Arculus, R.J., Ellis, D.J., and Frost, C.D., 2001, A geochemical classification for granitic rocks: Journal of Petrology, v. 42, p. 2033–2048.

GEOROC, 2007, Geochemistry of rocks of the oceans and continents: Max Plank Institute für Chemie, accessed May 2011 at *http://georoc.mpch-mainz.gwdg.de/georoc/*.

Gill, James, 1981, Orogenic andesites and plate tectonics: New York, Springer-Verlag, 390 p.

Gottfried, David, Rowe, J.J., and Tilling, R.I., 1972, Distribution of gold in igneous rocks: U.S. Geological Survey Professional Paper 727, 42 p.

Greenland, L.P., Gottfried, David, and Tilling, R.I., 1968, Distribution of manganese between coexisting biotite and hornblende in plutonic rocks: Geochimica et Cosmochimica Acta, v. 32, p. 1149–1163.

Greenland, L.P., Gottfried, David, and Tilling, R.I., 1974, Iridium in some calcic and calc-alkalic batholithic rocks of the western United States: Chemical Geology, v. 14, p. 117–122.

Greenland, L.P., Tilling, R.I., and Gottfried, David, 1971, Distribution of cobalt between coexisting biotite and hornblende in igneous rocks: Neues Jahrbuch für Mineralogie, Monatshefte, v. 1, p. 33–42.

Gunn, S.H., 1991, Isotopic constraints on the crustal evolution of southwest Montana: Santa Cruz, Calif., University of California at Santa Cruz Ph.D. dissertation, 190 p.

Hamilton, Warren, and Myers, W.B., 1967, The nature of batholiths: U.S. Geological Survey Professional Paper 554–C, 30 p.

Hanson, G.N., 1980, Rare earth elements in petrogenetic studies of igneous systems: Annual Review of Earth and Planetary Sciences, v. 8, p. 371–406.

Hildreth, Wes, and Moorbath, Stephen, 1988, Crustal contributions to arc magmatism in the Andes of central Chile: Contributions to Mineralogy and Petrology, v. 98, p. 455–489.

Irvine, T.N., and Baragar, W.R.A., 1971, A guide to the chemical classification of the common volcanic rocks: Canadian Journal of Earth Sciences, v. 8, p. 523–548.

John, D.A., Ayuso, R.A., Barton, M.D., Blakely, R.J., Bodnar, R.J., Dilles, J.H., Gray, Floyd, Graybeal, F.T., Mars, J.C., McPhee, D.K., Seal, R.R., Taylor, R.D., and Vikre, P.G., 2010, Porphyry copper deposit model, chap. B of Mineral deposit models for resource assessment: U.S. Geological Survey Scientific Investigations Report 2010–5070–B, 169 p.

Klepper, M.R., Robinson, G.D., and Smedes, H.W., 1971a, On the nature of the Boulder batholith of Montana: Geological Society of America Bulletin, v. 82, p. 1563–1580.

Klepper, M.R., Robinson, G.D., and Smedes, H.W., 1974, Nature of the Boulder batholith of Montana—Discussion: Geological Society of America Bulletin, v. 85, p. 1953–1960.

Klepper, M.R., Ruppel, E.T., Freeman, V.L., and Weeks, R.A., 1971b, Geology and mineral deposits, east flank of the Elkhorn Mountains, Broadwater county, Montana: U.S. Geological Survey Professional Paper 665, 66 p.

Klepper, M.R., Weeks, R.A., and Ruppel, E.T., 1957, Geology of the southern Elkhorn Mountains, Jefferson and Broadwater counties, Montana: U.S. Geological Survey Professional Paper 292, 82 p.

Knopf, Adolph, 1913, Ore deposits of the Helena mining region, Montana: U.S. Geological Survey Bulletin 527, 143 p.

Knopf, Adolph, 1950, The Marysville Granodiorite stock, Montana: American Mineralogist, v. 35, p. 834–845.

Knopf, Adolph, 1956, Argon-potassium determination of the age of the Boulder bathylith, Montana: American Journal of Science, v. 254, p. 744–745.

Knopf, A., 1957, The Boulder bathylith of Montana: American Journal of Science, v. 255, p. 81–103.

Knopf, Adolph, 1963, Geology of the northern part of the Boulder bathylith and adjacent area, Montana: U.S. Geological Survey Miscellaneous Geologic Investigations I–381, scale 1:48,000.

Knopf, Adolph, 1964, Time required to emplace the Boulder bathylith, Montana, a first approximation: American Journal of Science, v. 262, p. 1207–1211.

Lambe, R.N., 1981, Crystallization and petrogenesis of the southern portion of the Boulder Batholith, Montana: Berkeley, Calif., University of California Ph.D. dissertation, 171 p.

Lange, I.M., and Cheney, E.S., 1971, Sulfur isotopic reconnaissance of Butte, Montana: Economic Geology, v. 66, p. 63–74.

Le Maitre, R.W., 1989, A classification of igneous rocks and glossary of terms: Oxford, Blackwell Scientific, 193 p.

Lipman, P.W., 1992, Magmatism in the Cordilleran United States; Progress and problems, *in* Burchfiel, B.C., Lipman, P.W., and Zoback, M.L., eds., The Cordilleran orogen—Conterminous U.S.: Geological Society of America, The Geology of North America, v. G–3, p. 481–514.

Ludwig, K.R., 2001, Squid, version 1.02, A user's manual: Berkeley Geochronology Center Special Publication, No. 2, 21 p.

Ludwig, K.R., 2003, Isoplot/Ex version 3.00, A geochronological toolkit for Microsoft Excel: Berkeley Geochronology Center Special Publication, no. 4, 73 p.

Lund, Karen, editor, 2007, Earth science studies in support of public policy development and land stewardship; Headwaters Province, Idaho and Montana: U.S. Geological Survey Circular 1305, 92 p.

Lund, Karen, Aleinkoff, J.N., Kunk, M.J., Unruh, D.M., Zeihen, G.D., Hodges, W.C., du Bray, E.A., and O'Neill, J.M., 2002, Shrimp U-Pb and $^{40}Ar/^{39}Ar$ age constraints for relating plutonism and mineralization in the Boulder batholith region, Montana: Economic Geology, v. 97, p. 241–267.

Meyer, C., 1965, An early potassic type of wall-rock alteration at Butte, Montana: American Mineralogist, v. 50, p. 1717–1722.

Meyer, C., Shea, E.P., Goddard, C.C., Jr., Zeihen, L.G., Guilbert, J.M., Miller, R.N., McAleer, J.F., Brox, G.B., Ingersoll, R.G., Jr., Burns, G.J., and Wigal, T., 1968, Ore deposits at Butte, Montana, *in* Ridge, J.D., ed., Ore deposits of the United States, 1933–1967 (Graton-Sales v. 2): New York, American Institute of Mining and Metallurgical Engineers, p. 1373–1416.

Miller, R.N., 1973, Production history of the Butte district and geological function, past and present, *in* Miller, R.N., ed., Guidebook for the Butte field meeting of Society of Economic Geologists: Littleton, Colo., Society of Economic Geologists, p. F1–F10.

Miyashiro, Akiho, 1974, Volcanic rock series in island arcs and active continental margins: American Journal of Science, v. 274, p. 321–355.

O'Neill, J.M., Lund, Karen, Van Gosen, B.S., Desborough, G.A., Sole, T.C., and DeWitt, E.H., 2004, Geologic framework, *in* Nimick, D.A., Church, S.E., and Finger, S.E., eds, Integrated investigations of environmental effects of historical mining in the Basin and Boulder Mining Districts, Boulder River watershed, Jefferson county, Montana: U.S. Geological Survey Professional Paper 1652, p. 49–88.

Pearce, J.A., Harris, N.B.W., and Tindle, A.G., 1984, Trace element discrimination diagrams for the tectonic interpretation of granitic rocks: Journal of Petrology, v. 25, p. 956–983.

Proffett, J.M., 1973, Structure of the Butte district, Montana, *in* Miller, R.N., ed., Guidebook for the Butte field meeting of Society of Economic Geologists: Littleton, Colo., Society of Economic Geologists, p. G1–G12.

Richards, J.P., and Kerrich, R., 2007, Adakite-like rocks: their diverse origins and questionable role in metallogenesis: Economic Geology, v. 102, p.537–576.

Roberts, S.A., 1975, Early hydrothermal alteration and mineralization in the Butte district, Montana: Cambridge, Mass., Harvard University Ph.D. dissertation, 157 p.

Robinson, G.D., Klepper, M.R., and Obradovich, J.D., 1968, Overlapping plutonism, volcanism, and tectonism in the Boulder batholith region, western Montana *in* Coats, R.R., Hay, R.L., and Anderson, C.A., eds., Studies in volcanology: Geological Society of America Memoir 116, p. 557–576.

Ruppel, E.T., 1963, Geology of the Basin quadrangle, Jefferson, Lewis and Clark, and Powell counties, Montana: U.S. Geological Survey Bulletin 1151, 121 p.

Rusk, B.G., Reed, M.H., and Dilles, J.H., 2008, Fluid inclusion evidence for magmatic-hydrothermal fluid evolution in the porphyry copper-molybdenum deposit at Butte, Montana: Economic Geology, v. 103, p. 307–334.

Rutland, C., Smedes, H.W., Tilling, R.I., and Greenwood, W.R., 1989, Volcanism and plutonism at shallow crustal levels—The Elkhorn Mountains Volcanics and the Boulder batholith, southwestern Montana: International Geological Congress, 28th, Washington, D.C., Field Trip Guidebook T337, p. 16–31.

Sales, R.H., 1913, Ore deposits at Butte, Montana: Transactions of the Society of Mining Engineers of American Institute of Mining, Metallurgical and Petroleum Engineers, Incorporated, p. 1523–1626.

Sales, R.H., and Meyer, C., 1948, Wall-rock alteration, Butte, Montana: Transactions of the American Institute of Mining, Metallurgical and Petroleum Engineers, v. 178, p. 9–33.

Sales, R.H., and Meyer, C., 1949, Results for preliminary studies of vein formation at Butte, Montana: Economic Geology, v. 44, p. 465–484.

Sawka, W.N., Chappell, B.W., and Norrish, Keith, 1984, Light-rare-earth-element zoning in sphene and allanite during granitoid fractionation: Geology, v. 12, p. 131–134.

Schmidt, C.J., Smedes, H.W., and O'Neill, J. M., 1990, Syncompressional emplacement of the Boulder and Tobacco Root batholiths (Montana—USA) by pull-apart along old fault zones: Geological Journal, v. 25, p. 305–318.

Shand, S.J., 1951, Eruptive rocks: New York, John Wiley, 488 p.

Smedes, H.W., 1966, Geology and igneous petrology of the northern Elkhorn Mountains, Jefferson and Broadwater counties, Montana: U.S. Geological Survey Professional Paper 510, 116 p.

Smedes, H.W., Klepper, M.R., and Tilling, R.I., 1973, The Boulder batholith, Montana, *in* Miller, R.N., ed., Guidebook for the Butte field meeting of Society of Economic Geologists, 1973: Butte, Montana, Society of Economic Geologists, p. E1–20.

Smedes, H.W., Klepper, M.R., and Tilling, R.I., 1988, Preliminary map of plutonic units of the Boulder batholith, southwestern Montana: U.S. Geological Survey Open-File Report 88–283, scale 1:200,000.

Stacey, J.S., and Kramers, J.D., 1975, Approximation of terrestrial lead isotope evolution by a two-stage model: Earth and Planetary Science Letters, v. 26, p. 207–226.

Steiger, R.H., and Jäger, E., 1977, Subcommission on geochronology; Convention on the use of decay constants in geo- and cosmochronology: Earth and Planetary Science Letters, v. 36, p. 359–362.

Streckeisen, Albert, 1976, To each plutonic rock its proper name: Earth-Science Reviews, v. 12, p. 1–33.

Sun, S.-S., and McDonough, W.F., 1989, Chemical and isotopic systematics of oceanic basalts; implications for mantle composition and processes *in* Saunders, A.D., and Norry, M.J., eds., Magmatism in the ocean basins: Geological Society of London Special Publications, v. 42, p. 313–345.

Taylor, C.D., Winick, J.A., Unruh, D.M., and Kunk, M.J., 2007, Geochronology and geochemistry of the Idaho-Montana porphyry belt *in* Lund, Karen, ed., Earth science studies in support of public policy development and land stewardship—Headwaters Province, Idaho and Montana: U.S. Geological Survey Circular 1305, p. 26–39.

Tilling, R.I., 1964, Variation in modes and norms of an "Homogeneous" pluton of the Boulder batholith, Montana: U.S. Geological Survey Professional Paper 501–D, p. D8–D13.

Tilling, R.I., 1968, Zonal distribution of variations in structural state of alkali feldspars within the Rader Creek pluton, Boulder batholith, Montana: Journal of Petrology, v. 9, no. 3, p. 331–357.

Tilling, R.I., 1973, Boulder batholith, Montana—A product of two contemporaneous but chemically distinct magma series: Geological Society of America Bulletin, v. 84, p. 3879–3900.

Tilling, R.I., 1974, Composition and time relations of plutonic and associated volcanic rocks, Boulder batholith region, Montana: Geological Society of America Bulletin, v. 85, p. 1925–1930.

Tilling, R.I., 1977, Interaction of meteoric waters with magmas of the Boulder batholith, Montana: Economic Geology, v. 72, no. 5, p. 859–864.

Tilling, R.I., and Gottfried, David, 1969, Distribution of thorium, uranium, and potassium in igneous rocks of the Boulder batholith region, Montana, and its bearing on radiogenic heat production and heat flow: U.S. Geological Survey Professional Paper 614–E, p. E1–E29.

Tilling, R.I., Klepper, M.R., and Obradovich, J.D., 1968, K-Ar ages and time span of emplacement of the Boulder batholith, Montana: American Journal of Science, v. 266, p. 671–689.

Turekian, K.K., and Wedepohl, K.H., 1961, Distribution of the elements in some major units of the Earth's crust: Geological Society of America Bulletin, v. 72, p. 175–192.

Tysdal, R.G., 2000, Revision of Cretaceous Slim Sam Formation, Elkhorn Mountains area, Montana: U.S. Geological Survey Professional Paper 1601–B, 8 p.

Tysdal, R.G., Ludington, Steve, and McCafferty, A.E., 1996, Mineral and energy resource assessment of the Helena National Forest, west-central Montana: U.S. Geological Survey Open-File Report 96–683–A, 322 p., 6 plates.

Unruh, D.M., Lund, Karen, Snee, L.W., and Kuntz, M.A., 2008, Uranium-lead zircon ages and Sr, Nd, and Pb isotope geochemistry of selected plutonic rocks from western Idaho: U.S. Geological Survey Open-File Report 2008–1142, 36 p.

Wark, D.A., 1991, Oligocene ash flow volcanism, northern Sierra Madre Occidental; role of mafic and intermediate-composition magmas in rhyolite genesis: Journal of Geophysical Research, v. 96, p. 13,389–13,411.

Weed, W.H., 1912, Geology and ore depositions of the Butte district, Montana: U.S. Geological Survey Professional Paper 74, 262 p.

Wood, D.A., Joron, J.L., and Treuil, Michel, 1979, A re-appraisal of the use of trace elements to classify and discriminate between magma series erupted in different tectonic settings: Earth and Planetary Science Letters, v. 45, p. 326–336.

Publishing support provided by:
Denver Publishing Service Center
For more information concerning this publication, contact:
Center Director, USGS Central Mineral and Environmental Resources Science Center
Box 25046, Mail Stop 973
Denver, CO 80225
(303) 236-1562
Or visit the Central Mineral and Environmental Resources Science Center Web site at:
*http://minerals.cr.usgs.gov/*